DESIGN AND SIMULATION OF AN ELECTRIC VEHICLE CHARGER FOR SUSTAINABLE TRANSPORTATION

A DISSERTATION

SUBMITTED IN PARTIAL FULFILLMENT OF THE REQUIREMENTS FOR THE AWARD OF THE DEGREE

OF

MASTER OF TECHNOLOGY

In

POWER ELECTRONIC AND SYSTEM

Submitted by

SUSHANT CHATURVEDI

(2K21/PES/16)

Under the supervision of

Prof. ALKA SINGH

(Electrical Engineering Department, DTU)

DEPARTMENT OF ELECTRICAL ENGINEERING

DELHI TECHNOLOGICAL UNIVERSITY

(Formerly Delhi College of Engineering)

Bawana Road, Delhi-110042

MAY, 2023

DEPARTMENT OF ELECTRICAL ENGINEERING

DELHI TECHNOLOGICAL UNIVERSITY

(Formerly Delhi College of Engineering)

Bawana Road, Delhi-110042

CANDIDATE'S DECLARATION

I, SUSHANT CHATURVEDI, Roll No. 2K21/PES/16 student of M.tech (Power Electronic and Systems), hereby declare that the project Dissertation titled "**Design and simulation of an electric vehicle charger for sustainable transportation**" which is submitted by me to the Department of Electrical Engineering, Delhi Technological University, Delhi in the partial fulfillment of the requirement for the award of degree of Masters of Technology, is original and not copied from any source without proper citation. This work has not previously formed the basis for the award of any Degree, Diploma Associateship, fellowship or other similar title or recognition.

Place: Delhi SUSHANT CHATURVEDI

Date: 31st. May 2023

DEPARTMENT OF ELECTRICAL ENGINEERING

DELHI TECHNOLOGICAL UNIVERSITY

(Formerly Delhi College of Engineering)

Bawana Road, Delhi-110042

CERTIFICATE

I hereby certify that the Project Dissertation titled "**Design and simulation of an electric vehicle charger for sustainable transportation**" which is submitted by SUSHANT CHATURVEDI (2K21/PES/16), Electrical Engineering Department, Delhi Technological University, Delhi in partial fulfilment of the requirement for the award of the degree of Master of Technology, is a record project work carried out by the student under my supervision. To the best of my knowledge this work has not been submitted in part or full for any Degree or Diploma to this University or elsewhere.

Place: Delhi

Date: 31st MAY 2023

Prof. ALKA SINGH

(SUPERVISOR)

Department of Electrical Engineering

ACKNOWLEDGEMENT

It is a matter of great pleasure for me to present my dissertation report on "**Design and simulation of an electric vehicle charger for sustainable transportation**"**.** First and foremost, I am profoundly grateful to my guide Prof. Alka Singh, Department of Electrical Engineering for her expert guidance and continuous encouragement during all stages of thesis. Her help in form of valuable information and research papers at appropriate time brought life in this thesis. I feel lucky to get an opportunity to work with her. Not only understanding the subject, but also interpreting the results drawn thereon from the graphs was very thought provoking. I am thankful to the kindness and generosity shown by her towards me, as it helped me morally complete the project before actually starting it.

Besides my supervisors, I would also like to thank the following:

To my seniors, **Mr**.**Amarendra Pandey, Mr.Sudhanshu Mittal, Mr.Vineet Kumar** for being present during the best and the worst moments of this journey.

I would like to thank **my Family** for their help, encouragement and prayers for this duration. I dedicate my work to them.

Finally, I like to thank each and every person who was involved directly or indirectly in helping me to successfully complete this project.

Date: 31st May 2023

Place: DELHI SUSHANT CHATURVEDI

ABSTRACT

In recent years, electric vehicles have become increasingly popular due to growing concerns about climate change and the limited availability of fossil fuels. The battery charging system is a crucial component of electric vehicles, and it has received significant research attention, particularly in relation to vehicle-to-grid (V2G) power transfer. The primary objective of V2G is to facilitate peak load leveling for the grid and serve as a buffer for surplus renewable energy. This thesis focuses on single-phase on-board bidirectional chargers designed specifically for electric vehicle applications. The key areas of investigation include the design, control, and detection of islanding conditions in these chargers. This research entails a comprehensive examination of two different EV charging systems: one based on bidirectional power flow and other for unidirectional. The study involves an optimized design approach for both converters, which accurately assesses the high-frequency current ripple and damping resistor losses. The thesis also covers the design, simulation, and experimental validation of the controllers used in both converters. This study also focuses on examining the influence of 3rd harmonics on the performance of second-order generalized integrator (SOGI) phase-locked loops (PLLs). An analytical approach is used to predict the magnitude of the output harmonics that result from this impact. To enhance the harmonic rejection performance, two modified SOGI PLLs are introduced in the research. A 1KW and a 2KW prototype of the EV charger have been designed and simulated using MATLAB/Simulink. At full load, the power factor achieved is 0.999 with a THD under 5%.

Keywords: *Evs,PHEV,OBC,PFC,DC-DC,PSFB,THD,THD,SOGI,.*

TABLE OF CONTENTS

LIST OF ABBREVIATION

HEV	Hybrid Electric Vehicle
PHEV	Plug-in Hybrid Electric vehicle
EV	Electric Vehicle
DBR	Diode Bridge Rectifier
PFC	Power Factor Correction
OBC	On-Board Charger
THD	Total Harmonic Distortion
PF	Power Factor
RMS	Root Mean Square
EMI	Electro Magnetic Induction
RFI	Radio Frequency Interface
PCC	Point of Common Coupling
LPF	Low Pass Filter
LifePo4	Lithium iron phosphate
NIMH	Nickel-metal hybrid
CV	Constant Voltage
CC	Constant Current
VCO	Voltage Controlled Oscillator
PD	Phase Detector

LIST OF FIGURES

LIST OF TABLES

CHAPTER 1

INTRODUCTION

Designing an electric vehicle (EV) charger involves considering various factors such as power output, charging speed, safety features, and user interface. Here's a high-level overview of the design considerations for an EV charger [1]:

1. Power Output: First the power output capacity of the charger is determined, which is typically measured in kilowatts (kW). Consider the target charging time and the power limitations of the electrical grid. Common power outputs for EV chargers include 3.3 kW (Level 1), 7.2 kW (Level 2), and 50 kW (DC fast charging).

2. Connector Types: Select the appropriate connector type for compatibility with the target EV models and charging standards. Common connector types include the SAE J1772 (Type 1) for North America and IEC 62196 (Type 2) for Europe. DC fast chargers may use CHAdeMO, CCS (Combined Charging System), or Tesla Supercharger connectors.

3. Charging Speed: Determine the desired charging speed based on user requirements and available power. Level 1 chargers provide the slowest charging speed, Level 2 chargers are faster, and level 3 offer the highest charging speeds with DC fast charging.

4. Safety Features: Implement safety features to protect users and the charging infrastructure. This includes ground fault protection, overcurrent protection, thermal monitoring, and surge protection. Compliance with relevant safety standards is crucial.

5. User Interface: To design an intuitive user interface that provides clear instructions and feedback. It is important to include an interactive display or indicators to show charging progress, charging status, and any errors. Consider incorporating touch controls or physical buttons for user interaction.

6. Connectivity and Communication: There include communication capabilities to enable the charger to interact with the EV and other systems. This allows for features like remote monitoring, payment systems, and over-the-air updates. Common protocols used for communication include OCPP (Open Charge Point Protocol) and ISO 15118.

7. Physical Design and Durability: It is required to design a robust and weather-resistant enclosure suitable for indoor or outdoor installation. Consider factors such as heat dissipation, protection against dust and water (IP rating), and impact resistance. Ensure the design meets relevant standards and regulations.

8. Energy Efficiency: It is required to optimize the charger's energy efficiency to minimize power loss during charging. Use efficient power conversion techniques, standby power reduction, and energy management features. Incorporate smart charging algorithms to optimize charging based on grid conditions and user preferences.

9. Scalability and Modularity: The scalability of the charger design is another concern to accommodate future technological advancements and increasing demand. Modular designs can facilitate easier maintenance, upgrades, and expansion of charging infrastructure.

10. Compliance and Standards: The charger design must complies with relevant safety, electrical, and communication standards such as UL, IEC, CE, and local regulations. Adhering to industry standards promotes interoperability and compatibility.

It's important to note that designing an EV charger involves technical expertise in electrical engineering, power electronics, software development, and compliance with local regulations. Engaging with specialists in the field can help ensure a safe and efficient charger design.

1.1 Background

In an era marked by the pressing need to mitigate climate change and reduce our dependence on fossil fuels, electric vehicles (EVs) have emerged as a promising solution for sustainable transportation. As the demand for EVs continues to rise, the development of efficient and accessible charging infrastructure is essential to support this transformative shift. At the heart of this infrastructure lies the electric vehicle charger, a vital component that enables drivers to conveniently and reliably power their vehicles [1, 2].

Electric vehicle chargers provide a means to replenish the energy stored in an EV's battery, allowing drivers to embark on their journeys with confidence and peace of mind. These chargers come in various forms and capabilities, catering to the diverse needs of EV owners. From home chargers that facilitate overnight charging in residential settings to public charging stations strategically located along highways, urban centers, and commercial areas, the network of chargers is rapidly expanding to accommodate the growing fleet of electric vehicles [3].

The technology behind electric vehicle chargers has evolved significantly, offering faster charging times and improved energy efficiency. Today, advanced chargers

incorporate features such as smart connectivity, enabling drivers to monitor and control the charging process remotely through mobile applications. Additionally, some chargers are equipped with innovative technologies like bidirectional charging, allowing EVs to serve as mobile energy storage units that can supply electricity back to the grid during peak demand or in emergency situations.

The deployment of electric vehicle chargers not only supports the needs of individual EV owners but also contributes to the larger goal of building a sustainable transportation system. By providing a reliable and widespread charging infrastructure, we can encourage more individuals to adopt EVs, thereby decreasing emission of greenhouse gases, improving air quality, and promoting energy diversification.

In this era of rapid electrification, the significance of electric vehicle chargers cannot be overstated. They are the vital enablers of electric mobility, fostering a cleaner and greener future for transportation. Through continued innovation, collaboration among stakeholders, and investment in charging infrastructure, we can unlock the full potential of electric vehicles and pave the way for a sustainable and emission-free transportation landscape.

1.2 IC engine vs Electric Vehicle

IC Engine vehicles and Electric Vehicles represent two distinct approaches to transportation, each with its own set of advantages and disadvantages. [4]

ICE vehicles have been the dominant mode of transportation for over a century. They rely on combustion engines that convert the chemical energy into mechanical energy, propelling the vehicle forward. ICE vehicles offer a long-established infrastructure, with readily available fuel stations and a wide range of models to choose from. They also tend to have a longer driving range and shorter refueling times compared to EVs. However, ICE vehicles [5] contribute significantly to air pollution and climate change through the emission of greenhouse gases and harmful pollutants.

On the other hand, EVs are gaining momentum as a cleaner and more sustainable alternative. They utilize electric motors powered by rechargeable batteries to generate motion. EVs produce zero tailpipe emissions, leading to improved air quality and reduced dependence on fossil fuels. Moreover, EVs offer a quieter and smoother driving experience, with instant torque and responsive acceleration. While the initial cost of EVs may be higher, they often have lower operating costs due to cheaper electricity compared to gasoline or diesel.

However, EVs face some challenges. The limited driving range of early EV models has improved with advancements in battery technology, but it still remains a concern for long-distance travel. Charging infrastructure, though expanding, is not as widespread as traditional fuel stations, which can cause range anxiety for EV owners. Additionally, the production and disposal of EV batteries raise concerns regarding the environmental impact of their life cycle.

As the world transitions towards cleaner and more sustainable transportation, both ICE vehicles and EVs play a role. While ICE vehicles continue to dominate the roadways, advancements in EV technology, increased charging infrastructure, and environmental concerns are driving the shift towards electric mobility. The choice between an ICE vehicle and an EV ultimately depends on factors such as driving needs, environmental consciousness, and the availability of charging infrastructure. Ultimately, both technologies are coexisting, and their coexistence paves the way for a more diverse and sustainable transportation landscape.

1.3 Hybrid EV vs. Electric Vehicle

Electric Vehicles and Plug-In Hybrid Electric Vehicles (PHEVs) [5] are two types of vehicles that share the goal of reducing emissions and promoting sustainable transportation, but they employ different technologies to achieve this.

Electric Vehicles, or EVs, are fully electric vehicles that run solely on electric power. They are powered by rechargeable batteries and employ electric motors to generate motion. EVs produce zero tailpipe emissions, providing substantial ecological advantages through the mitigation of air pollution and the reduction of greenhouse gas emissions. They offer a quiet and smooth driving experience, instant torque, and typically exhibit higher energy efficiency compared to traditional internal combustion engine vehicles. However, EVs typically have limited driving ranges and require access to charging infrastructure for recharging, which can present challenges for long-distance travel and in areas with limited charging stations.

HEVs, combine an IC engine with an motor and battery system. HEVs are designed to optimize fuel efficiency and reduce emissions. They utilize the internal combustion engine to power the vehicle at higher speeds or when additional power is needed, while the electric motor assists during acceleration and low-speed driving. HEVs offer better fuel economy and lower emissions compared to conventional vehicles, as they can rely on electric power for certain driving conditions. They also eliminate the range

limitations associated with fully electric vehicles since they can rely on the internal combustion engine for extended driving ranges. However, HEVs still rely very much on fossil fuels and hence may not offer the same level of emissions reduction as fully electric vehicles.

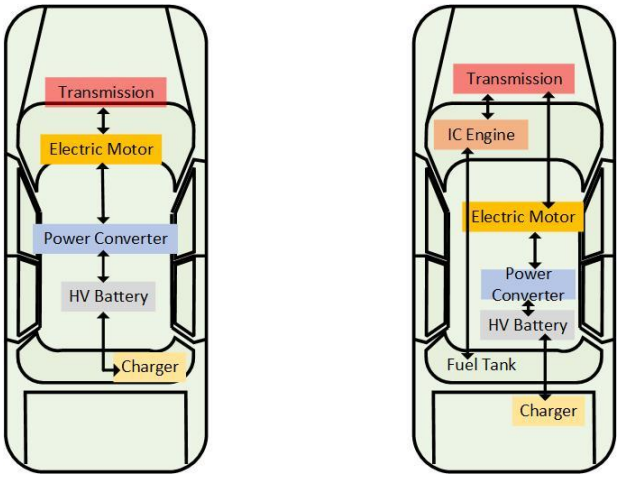

(a) **(b)**

Figure 1.1: Flow in EVs (a) BEVs (b) HEV [4]

In summary, Electric Vehicles are fully electric, relying solely on rechargeable batteries, while HEV combines both an IC engine along with an EV motor and battery system. EVs offer zero emissions but have limited range and require charging infrastructure, while HEVs offer improved fuel efficiency and lower emissions but still rely on fossil fuels. The choice between an EV and an HEV depends on factors such as driving patterns, infrastructure availability, and environmental priorities. Both types of vehicles contribute to the goal of reducing emissions and transitioning towards a more sustainable transportation future.

1.4 Battery Chargers for Plug-In Electric Vehicles [7-9]

As the world embraces the transition to sustainable transportation, battery chargers for electric vehicles play a crucial role in enabling convenient and efficient recharging. These chargers are essential components of the electric vehicle infrastructure, providing a reliable and accessible means to replenish the energy stored in the vehicle's battery.

Battery chargers for PEVs come in various forms and charging levels, catering to the diverse needs of electric vehicle owners. At the most basic level, Level 1 chargers are designed for residential charging and can be plugged into a standard household outlet. While Level 1 chargers offer the slowest charging rate, they provide a convenient option for overnight charging, ensuring that the vehicle is ready for daily use.

For faster charging, Level 2 chargers are commonly installed in homes, workplaces, and public charging stations. These chargers require a dedicated charging unit and can deliver higher power levels, significantly reducing charging times compared to Level 1 chargers. Level 2 chargers are an ideal solution for regular charging needs, allowing PEV owners to top up their vehicles in a matter of hours.

For even greater charging speed and convenience, DC fast chargers, also known as Level 3 chargers, are available at select public charging stations. DC fast chargers utilize direct current (DC) to rapidly charge the vehicle's battery. They can provide a substantial charge in a short period, typically within 30 minutes or less, making them ideal for long-distance travel and quick charging on the go.

The battery charger plays a vital role in maximizing the utilization the battery to its full capacity. Efficiency and sustainability, charging time and power density are key factors that contribute to the notable characteristics of a battery charger. These features in the device are determined by choice of components, methods of switching, and controller. Microcontrollers are utilized to implement control algorithms digitally. The Figure 1.2 represents a general architectural diagram of an EV charger. Charger is made to work in two stages. initial component is the PFC modules AC to DC converter, which transforms the AC grid voltage into DC while maintain a good pf and low total harmonic distortion (THD). In the subsequent stage, the method chosen determines how the battery's charging current and voltage are regulated and modified.

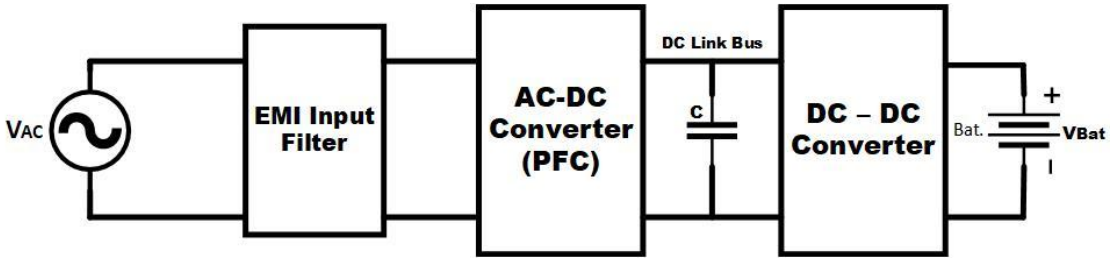

Figure 1.2: Block diagram of EV charger architecture

This charger operates in either a unidirectional manner, which means it can solely charge the electric vehicle (EV) battery from the grid, or in a bidirectional manner, which allows it to charge the battery from the grid during the charging mode and also transfer excess power from the battery back into the grid. Both isolated and non-isolated topologies can be utilized for the charger. Comprehensive explanations of each stage are provided in the following chapters, covering all the necessary details.

1.5 Battery study

1.5.1 Introduction

As the world embraces the transition to sustainable transportation, battery chargers for plug-in electric vehicles (PEVs) play a crucial role in enabling convenient and efficient recharging. These chargers are essential components of the electric vehicle infrastructure, providing a reliable and accessible means to replenish the energy stored in the vehicle's battery.

Battery chargers for PEVs come in various forms and charging levels, catering to the diverse needs of electric vehicle owners. At the most basic level, Level 1 chargers are designed for residential charging and can be plugged into a standard household outlet. While Level 1 chargers offer the slowest charging rate, they provide a convenient option for overnight charging, ensuring that the vehicle is ready for daily use.

For faster charging, Level 2 chargers are commonly installed in homes, workplaces, and public charging stations. These chargers require a dedicated charging unit and can deliver higher power levels, significantly reducing charging times compared to Level 1 chargers. Level 2 chargers are an ideal solution for regular charging needs, allowing PEV owners to top up their vehicles in a matter of hours.

For even greater charging speed and convenience, DC fast chargers, also known as Level 3 chargers, are available at select public charging stations. DC fast chargers utilize direct current (DC) to rapidly charge the vehicle's battery. They can provide a substantial charge in a short period, typically within 30 minutes or less, making them ideal for long-distance travel and quick charging on the go.

The evolution of battery charger technology has also introduced features like smart connectivity, enabling PEV owners to monitor and control the charging process remotely through smartphone applications. Some chargers incorporate advanced features such as load management, allowing users to schedule charging during off-peak hours, maximizing energy efficiency and cost savings.

The widespread availability and accessibility of battery chargers for PEVs are vital for promoting electric vehicle adoption and addressing range anxiety concerns. By expanding the charging infrastructure, governments, businesses, and individuals can contribute to a cleaner and greener future of mobility. Investment in charging

infrastructure and collaboration among stakeholders are essential to ensure seamless charging experiences for PEV owners, enabling the continued growth of electric vehicle usage.

Battery chargers for plug-in electric vehicles are more than just charging devices; they are enablers of the electric mobility revolution. With their ability to efficiently recharge PEVs, these chargers empower drivers to embrace sustainable transportation, reduce emissions, and contribute to a cleaner, healthier, and more sustainable future for all.

1.5.2 Battery [9]

A common electrical model used to represent a lithium-ion (Li-ion) battery is the equivalent circuit model, as in Figure 1.3. This model consists of several circuit elements that approximate the behavior of a Li-ion battery under different conditions. Here is a simplified representation of the electrical model:

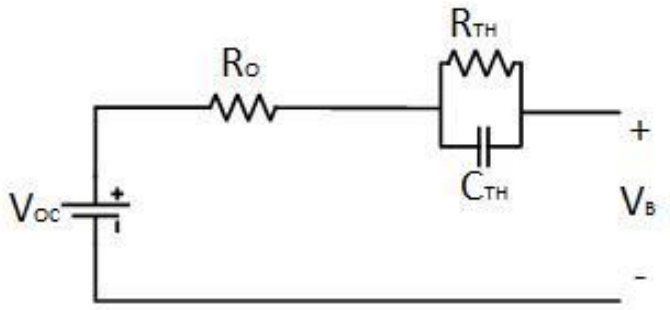

Figure 1.3: Electrical Equivalent Model of Li-Ion Battery

1. Open-Circuit Voltage (V_{OC}): The V_{OC} represents the voltage of the battery when no current is flowing. It is battery's' state of charge (SoC) dependent and is usually determined through calibration or measurement.

2. Internal Resistance: The internal resistance represents the resistance to the flow of current within the battery. It includes various sources of resistance such as electrode resistance, electrolyte resistance, and contact resistance. The internal resistance causes voltage drops and power losses within the battery. Here in this model both ohmic resistance R_o and polarization resistance R_{TH} are accounted for the internal resistance.

3. Capacitance (C_{TH}): Capacitance represents the ability of the battery to store and release charge. It accounts for the double-layer capacitance at the electrode-electrolyte interface and the intercalation capacitance.

4. The operative voltage of the battery is indicated by the variable V_B.

The charging characteristics of a lithium-ion battery are shown in figure 1.4

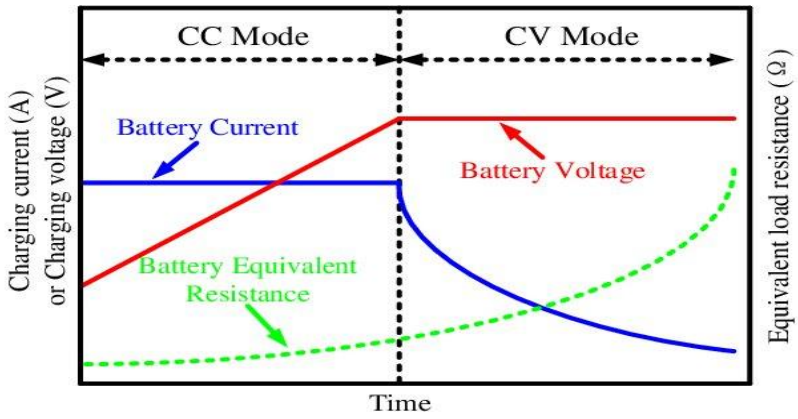

Figure 1.4: Charging behavior of a single Li-ion cell

The most frequently employed charging method for Li-ion batteries is the CC/CV (constant current/constant voltage) mode. Figure 1.4 illustrates The charging performance of an individual lithium-ion cell with a designated nominal voltage. Four notable stages can be identified during the charging process [5]. Beginning and ending points of the charging process correspond to the initiation and termination of charging. The nominal value signifies when the battery reaches to the steady state, while the turning point indicates transition from the constant current (CC) charging mode to the constant voltage (CV) charging mode. The cell voltage drops below its nominal rating when it is depleted. Initially, battery begins charging in a Constant Current operation until it reaches the point of turning, point were the voltage of the battery must have reached its maximum value with 100% state of charge (SoC). After that, the battery gets charge in a constant voltage mode till the charging current drops below a certain acceptable threshold.

1.6 Literature Review

Paper [7], Charger necessitates a quad operating AC to DC converter to enable power factor correction (PFC), along with full bridge DC to DC converter for constant current and constant voltage charging behavior. Design of the controller for PFC to incorporate battery voltage and current references, which leads to increased complexity in the control circuit.

Paper [8] introduces a level 2 charger that incorporates a bridgeless boost power factor correction (PFC) converter as the first converter known as front end device and a PSFB

DC to DC converter. The charger employs silicon carbide (SiC) power switches to achieve high density and efficiency. Operating at a frequency of above 200 kHz, the charger achieves efficiency above to 92% and a minimum total harmonic distortion (THD) of 4.2%.

Paper [9] provides a description of the operating modes of (EVs) in homes and Smart Grid systems. Typically, two primary ways of power transfer exist between the vehicle and the grid, Grid to Vehicle (G2V) and Vehicle to Grid (V2G). Proposing two additional modes: Vehicle for Grid (V4G) and Home to Vehicle (H2V). A new mode called Vehicle to Home (V2H) is also suggested.

In the mode, current of charger is adjusted based on the power consumption of household appliances. The V4G operation aims to compensate for reactive power within the home using the charger. In the V2H mode, the vehicle supplies power to a small home, while in the V2G mode, vehicle is intended to transfer power to the grid. To enable all these modes of working, a prototype of a 3.6 kW charger has been created, featuring the ability to facilitate power flow in both directions (bidirectional).

A EV on board charger (OBC) was presented in [10], specifically designed for electric scooters. This device is specifically designed for a lead-acid battery with a voltage at around 200 V and a capacity of 12 Ah. It is capable of charging the battery using a standard single-phase. DC-DC converters for low voltage (LDC) were also introduced in the study. Additionally, DC-DC converter is proposed to facilitate the charging of a 12 V auxiliary.

Paper [11], Resonant synchronous mode of operation, DC to DC converter operating in discontinuous conduction mode is introduced. The study proposes a method to calculate the necessary dead time and reversed current for achieving zero voltage switching (ZVS) operation throughout the entire operating range. The selection of parameters can be performed using the provided datasheets of components, eliminating the need for simulation or experimental verification.

Various power factor correction (PFC) topologies, including the Diode Bridge followed by non-isolated DC-DC Converter, can be utilized for supplying Brushless DC Motors. In reference [12], various PFC topologies are studied to determine the most suitable one for a specific application. The paper suggests that DBR based PFC topologies are the optimal choice for low-power applications. Boost PFC topology offers an advantage when the desired output DC voltage is higher than the input voltage. For applications requiring an output DC voltage lower than the root mean square of the supply, Buck-

based PFC topologies are suitable. Buck-Boost-derived topologies such as Cuk and SEPIC are advantageous for power levels below 500 W. Half Bridge and Push Pull topologies exhibit lower total harmonic distortion (THD) and are suitable for medium-power operations compared to the Boost PFC converter. However, the selection of topology should consider the trade-off between performance, cost, and complexity, as the component count increases with certain topologies.

Paper [13], a Buck power factor correction (PFC) converter employing Constant On-Time control is introduced. The proposed design is experimentally validated for a power output of 100 W and a input voltage of 90 V. The design successfully matches the harmonic standards specified by IEC61000-3-2. The efficiency of the converter is calculated to be 0.96 under full load and universal voltage operation. It is worth noting that a drawback of buck PFC converters is the discontinuous input current, which necessitates the use of a larger input filter.

Paper [14], a new and innovative two-switch Boost-interleaved buck-boost topology is presented. This designed converter offers several advantages, including reduced stress on the power switching devices, lower conduction loss in the switching devices, inductive components, and a smaller overall size. The converter achieves an efficiency of 93% when operating with a universal line voltage input, while maintaining low total harmonic distortion (THD).

1.7 Objective

The aim of this thesis is to design an Electric Vehicle OBC specifically designed for level 1 requirement. The designed charger consists of two stages: A Power Factor Correction (PFC) known as the front end to convert AC to high power factor DC, and an Isolated DC-DC converter in the second stage for regulating the power transfer to battery. The propulsion battery used in the system is a Li-Ion type, and a charging algorithm based on constant current/constant voltage (CC/CV) is developed for efficient charging.

1.8 Outline of Thesis

The structure of the Thesis is arranged as follows.

Chapter 1: In this chapter, the reader is introduced to general Electric Vehicle (EV) technology and is provided with a background on the significance of control structure. Additionally, the chapter addresses the various issues that can occur on the grid in relation to EVs.

Chapter 2: A PFC based AC-DC converter is explained, necessary to transform the grid voltage into a acceptable DC voltage while minimizing current harmonics while keeping good power factor. Different PFC configuration are discussed and simulated.

Chapter 3: This chapter considers the design of few synchronization techniques such as SFL-PLL, SOGI-PLL which are integrated into the control technique when distorted grid is present.

Chapter 4: The second stage of the On-Board Charger (OBC) is described in this chapter, which involves a DC-DC converter responsible for regulating power while charging. Additionally, the chapter presents the concept of V2G and G2V operating modes of the charger.

Chapter 5: In this chapter, the validation of the results is conducted, with simulation results for 1kW and 2kW EV charger.

Chapter 6: In this chapter, the contributions of this thesis are summarized, and the potential for future research opportunities is highlighted.

1.9 Conclusion

In Chapter 1 of this thesis, the fundamental distinction between IC Engine (ICE) and Electric Vehicles (EVs) is outlined. Additionally, a concise explanation of the Hybrid Electric Vehicle (HEVs) and Electric Vehicles (EVs), highlighting the power devices required for each stage for conversion. Explanation of the two-stage EV charger, highlighting the need of power devices for each stage are mentioned.

The advancements in EVs and HEVs have led to the utilization of high-voltage Lithium-Ion battery packs for propulsion. The numerous advantages of Li-ion batteries are discussed, along with the recommended charging profile known as CC/CV mode, as suggested by battery manufacturers. Furthermore, an in-depth explanation of the equivalent electrical model of the battery is provided.

Literature reveiw focuses on the classification of EV chargers based on power levels and power flow capabilities, distinguishing between unidirectional and bidirectional chargers. The section also reviews previous works related to EV chargers and the associated converters.

A Basic Block diagram of the EV charger configuration is provided which comprises PFC as front end converter and another DC-DC converter of appropriate rating and design.

CHAPTER 2

FRONT END AC-DC PFC CONVERTER

2.1 Introduction

Electric vehicles (EVs) rely on high-voltage DC (direct current) power stored in the battery pack to operate their electric drivetrains. However, the power supplied by the electrical grid or charging stations is typically AC (alternating current). To bridge this gap, EVs incorporate an AC-DC converter, also known as an onboard charger or rectifier, to convert the incoming AC power to DC power for charging the vehicle's battery.

The AC-DC converter performs the essential function of converting the g AC from supply to a steady DC level that the vehicle's battery can accept. It ensures efficient power transfer and enables the charging process to occur safely and effectively. The converter operates in two stages: rectification and conversion.

1. Rectification: In this stage, the AC input from the grid is rectified to produce a pulsating DC waveform. This is typically achieved using diodes that allow the positive half-cycles of the AC voltage to pass through while blocking the negative half-cycles, resulting in a unidirectional current flow. The rectified output is an intermediate DC voltage.

2. Conversion: The rectified DC voltage is further converted to the specific voltage level required for charging the EV battery. This conversion is accomplished through power electronics circuits, such as a DC-DC converter, which steps up or steps down the voltage as needed. The converter ensures that the DC output voltage is stable and regulated, efficient for charging the battery pack.

The AC-DC converter in an electric vehicle requires sophisticated control algorithms to manage the power flow, monitor the charging process, and maintain safety. It integrates with the vehicle's battery management system (BMS) to optimize charging efficiency, monitor battery health, and implement safety features like over current and overvoltage protection.

In addition to charging the vehicle, the AC-DC converter may also serve as a power source for auxiliary systems in the vehicle, such as the onboard electronics and accessories. This allows the converter to provide low-voltage DC power to various components, reducing the need for separate DC-DC converters.

Efficiency and power factor correction are key considerations in AC-DC converter design. Higher efficiency ensures minimal energy loss during the conversion process,

optimizing charging efficiency and reducing electricity consumption. Power factor correction (PFC) techniques are employed to improve the power quality by minimizing reactive power demand, reducing harmonic distortion, and maximizing the utilization of the grid's power resources.

Overall, the AC-DC converter in an electric vehicle plays a vital role in converting grid AC power to the required DC power for charging the vehicle's battery. It enables efficient power conversion, integrates with the vehicle's systems, and ensures a safe and reliable charging experience, contributing to the widespread adoption and usability of electric vehicles.

The Electric Vehicle (EV) can be charged through an On-Board Charger (OBC), where AC to DC converter serves as initial part, converting the available AC supply into DC. The desired output from the AC-DC converter is a constant voltage with minimal ripple, which can be utilized by loads or other converters. The DBR with a capacitance for filtering and phase-controlled rectifiers are the most common rectifier topologies. The former is prior for lower rating applications, while the latter is suitable for high rating and 3-phase applications.

However, conventional rectifiers have a significant drawback in the form of harmonic components in the line current. These harmonics distort the voltage at the PCC due to source inductance, resulting in distorting effects. One of the consequences is a worsening power factor caused by the presence of harmonics. The adverse effects of low pf and higher value of THD are discussed in detail ahead.

2.2 Basic Definitions [15]

Power factor can be defined as the ratio of power consumed by system to total power delivered by grid. Real power is obtained by taking the product of voltage and current over a complete cycle, while apparent power is calculated as the product of the RMS voltage and RMS current.

The power factor (PF) is defined as the cosine of the angle between the voltage phasor and the current phasor. However, it should be noted that this definition is not universally applicable, particularly in the presence of non linear loads. The definition is valid only for all loads [15].

Considering a non linear load with an ideal voltage supply. In this case, the voltage and current signal are represented as v(t) and i(t) respectively.

$$v(t) = V_m \sin wt \tag{2.1}$$

$$i(t) = I_O + \sum_{n=1}^{\infty} I_n \sin(nwt + \phi_n) \tag{2.2}$$

V_m is the peak value voltage. I_n is the peak value of $n\ th$ harmonics component of current and $\emptyset n$is the nth harmonic phase displacement.

The RMS current is calculated mathematically and represented as

$$I_{RMS} = \sqrt{I_O{}^2 + \Sigma_{n=1}^{\infty} I_n{}^2} \tag{2.3}$$

The power factor can be stated as the product of displacement and the distortion factor. Prior denoted as $k\emptyset$, is defined as the cosine of the angle between the fundamental components of voltage and current.

$$k_\phi = \cos\phi \tag{2.4}$$

Here, $\emptyset$ represents the phase displacement between the fundamental voltage and current components.

Total Harmonic Distortion (THD) is a measurement that quantifies the level of harmonic distortion present in an electrical or electronic system. Harmonics are additional frequencies that occur in a system due to nonlinearities in the devices or circuits. In an ideal system, the voltage and current waveforms would be perfect sinusoids with no distortion. However, in real-world systems, non-linear loads like power electronic devices, electric motors, or certain types of lighting can introduce harmonics into the system.

THD is typically expressed as:

$$THD(\%) = \frac{1}{\sqrt{g^2 - 1}} \tag{2.5}$$

Where g is the distortion factor and can be defined as:

$$g = \frac{I_{1(RMS)}}{\sqrt{I_O{}^2 + \sum_{n=1}^{\infty} I_n{}^2}} \tag{2.6}$$

From here pf can also be defined as the product of displacement factor and distortion factor.

$$pf = g \times k\phi \tag{2.7}$$

When the fundamental component of current is in phase with the voltage, the displacement factor is 1 and the $pf = g$

2.2.1Effects of current Harmonics:

Current harmonics can have several negative effects on electrical systems and equipment. Some of the major impacts include:

1. Increased losses: Harmonic currents can cause additional losses in electrical distribution systems, including transformers, cables, and other components. These losses result from the resistive heating effects of harmonic currents flowing through system impedances. Increased losses lead to reduced system efficiency, higher energy consumption, and increased operating costs.

2. Overheating and reduced equipment lifespan: Harmonic currents can cause overheating in electrical equipment such as transformers, motors, and capacitors. The additional heat generated by harmonics can exceed the design limits of the equipment, leading to accelerated aging, insulation degradation, and reduced equipment lifespan. Overheating can also increase the risk of equipment failures and potential safety hazards.

3. Voltage distortion: Harmonic currents interact with the impedance of the electrical system, resulting in voltage distortion. Voltage distortion can lead to various issues such as flickering lights, malfunctions of sensitive electronic equipment, and interference with communication systems. Excessive voltage distortion can also violate the permissible limits set by voltage quality standards and regulations.

4. Power quality issues: Harmonic currents can degrade overall power quality. They can cause voltage fluctuations, voltage unbalance, and harmonic resonance. Harmonic resonance occurs when the natural frequency of a system coincides with a harmonic frequency, leading to a significant increase in harmonic voltage and current levels. Resonance can result in severe equipment damage, voltage distortion, and even system instability.

5. Interference with other systems: Harmonic currents can interfere with neighboring electrical systems, communication networks, and sensitive electronic devices. Harmonics can generate electromagnetic interference (EMI) and radio frequency interference (RFI), affecting the performance and reliability of nearby equipment and systems.

To mitigate the adverse effects of current harmonics, various measures can be taken, including:

- Applying harmonic filters: Installing harmonic filters at the affected loads or at the point of common coupling can help mitigate the impact of harmonics by providing a low impedance path for harmonic currents to flow.

- Implementing power factor correction: Improving power factor by adding power factor correction capacitors can reduce the level of harmonics in the system.
- Conducting harmonic studies: Performing detailed harmonic studies and assessments can help identify the sources of harmonics, evaluate their impact, and develop appropriate mitigation strategies.
- Compliance with standards: Adhering to relevant standards and guidelines, such as IEEE 519 and IEC 61000-3-4, ensures that harmonic distortion remains within acceptable limits.

Overall, mitigating the effects of current harmonics is crucial to maintaining the reliability, efficiency, and safety of electrical systems while minimizing the risks associated with harmonic distortion.

2.2.2 Effect of low power factor

A low power factor in an electrical system can have several negative effects, including:

1. Increased energy costs: Utilities often charge penalties or additional fees for low power factor. This is because a low power factor indicates inefficient utilization of the electrical system, requiring the utility to supply more current to meet the actual power demand. As a result, consumers with low power factors may face higher electricity bills due to the increased demand for reactive power.
2. Reduced system efficiency: Low power factor means that a significant portion of the current flowing through the system is reactive power, which does not perform useful work. Reactive power causes increased losses in electrical equipment, such as transformers, motors, and cables, leading to reduced system efficiency. The additional losses result in wastage of energy and can result in increased heat generation, which can further decrease equipment lifespan.
3. Overloading of electrical equipment: A low power factor increases the current drawn from the electrical system to meet the real power demand. The increased current can lead to overloading of electrical equipment, such as transformers, cables, and switchgear. Overloading can cause overheating, voltage drop, and premature failure of equipment.
4. Voltage drop: Low power factor causes an increase in reactive power flow, which leads to an increase in voltage drop across the system. Voltage drop can cause a decrease in the voltage supplied to equipment, affecting its performance and causing malfunctions or inefficiencies. This can be particularly problematic in systems with long transmission or distribution lines.

5. Reduced system capacity: A low power factor decreases the effective capacity of the electrical system. Since reactive power does not contribute to useful work, it limits the amount of real power that can be supplied by the system. This reduction in capacity can result in limitations on the addition of new loads or expansion of the electrical system.

6. Power quality issues: Low power factor can lead to power quality problems such as voltage flicker, voltage unbalance, and harmonics. These issues can affect the performance and lifespan of sensitive electronic equipment and lead to operational disruptions.

To mitigate the negative effects of low power factor, power factor correction techniques can be implemented. Power factor correction involves adding power factor correction capacitors or using power factor correction devices to compensate for the reactive power in the system, thereby improving the power factor and overall system efficiency. Power factor correction helps reduce energy costs, alleviate equipment overloading, improve voltage regulation, and enhance the capacity and performance of electrical systems.

2.3 Harmonic standards.[16]

As per the IEEE 519 - 2014 standard, the measurement of current harmonics is determined by proportion of the current demanded at load to the short circuit current. This ratio can also be defined as the proportion of the load kilovolt-ampere to the short circuit kilovolt-ampere (kVA) at the point of common coupling (PCC).

Table 1: Recommended Limits of voltage distortion and THD Levels.

BUS voltage at PCC	Individual Voltage Distortion	THD%
V< 1kV	5	8
1kV < V < 69kV	3	5
69kV < V < 161kV	1.5	2.5
161kV < V	1	1.5

High-voltage systems may exhibit a total harmonic distortion (THD) of up to 2.0%, which can be attributed to an HVDC terminal. However, the impact of this terminal tends to diminish as it propagates through the network, potentially affecting future users who may be connected.

2.4 Diode Rectifier

A diode rectifier is an electronic circuit that converts alternating current (AC) into direct current (DC). It uses diodes as seen in figure 2.1, which are semiconductor

devices, to allow the flow of current in one direction while blocking it in the opposite direction. During the positive half-cycle of the input AC voltage, diodes D1 and D4 conduct, allowing current to flow through them. Diode D2 and D3 are reverse-biased and block the current. The current flows through the load in the desired direction, creating a positive half-wave rectified output. Negative half-cycle: During the negative half-cycle of the input AC voltage, diodes D2 and D3 conduct, while diodes D1 and D4 are reverse-biased. Again, the current flows through the load in the desired direction, creating a negative half-wave rectified output.

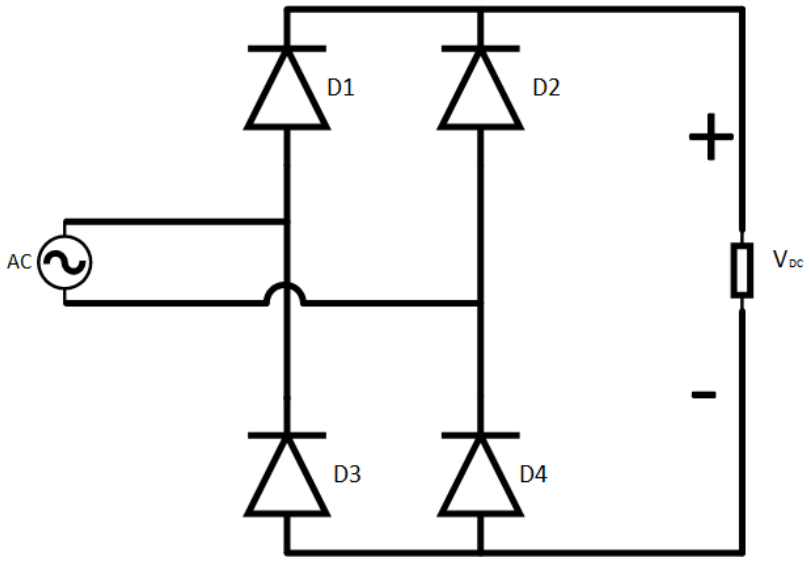

Figure 2.1: Diode Bridge Rectifier (DBR)

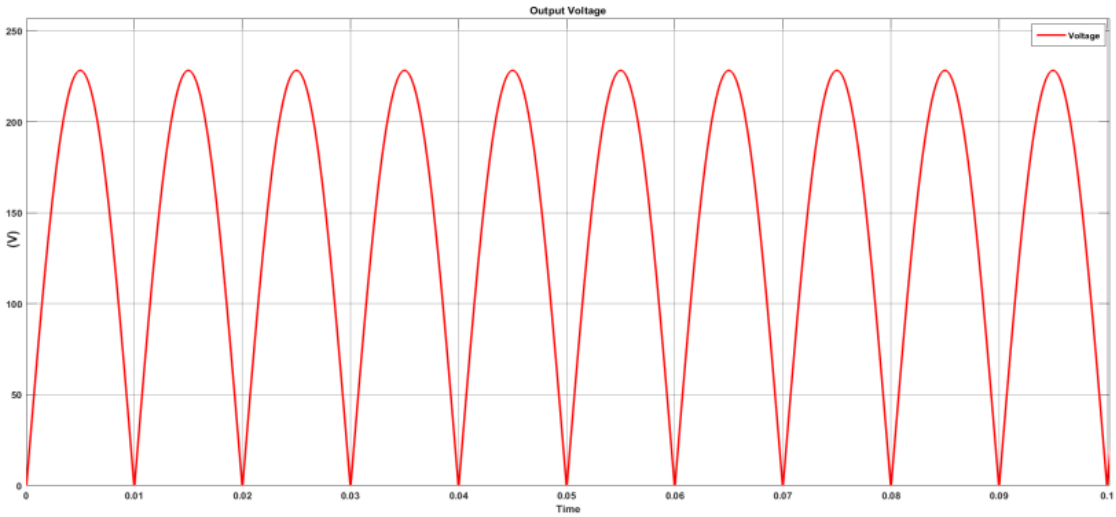

Figure 2.2 Output Voltage of DBR

By referring to Figure 2.2, it is evident that the output of the rectifier or voltage of load (V_{DC}) takes form of a sinusoidal waveform. However, the V_{DC} exhibits significant

ripple, which are need be cut down to none. In many scenarios, this V_{DC} serves as the input to a DC-DC converter, which requires a DC voltage input with an acceptable level of ripple. In order to minimize the ripple in this output, different filters can be implemented.

2.4.1 Diode Rectifier with C filters.

To reduce these voltage fluctuations at the output and optimize the average of output, filters are incorporated into the basic DBR circuit. One commonly used and fundamental filter is the capacitive filter. Typically, the value of filter capacitor is determined depending on the permissible level of ripple allowed in the output voltage.

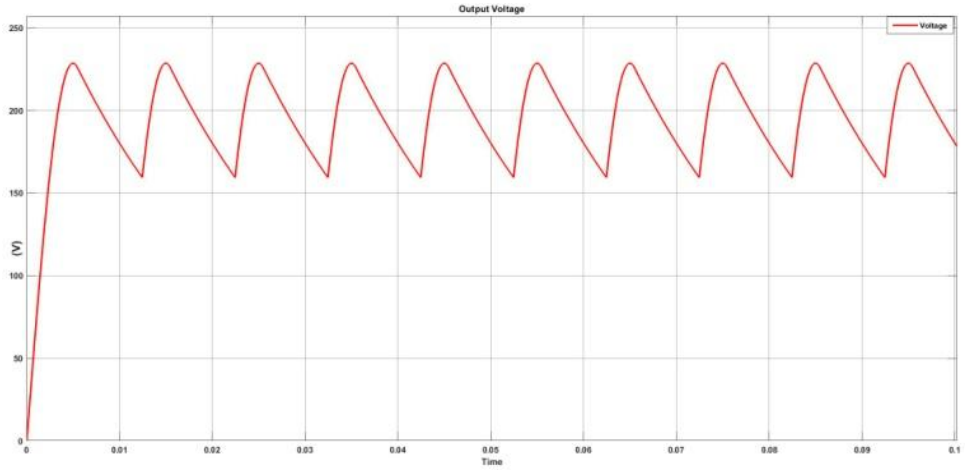

(a)

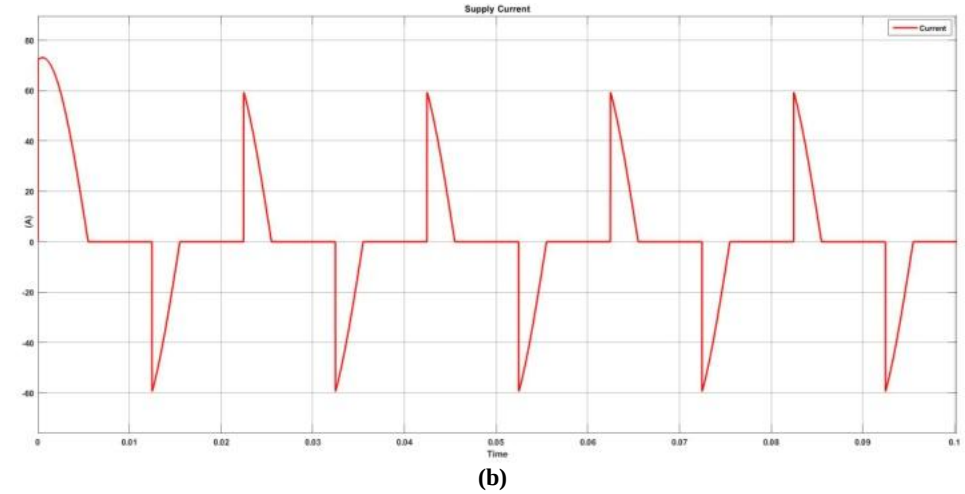

(b)

Figure 2.3: (a) Output Voltage of DBR with C (200µF), (b) Supply Current with C (200µF)

As shown in Figure 2.3(a), the voltage exhibits a peak-to-peak ripple of 60 V. To further reduce the ripple, the value of the filter capacitor can be increased. However, it

is important to note that the current supplied is not sinusoidal and carry harmonics in it, seen in Figure 2.3(b) and as evident from the Fast Fourier Transform (FFT) analysis of the supply current shown in Figure 2.4.

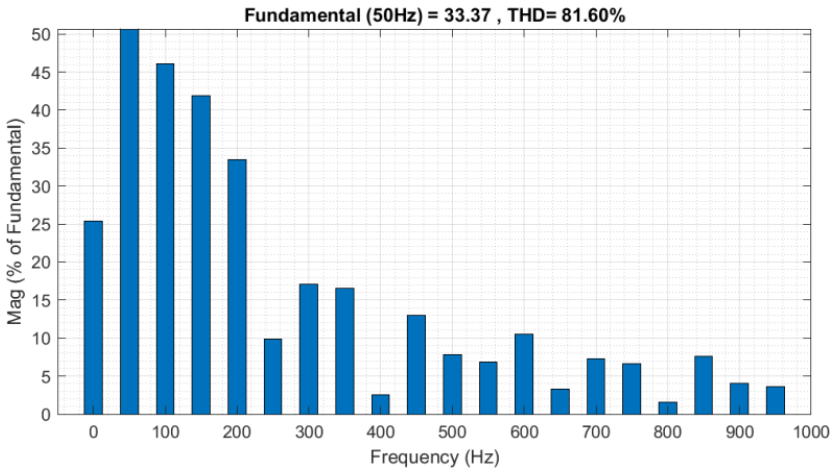

Figure 2.4: FFT analysis of the input current (Vs = 230V RMS and C=200uF)

The input current is characterized by its disrupt nature, meaning that the one leg of diodes do not conduct for half cycle of the supply. With the increase in the capacitance, diodes conduction period decreases, resulting in an increase in the peak of the input current and an increase in the total harmonic distortion (THD). The underlying reason for this momentary current behavior will be explained in the following section.

Figure 2.3(b) illustrates the waveforms of the V_C in steady state and current at input. When the voltage at input is lower than the capacitor voltage, the diodes are in a reverse-biased state, resulting in no current flow into the converter. During this time, capacitor supplies the load.

On the other hand, when the supply exceeds the voltage across capacitor, the diodes become forward biased, and the capacitor acts as a load and draws current from the supply.

If the capacitance tends toward a very large value, the input current becomes an impulse current only. The power factor of the converter in this case is 0.657, and the total harmonic distortion (THD) is 144.5%, which exceeds the relevant standards.

2.4.2 Diode Rectifier with LC filters.

When an inductor filter is used, the rectifier can operates between two modes: Continuous Conduction Mode and Discontinuous Conduction Mode. In CCM, the inductor is kept at larger value than the capacitor, which prevents sudden changes in current. As a result, the inductor current remains constant, and at least two diodes

conduct to supply the constant inductor current. The input current is in phase with the input voltage, resulting in a unity displacement factor. However, the shape of the current is not sinusoidal, introducing Total Harmonic Distortion.

In DCM, the value of inductance is smaller as to capacitance. This leads to an increase in the width of the input current due to the presence of the inductor. The inductor helps in smoothing out the current waveform.

Multiple branches can be interconnected to form a LC filter, and a harmonic filter can be incorporated on the input side with a series RLC branch. By adding an inductor at the output DBR, both Total Harmonic Distortion (THD) and hence Power Factor (PF) is improved. The outcomes of FFT analysis is shown in Figure 2.6

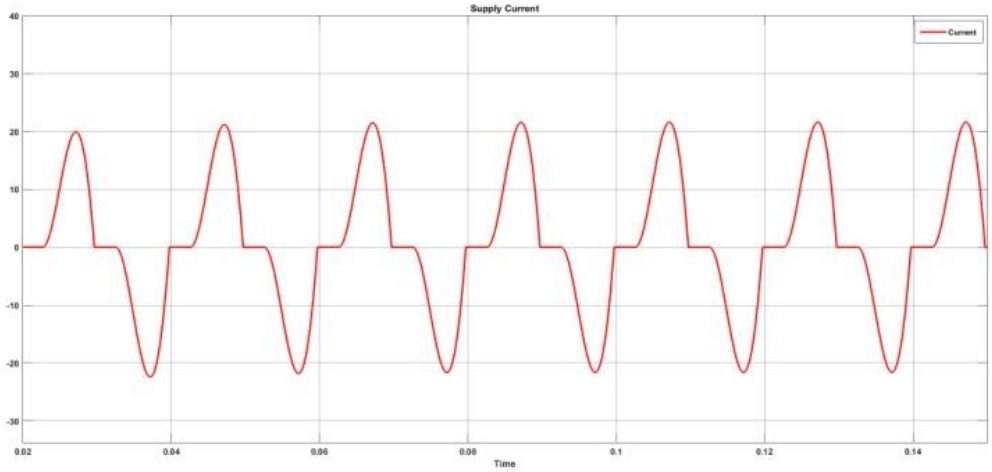

(a)

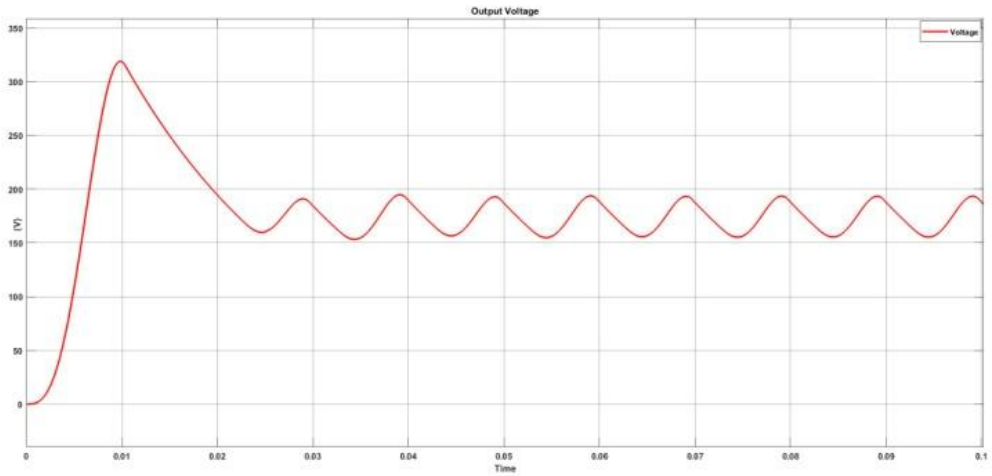

(b)

Figure 2.5: Waveform of (a) Supple Current, (b) output Voltage of DBR with LC filter at output. (Vs=240V RMS, L=10mH, C=200 μF)

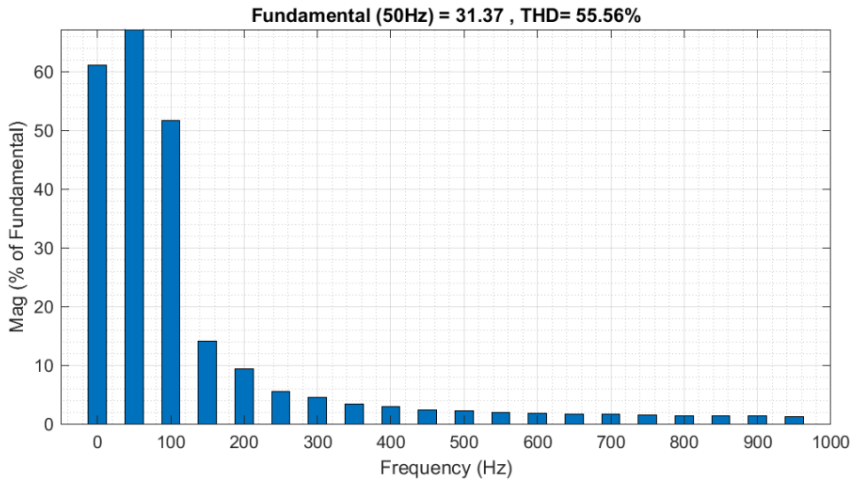

Figure 2.6: FFT analysis of input current with LC filter

By incorporating a filter inductance, the Total Harmonic Distortion (THD) value is reduced from 81% to 55%. Increasing the value of the inductance further decreases the THD; however, it also leads to a decrease in the output. For maintaining the needed output, an additional DC to DC converter working in boost mode is required. The (THD) performance is enhanced when a harmonic trap filter is implemented on the input side. Figure 2.7 displays the relationship between the inductance value and THD. It should be noted that even with an infinite inductance, the power factor (pf) cannot exceed 0.9 [17].

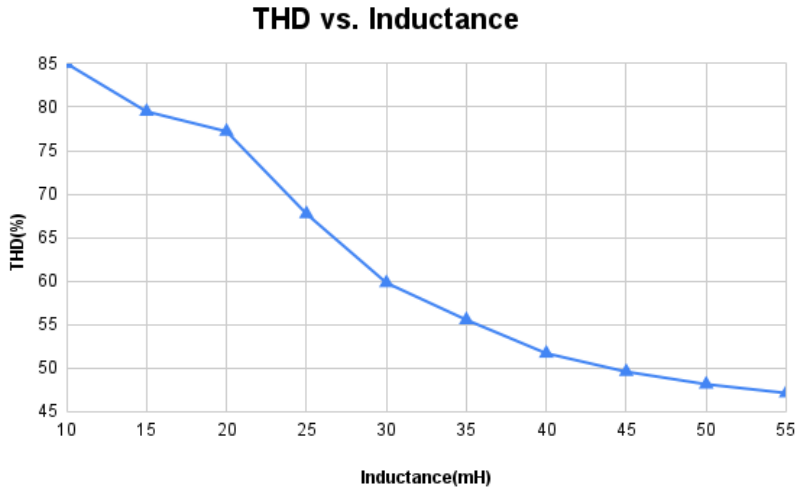

Figure 2.7: Relation THD (%) with inductance value (mH) of the system.

Passive filters have limitations in improving the power factor, typically achieving a maximum of 0.75, and they are primarily suitable for low power applications. These filters are associated with drawbacks such as large size, high Total Harmonic Distortion

(THD), low power factor (pf), and the potential for unwanted resonance. Consequently, at higher power levels, active techniques are preferred and implemented to overcome these disadvantages.

2.5 Active PFC Converter [16-19]

Active power factor correction (APFC) is a technique used to improve the power factor of an electrical system by actively controlling the input current waveform. It involves the use of active electronic components, such as power factor correction (PFC) controllers and power switches, to shape the current drawn from the AC power source.

The primary goal of APFC is to minimize reactive power and bring the power factor closer to unity (1.0). By reducing the reactive power component, APFC helps to optimize power utilization, improve system efficiency, and mitigate the negative effects of low power factor.

The block diagram shown in Figure 1.2 illustrates a fundamental AC-DC converter with power factor correction. In the context of an On-Board EV charger, the DBR is only suitable for power to flow in one direction (unidirectional), specifically for charging the battery of vehicle. However, in order to facilitate bidirectional power flow in both Grid-to-Vehicle (G2V) and Vehicle-to-Grid (V2G) modes, the diode is substituted with IGBT or MOSFET components. This modification allows the rectifier to function as an inverter during V2G operation, enabling power flow from the Vehicle back to the Grid.

The DC-DC converter used in the system can take the form of a step down, up, or Buck-Boost converter, depending on the requirement. A step down (A.K.A Buck converter) generates an output that is lower than the input, while a step up(A.K.A Boost converter) produces a output higher than the input. In the case of a Buck-Boost converter, the output voltage can be either higher or lower than the supply voltage. However, it is important to note that the voltage stress on components in a Buck-Boost converter gets double compared to other two, making it less efficient.

The DC to DC conversion can also be done by an isolated converter, which provides galvanic isolation between the supply and Vehicle. The operation of these converters in Continuous Conduction Mode or Discontinuous Conduction Mode determine by continuity or discontinuity of current across inductor. In discontinuous mode, the current reaches zero within each switching cycle, while in a continuous, the current

never touches zero and exhibits less ripple. It is worth noting that only in the case of a Boost converter, the input current is continuous, whereas in Buck and Boost converters, it is discontinuous due to the switch interruption in each switching cycle.

Table shows different PFC topologies along with the efficient power rating.

Table 2: Power levels of different PFC topologies

PFC Topologies	Power Level
Boost PFC	<3.6kW
Interleaved Boost PFC	2-3.6kW
Semi-Bridgeless PFC	7kW
Totem Pole PFC	<10kW
Vienna PFC (3-Phase unit)	>10kW

2.6 Boost PFC Converter[16]

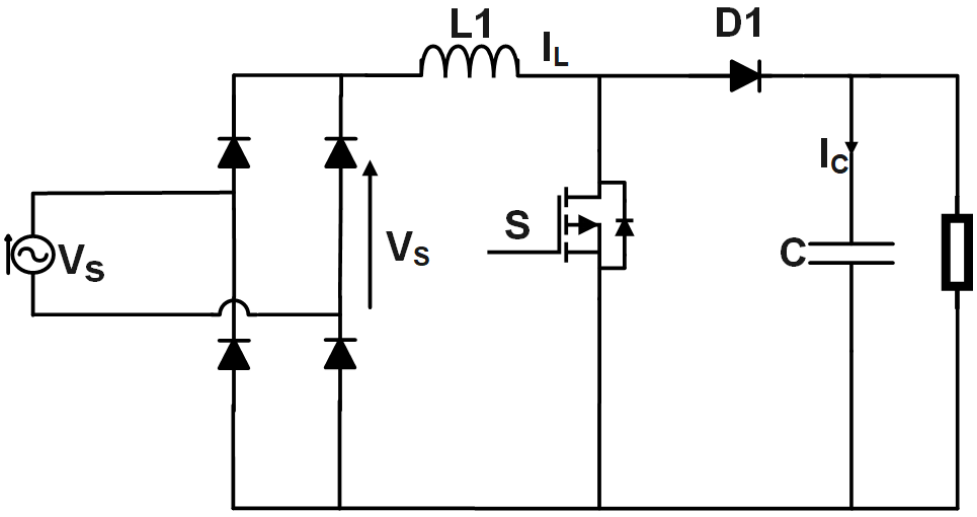

Figure 2.8 Circuit Diagram of a Boost PFC Converter

The Figure 2.8 shows a conventional circuital diagram of a PFC converter in boost mode. The initial step involves rectifying the input supply voltage using a diode bridge rectifier. Subsequently, a Boost converter is introduced to modify the current waveform, ensuring it resembles a sinusoidal shape.

2.6.1 Different modes of operation

Boost converter operation can be categorized into three different types based on the waveform of the inductor current. These types are Continuous Conduction Mode, Discontinuous Conduction Mode, and Critical Conduction Mode or Boundary Conduction Mode.

In Continuous Conduction Mode , the current across the inductor remains non-zero throughout the switching cycle. As indicated by working study of boost pfc, current first increases during the ON time and then drops during the OFF time. However,

during the OFF time, there is a possibility of transitioning to Discontinuous Conduction Mode (DCM) if the inductor current reaches zero. CCM offers advantages such as higher converter efficiency. However, it requires a independent current controller to shape the input current and ensure that it follows the input voltage.

In Discontinuous Conduction Mode (DCM), the inductor current reaches zero during each OFF interval of the switching cycle. This mode of operation results in higher voltage and current stress on the power devices. However, DCM offers the advantage of naturally shaping the input current without the need for a separate current controller.

In BCM, the inductor current is on boundary of continuous and discontinuous.

2.7 Interleaved Boost PFC [17]

In an interleaved Boost PFC configuration, two or more identical boost converter stages are connected in parallel, diagram shown in Figure 2.9. Each stage operates with a phase shift in switching, achieved by employing a phase delay or phase-shifted control. The key idea is to distribute the load current equally among the phases, allowing for reduced current stress on individual components and improved overall system efficiency.

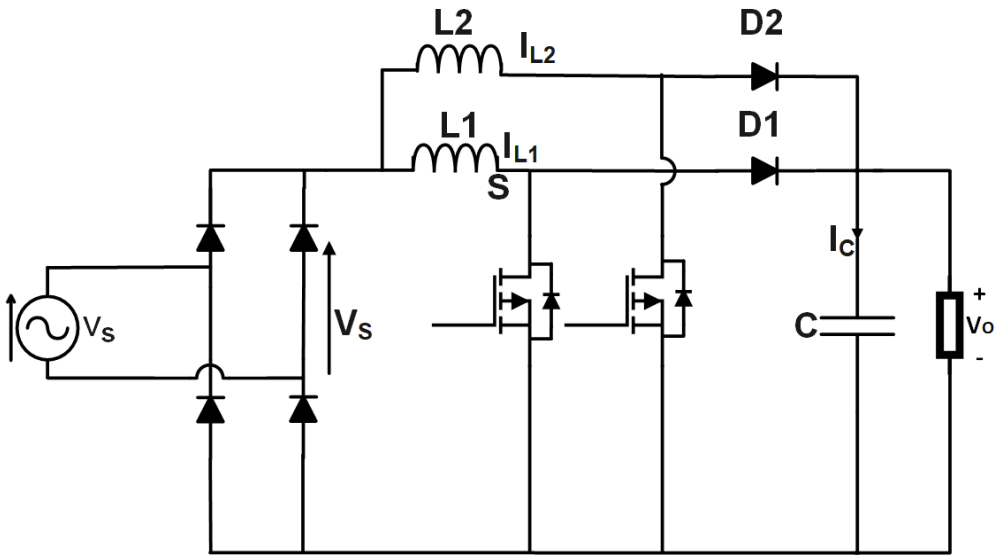

Figure 2.9: Circuit Diagram of a two leg interleaved Boost PFC Converter

2.8 Semi-Bridgeless and Bridgeless PFC Converter [18]

In a semi-bridgeless PFC converter Figure 2.10(a), instead of using a full bridge rectifier and full bridge boost converter, it utilizes a combination of a diode bridge rectifier and a single active switch (usually a MOSFET) in the boost converter stage.

This configuration reduces the switching losses and conduction losses associated with the active switches, leading to improved efficiency.

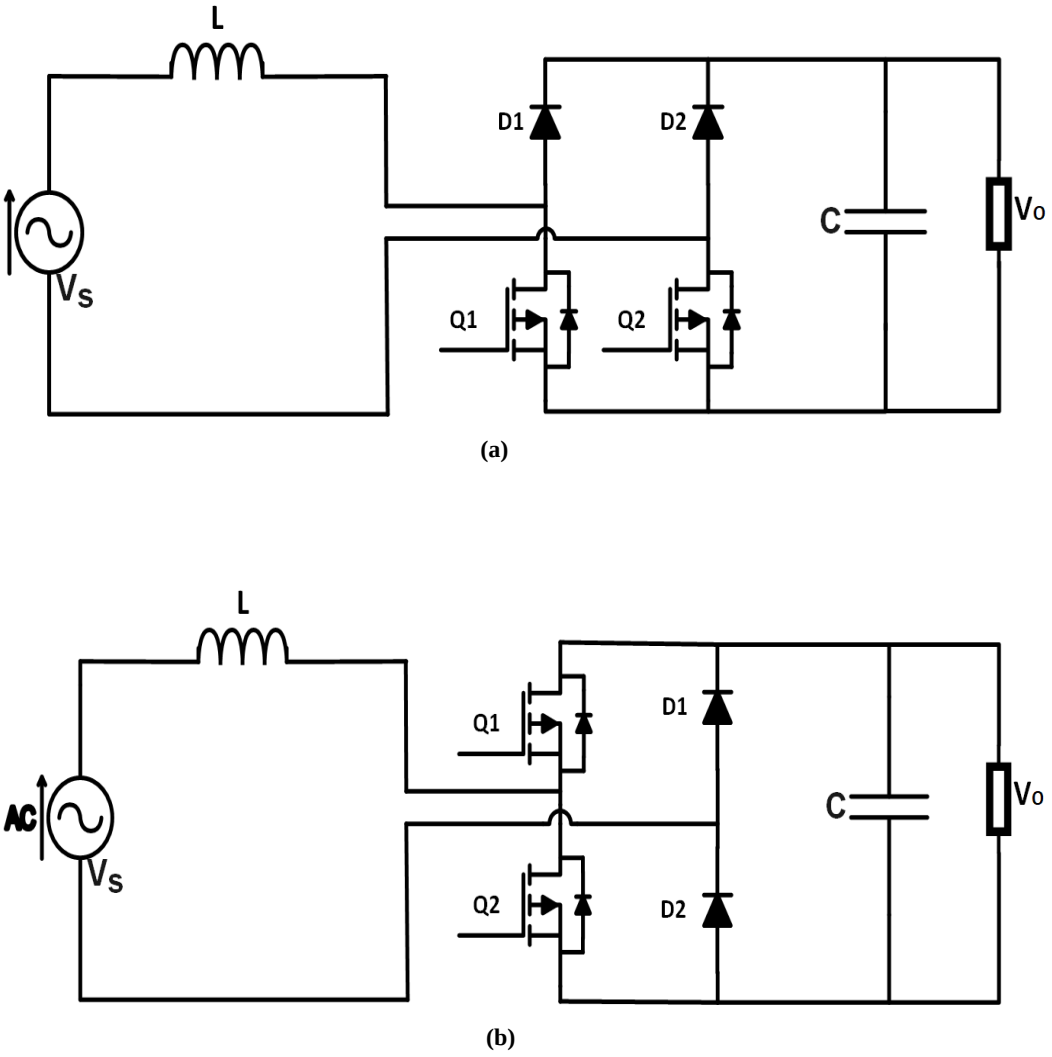

Figure 2.10: Circuit Diagram shown of (a) Semi-Bridgeless, (b) Bridgeless totem pole PFC Converter

Bridgeless PFC converters aim to improve the power factor and efficiency of the PFC circuit by eliminating the need for a diode bridge rectifier, circuit diagram of it is shown in Figure 2.10(b).

In summary, the main difference between semi-bridgeless and bridgeless PFC converters lies in the rectification approach. The semi-bridgeless configuration uses a diode bridge rectifier, while the bridgeless configuration directly connects the AC input to the boost converter. Both topologies aim to improve power factor and efficiency, but the choice between them depends on factors such as design requirements, cost considerations, and desired performance characteristics for a specific application.

2.9 Vienna PFC Converter.[18]

Shown in Figure 2.11, Vienna PFC converter is based on the concept of a boost converter and utilizes two active switches (usually MOSFETs) and two diodes. It consists of an inductor, a capacitor, and a control circuit. The converter operates by shaping the input current waveform to be in-phase with the input voltage waveform, thus minimizing the reactive power drawn from the power source.

The key advantage of the Vienna PFC converter is that it achieves power factor correction with a single-stage conversion, unlike other PFC solutions that require a two-stage conversion process. This leads to a more compact and efficient power supply design.

The control circuit of the Vienna PFC converter uses a feedback loop to regulate the output voltage and maintain a high power factor. It dynamically adjusts the duty cycle of the active switches based on the input voltage and load conditions. The control algorithm ensures that the input current waveform follows the shape of the input voltage waveform, reducing harmonic distortion and achieving a power factor close to unity.

The Vienna PFC converter is commonly used in various applications, including power supplies for computers, LED lighting systems, motor drives, and other electronic devices where power factor correction is required to comply with energy efficiency standards and regulations. The Vienna PFC converter's control circuit continuously

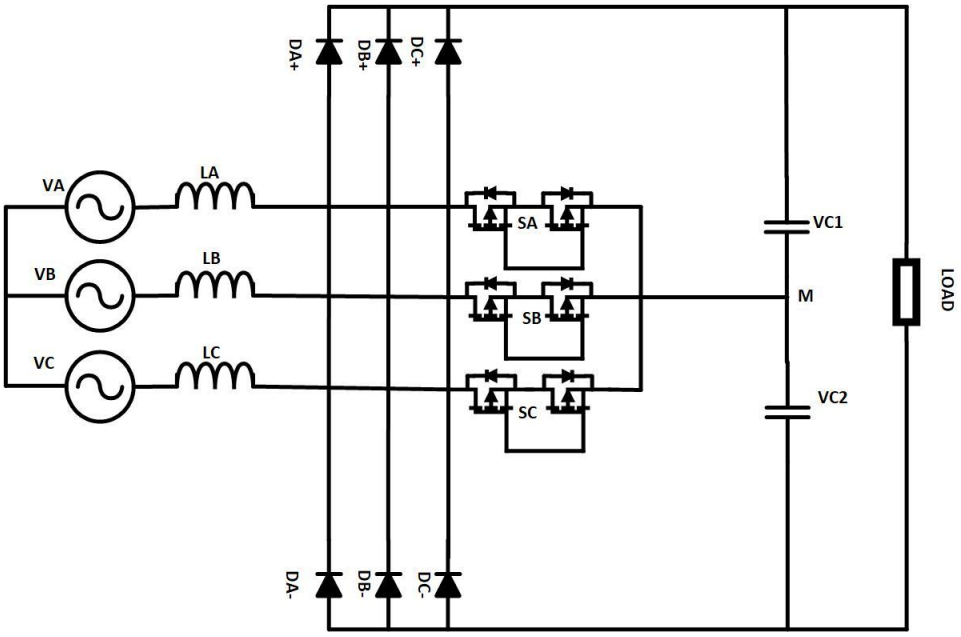

Figure 2.11: Circuit Diagram of 3-phase Vienna PFC Converter

regulates the duty cycle of the active switches to maintain the desired output voltage and achieve power factor correction. This efficient operation not only reduces reactive power but also enables compliance with energy efficiency standards and regulations. It's worth noting that the field of power electronics is constantly evolving, and new converter topologies and control techniques may emerge over time. Therefore, it's always a good idea to refer to the latest research and literature for the most up-to-date information on specific power converter technologies

2.10 Controller Design [19-21]

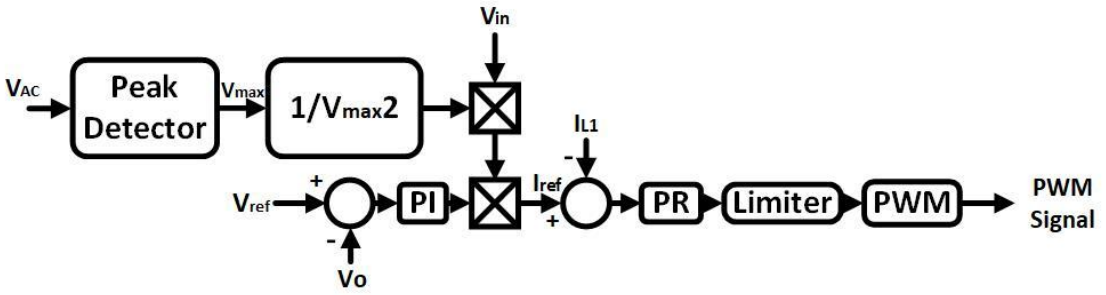

Figure 2.12 Block Diagram of a conventional PFC Controller

The PFC controller aims to correct this power factor by manipulating the input current waveform. It actively controls the power flow to the load, ensuring that the current follows the voltage waveform as closely as possible. This is typically achieved by employing control techniques, such as pulse-width modulation (PWM) or resonant converters, to shape the input current.

Devices are controlled by a controller in a close loop maintaining needed voltage current. This is typically achieved by employing control techniques, such as pulse-width modulation (PWM) or resonant converters, which continuously monitors the input voltage and current and adjusts the switching frequency or duty cycle based on the feedback received, to shape the input current.

Figure 2.12 illustrates the controller integrated with the PFC converter. The controller comprises two loops: an outer voltage loop responsible for regulating the desired voltage at the output terminals, and an inner current loop that controls the characteristics of the input current, allowing it to align with the shape of the input voltage.

The inner current loop operates at a significantly faster rate compared to the outer voltage loop. Typically, the bandwidth of the current loop ranges from one-fifth to one-

tenth of the switching frequency, while the voltage loop bandwidth is approximately one-tenth of the current loop bandwidth or one-fifth of the supply frequency.

The voltage loop compares the required output with the actual output and generates an voltage signal based on the resulting difference or error. This reference signal is then multiplied by a sinusoidal waveform to generate a current. The reference current is compared to the actual rectified current and fed into the current controller. The current controller adjusts its output to track the reference current. The amplitude of the reference current is determined by the output of the voltage controller.

The voltage error amplifier output is multiplied by the sensed DC output voltage of the diode bridge rectifier, V_C, which represents a rectified sinusoidal waveform. This multiplication generates a sinusoidal reference current, ref I. The reference current is then compared with the actual inductor current. Based on the error between the reference and actual current, the current controller generates a control signal. This control signal is compared with a saw tooth wave to generate the gate pulse for the switch BS. The frequency of the saw tooth carrier wave matches the predetermined f_{sw} of the converter.

2.10.1 Current Control Loop

The primary function of the current controller is to generate a control signal that adjusts the switching frequency or duty cycle of the PFC converter. By manipulating the switching operation, the controller regulates the input current to maintain a desired reference current waveform.

The current controller typically operates in a closed-loop feedback system. It monitors the actual input current through current sensing techniques, such as current transformers or shunt resistors. The sensed current is compared to a reference value, and any deviation triggers the control action to adjust the switching frequency or duty cycle.

There are different control techniques and algorithms used in current controllers for PFC systems. Some common approaches include:

1. Average Current Mode Control: This control technique measures the average value of the input current and compares it with a reference value. The controller adjusts the duty cycle of the converter to keep the average current in line with the reference.

2. Peak Current Mode Control: In this approach, the controller detects the peak value of the input current and uses it to regulate the duty cycle. By controlling the peak current, the controller achieves accurate current shaping and improved transient response.

Hysteresis Current Control: This technique sets upper and lower thresholds for the input current. If the current exceeds the upper threshold, the controller reduces the duty cycle, and if it falls below the lower threshold, the duty cycle is increased. This creates a hysteresis loop that keeps the current within a desired range.

2.10.2 Voltage Control Loop

The primary function of the voltage controller is to generate a control signal that adjusts the operation of the PFC converter to maintain the desired output voltage. It monitors the output voltage and compares it to a reference value, and based on the difference between the two, it generates a control signal to regulate the PFC converter.

The voltage controller typically operates in a closed-loop feedback system. It continuously monitors the output voltage through voltage sensing techniques, such as voltage dividers or voltage sensors. The sensed voltage is compared to a reference value, and any deviation triggers the control action to adjust the PFC converter's operation. The voltage controller plays a critical role in ensuring stable and regulated output voltage in a PFC system. It allows for effective power factor correction while maintaining the desired voltage level, contributing to improved power quality and efficient operation of the load.

There are different control techniques and algorithms used in voltage controllers for PFC systems. Some common approaches include:

1. Voltage-Mode Control: This control technique compares the output voltage to a reference voltage and generates a control signal based on the difference. The control signal is used to adjust the duty cycle or switching frequency of the PFC converter, ensuring that the output voltage remains close to the reference.

2. Peak Current Mode Control with Voltage Feed forward: This technique combines voltage control with current control. The controller detects the peak value of the input current and uses it to regulate the duty cycle, while also considering the output voltage. By incorporating voltage feed forward, the controller compensates for changes in the output voltage, resulting in improved dynamic response.

3. Average Current Mode Control with Voltage Compensation: This approach combines current control with voltage compensation. The controller measures

the average value of the input current and compares it to a reference, adjusting the duty cycle accordingly. Additionally, it incorporates voltage compensation to account for variations in the output voltage, ensuring stable and accurate control.

2.11 Simulation and Results

The different PFC converters described above working in CCM are simulated here using MATLAB/Simulink at full load condition and simulated results are shown below.

2.11.1 Boost PFC Converter

It can be seen from the Figure 2.13 that the output voltage is kept constant at 400V with the ripple of 10Vp-p and at figure 2.14 shows that the supply current is in phase and follows the voltage waveform in synchronous manner. The input current has been enlarged 5 times to its original value for better understanding purposes.

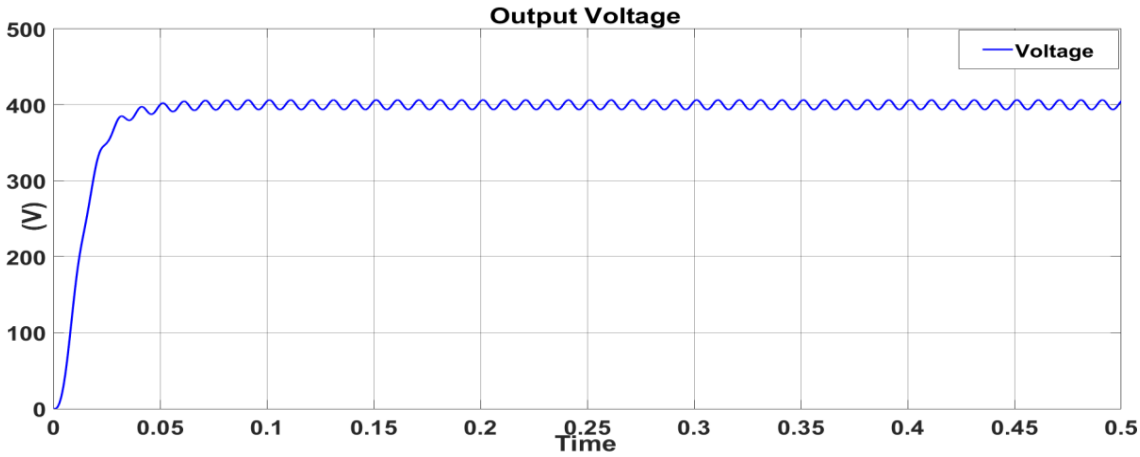

Figure 2.13: Waveform of output voltage

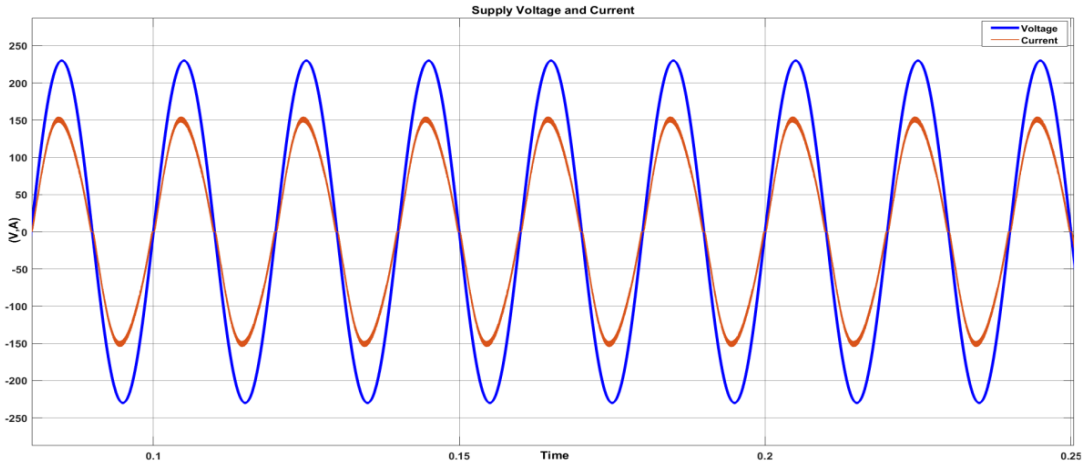

Figure 2.14: Sinusoidal Waveform of input voltage and current.

In the FFT analysis of input current the % of THD is found out to be 5.64% and the same is shown in the Figure 2.15. and using the equation 2.7 the pf is calculated to be 0.998.

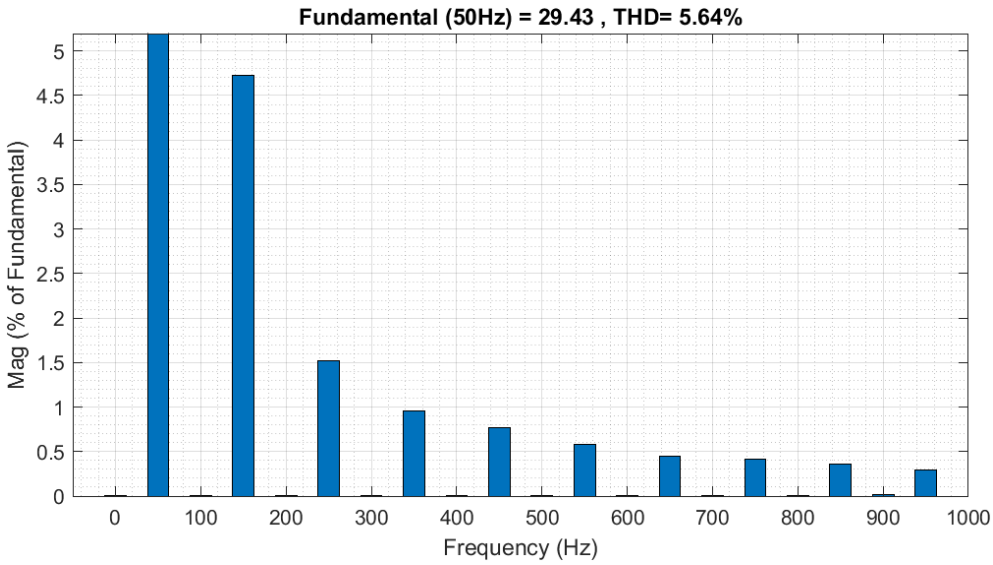

Figure 2.15: FFT analysis of input current

Inductor Current can be seen in Figure. 2.16 showing that the designed converter is indeed working in CCM mode as were indented for desired operation.

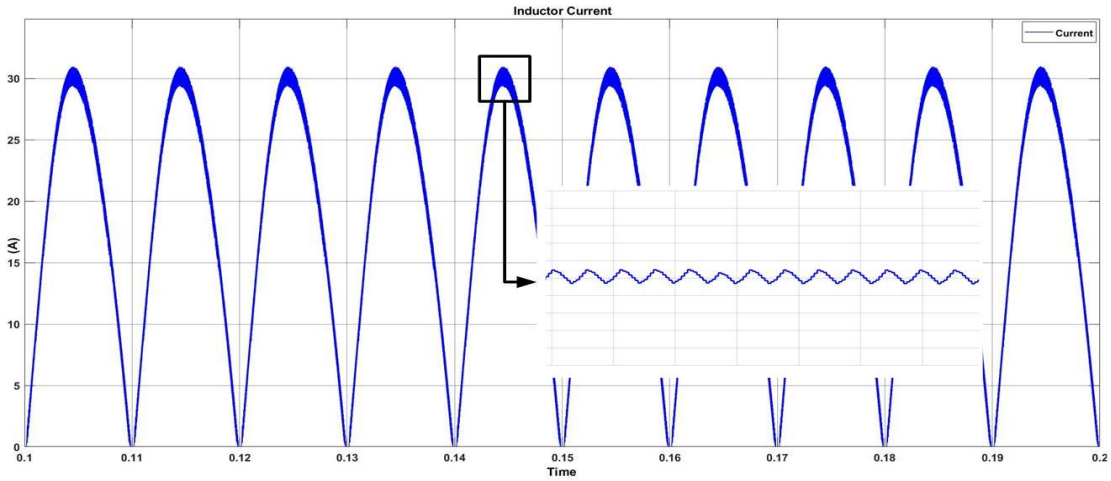

Figure 2.16: Waveform of inductor current

Figure 2.17 shows the input and output current waveforms under varying load of 3200W to 1600W. Upon the change in the load to half load from full, the value of output current is drops proportionally to half as well. The output voltage settles back to desired value of 400V after few cycles in 150ms.

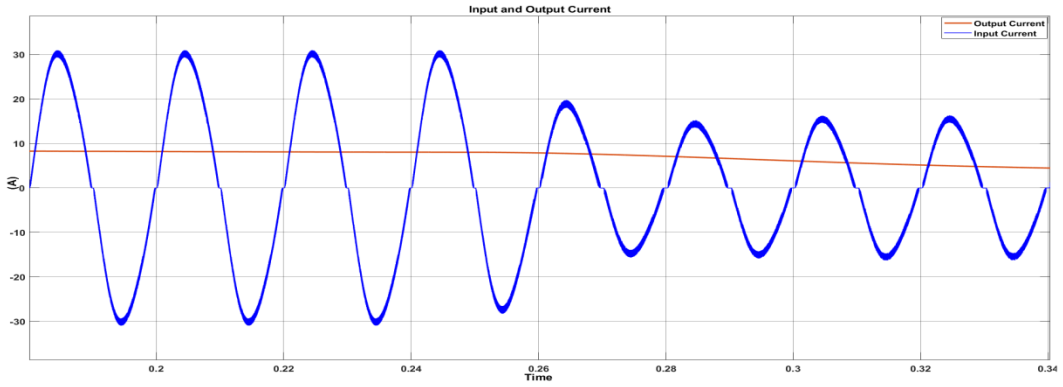

Figure 2.17: Input and output current waveform under varying load condition.

2.11.2 Interleaved Boost PFC Converter

Figure.2.18 shows different results of the interleaved PFC converter running at on a full load (i.e 3200W), (a) gives the waveform of input current and voltage running in phase, input current has been enlarged 5 times for the better study and understanding, (b) shows the voltage from the output of DBR, (c) gives the value of value of inductor current (iL1 and iL2), (d) shows the value of output voltage of the PFC converter. The output was settled at its correct value after 550ms.

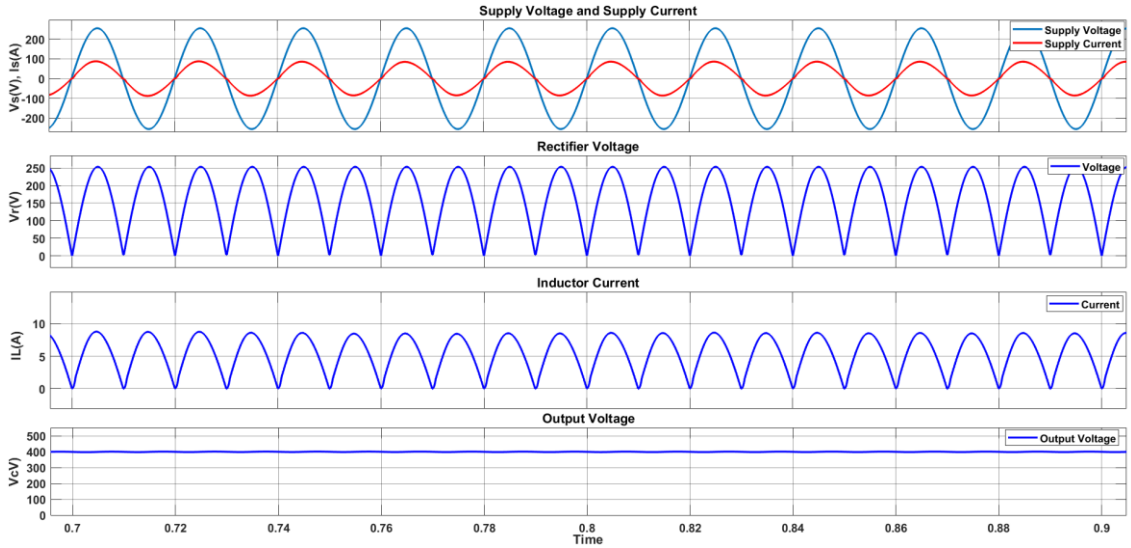

Figure 2.18: Waveforms of (a) supply voltage and current, (b) DBR output, (c) Inductor Current, (d) output voltage

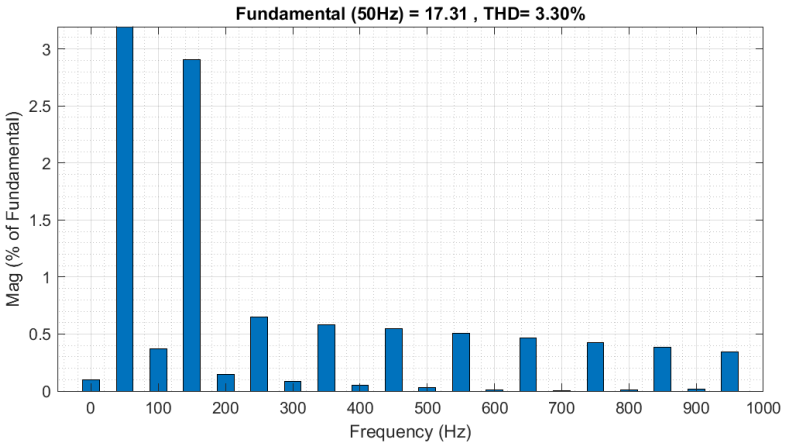

Figure 2.19: FFT Analysis of the supply current.

Figure.2.19 gives the THD % of the system after FFt analysis of the input current which turn outs to be 3.30%

Figure 2.20 shows the dynamic behavior of the system with variation in input supply. (a) Shows the increment of input voltage. (b) Shows the change in rectified voltage of DBR with change in supply. (c) gives the dynamic behavior of the inductor current (iL1 and iL2) with variation in the supply. (d) Shows the output voltage of the system running almost at constant voltage even with variation in supply voltage.

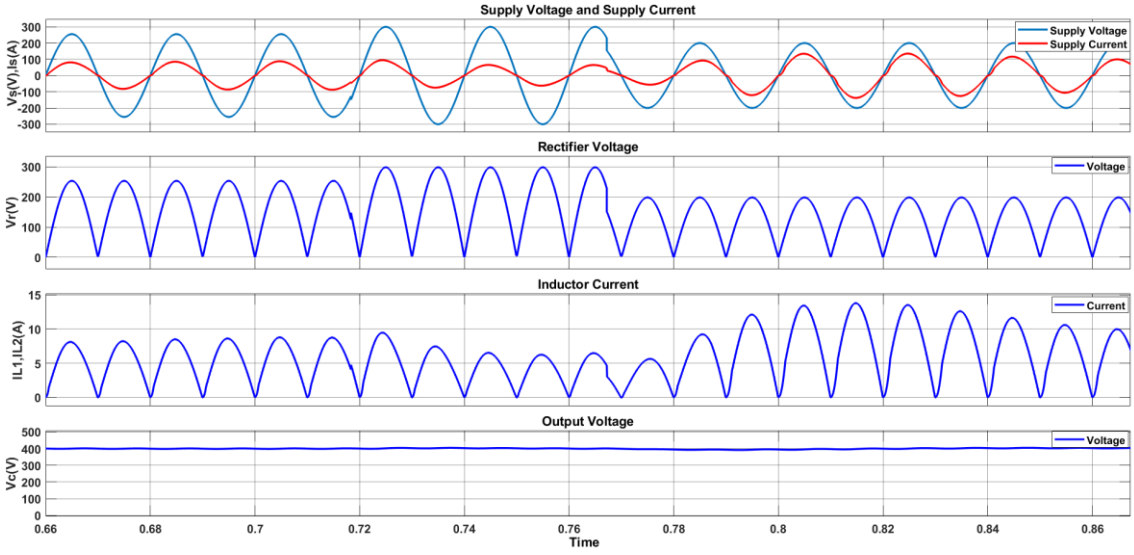

Figure 2.20: Dynamic behavior of the Interleaved Boost Converter under load vitiation from full to half load.

2.11.3 Semi-bridgeless PFC Converter.

Figure 2.21 shows the waveform of the supply voltage and current running in phase followed by Figure 2.22 giving the output voltage of the converter and Figure 2.23 giving the FFT analysis of the supply current which gives the THD% value of 4.53%.

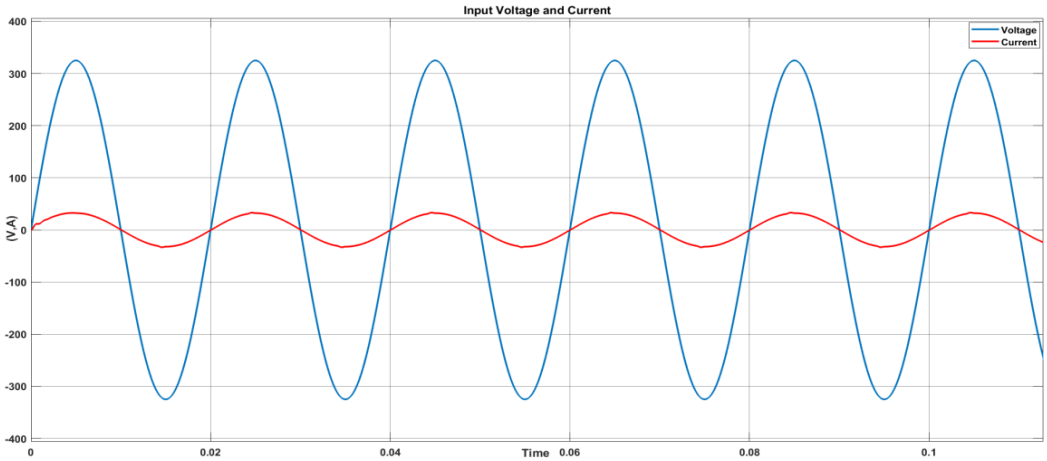

Figure 2.21: Supply voltage and current of semi-bridgeless PFC Converter

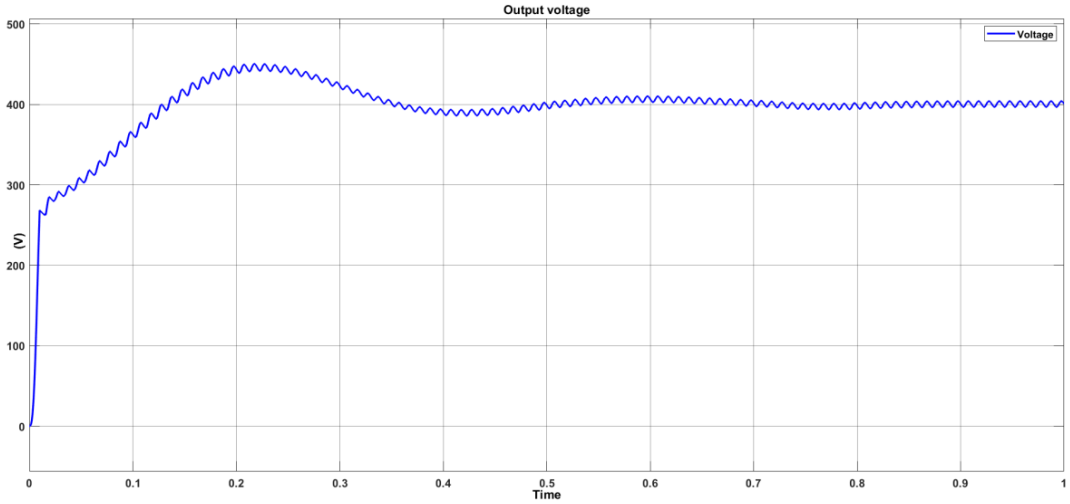

Figure 2.22: Output voltage waveform of the converter settling at 400V.

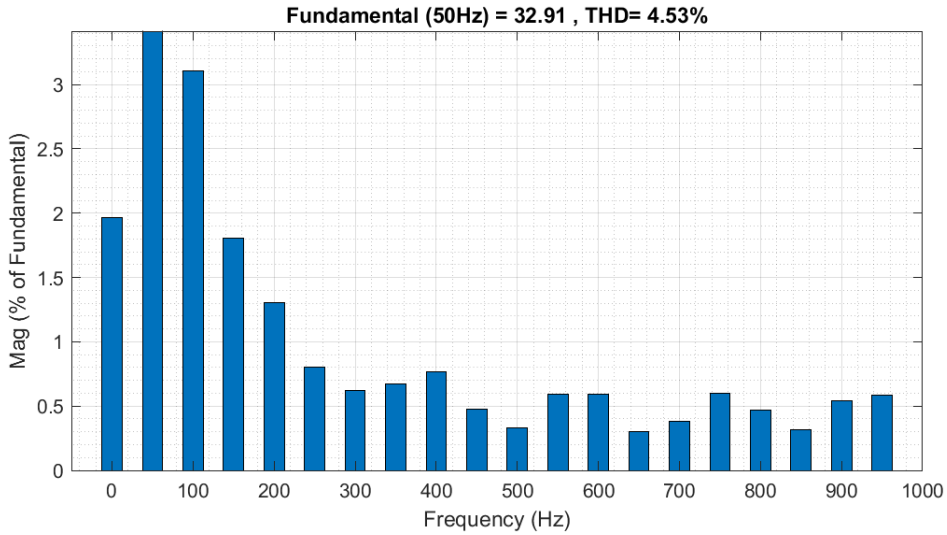

Figure 2.23: FFT analysis of the supply current.

2.11.4 Bridgeless PFC Converter.

Figure 2.24 shows the input current in phase with the input voltage and Figure 2.25 shows the output voltage of the converter, it can be observed that the overshoot for the bridgeless converter is least compared to other PFC converters.

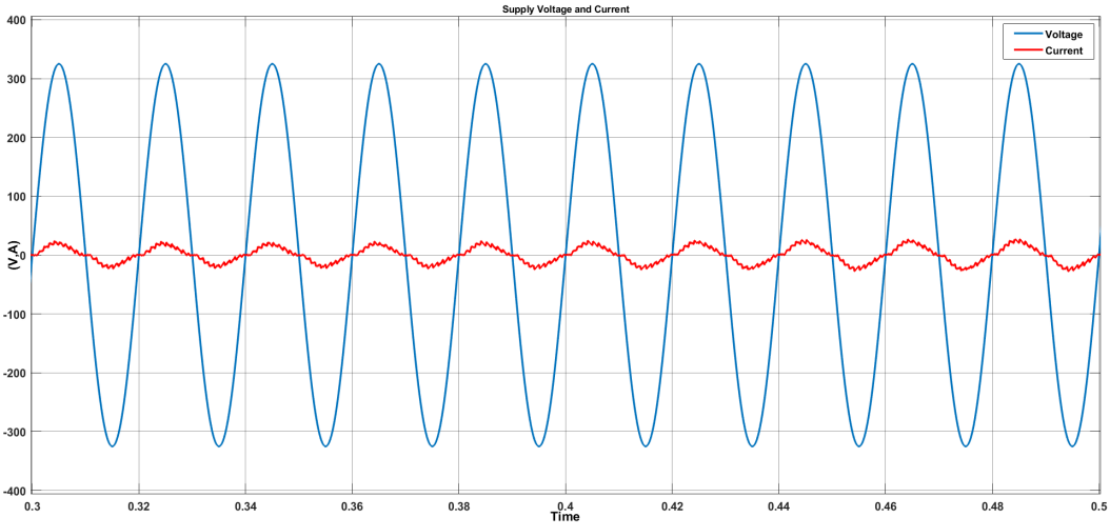

Figure 2.24: Waveform of Supply Voltage and Supply Current running in phase.

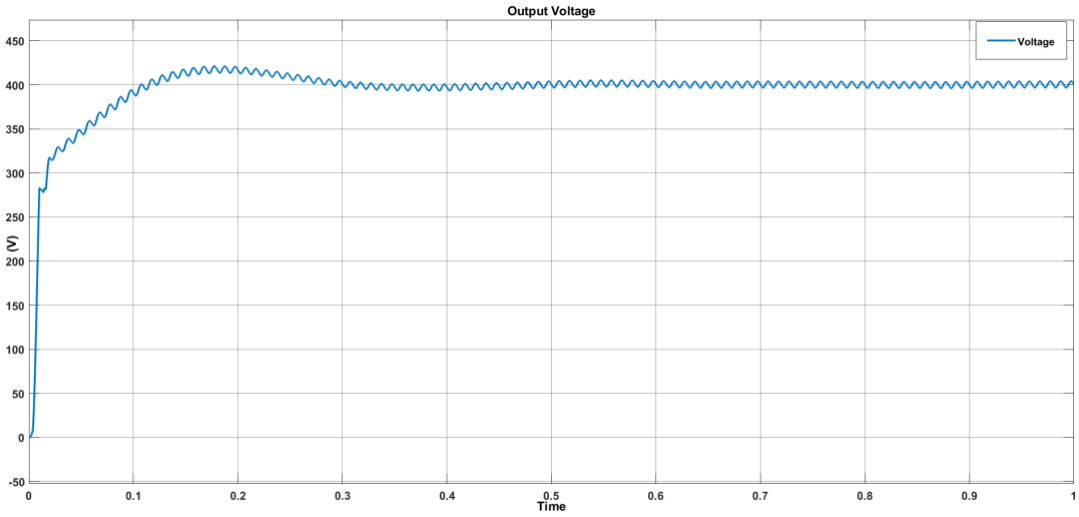

Figure 2.25: Output Voltage Waveform settling at 400V.

2.12 Conclusion

In this chapter, the fundamental concepts and mathematical models of pf and THD are presented. The limitations of DBR are highlighted, and the issue of THD is addressed through the use of active power factor correction (PFC) converters. Various topologies of active PFC converters are discussed, and their performance is evaluated through simulations and experiments. Under full load conditions, the input current is found to be sinusoidal with minimal harmonic content. However, variations in output power or input voltage can affect the THD and power factor. In the case of an onboard charger (OBC), the PFC converter is followed by a DC-DC converter that requires variable power depending on the battery's state of charge. Additionally, practical scenarios may involve fluctuations in the grid supply. Therefore, the dynamic behavior of the converters is studied by varying both the load demand and the grid supply. The output power of the DC-DC converter is varied from half load to full load, while the supply voltage is adjusted to 10% of its nominal value. It is observed that the designed PFC models maintain a constant output and keep the THD within the desired level under all variation.

CHAPTER 3

Grid Synchronization

3.1. Introduction

Grid synchronization is a crucial aspect to consider in the design of any on-board/off-board EV chargers, as these chargers are designed for use in residential settings with Power supplied in AC. Grid synchronization involves obtaining the real-time components voltage vector from the grid, which is necessary for effectively connecting the converting device to the grid facility. These parameters encompass the magnitude, phase angle, and frequency of the fundamental waveform for standard power converters. Additionally, in different applications, it is essential to detect and analyze any harmonic components present in the grid voltage. By achieving grid synchronization, the charger can ensure efficient and reliable interaction with the utility grid [30].

To ensure the efficiency of these power converters, the synchronization method employed must be capable of adapting to the various transients and abnormal conditions that can occur in the utility grid. These transients can arise from fluctuations in load, faults, and third party error. It is essential for the synchronization method to swiftly respond and adjust to these transients, minimizing any disruptions and enabling the power converter to operate optimally. By quickly adapting to changes in the grid, the synchronization method ensures the overall efficiency of the power conversion process.

There are two main categories of grid synchronization techniques: those based on the frequency domain and those based on the time domain. Frequency domain methods utilize adaptive band-pass filters in conjunction with a form of DFT to extract the phase and magnitude information from the grid voltage signal. However, DFT based methods can experience errors in phase angle and magnitude when the grid frequency deviates from its nominal value. This occurs because the number of samples within one cycle of the input signal may not be an exact multiple of the sample window. Nonetheless, there have been proposed methods to address and mitigate this issue, as discussed in references [36, 37].

One of the simplest time domain-based grid synchronization methods involves zero crossing detection iof the grid voltage. This method utilizes a comparator, a timer (and integrator), to detect each transition of the input signal's half cycle and compute the

frequency and its phase information. While this method is straightforward to implement, it is sensitive to the quality of the input signal, and distortion signal can lead to detection errors. Proposed methods to address these issues include adaptive compensation techniques described in [38] and the use of dynamic hysteresis or interpolation as presented in [39].

Other time domain-based synchronization methods commonly employ a variable frequency oscillator in a control loop, where the output signal tracks the frequency and phase of the input signal. Examples of such methods include the phase-locked loop (PLL) and the frequency-locked loop (FLL).

3.1.2. Phase-Locked Loop (PLL)

The phase locked loop is the most widely used synchronization structure in various fields such as power converters, motor drives, and communication. The concept of PLL was initially proposed by Appleton [40] in 1923, and subsequent analytical descriptions were provided in [40, 41]. However, it was not until the 1970s, with the widespread use of integrated circuits (ICs), that the practical application of PLLs became prevalent. In motor drives, the application of PLLs in analog electronics emerged around the same period, and later transitioned to digital systems with the rapid development of microprocessor technology in the 1980s [31].

Over time, numerous variations of PLLs have been developed, primarily distinguished by the architecture of their phase detection methods. The most basic form of PLL is often referred to as the power-PLL (pPLL), which utilizes a multiplier for phase detection [33]. A comprehensive examination of the conventional PLL and its applications has been conducted in [31].

Structure of the PLL

The pPLL (programmable Phase-Locked Loop) can be segmented into three primary functional components, illustrated in Figure 3.1. These components are commonly known as the phase detector (PD), loop filter (LF), and voltage-controlled oscillator (VCO). The PD generates an error signal (v_{err_pd}) that represents the phase difference between the input signal and the output signal of the PLL.

When utilizing the pPLL, the phase detector (PD) incorporates a multiplication operation that leads to the generation of a double-frequency tone in the error signal, alongside the DC error component. The equation (3.1) presents the expression for the error output signal of the PD. It is notable that when the PLL is locked in a steady

condition ($\omega = \omega_o, \phi = \phi_o$), this behavior can be observed. The second term in the equation represents the undesired double-frequency component.

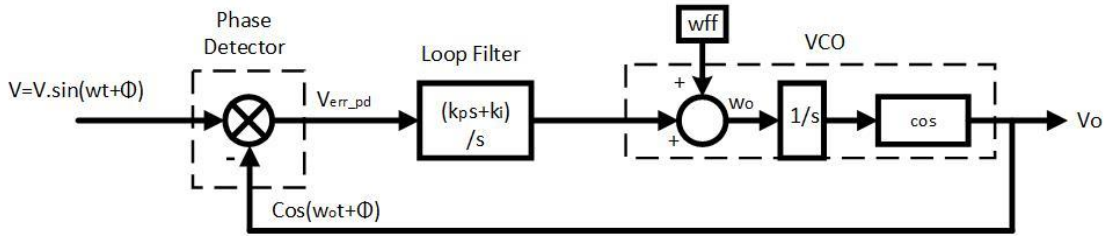

Figure 3.1: Structural diagram of PLL

$$v_{err\_pd} = \frac{V}{2}\left\{\left(\sin\left[\omega - \omega_o\right]t + \left[\phi - \phi_o\right]\right) + \sin\left(\left[\omega + \omega_o\right]t + \left[\phi + \phi_o\right]\right)\right\} \quad (3.1)$$

The loop filter (LF) performs low pass filtering on v_{err_pd} in order to extract the DC component from the error signal. Typically, the LF incorporates a proportional-integral (PI) controller, which naturally exhibits a low pass frequency response.

The role of a voltage-controlled oscillator (VCO) is to produce a signal with a frequency that is directly proportional to the input magnitude. Consequently, the filtered signal from the LF is used to drive the VCO, which generates the phase angle at a frequency centered on the nominal grid frequency (ω_{ff}), which is a feed forward term to facilitate fast locking. The output signal of the VCO (vo) is then derived from the phase angle (θ_o) with a cosine function. In the case of the pPLL, the VCO consists of an integrator function.

Linearised model of pPLL

Assuming that the initial frequency output of the PLL is equal to the input frequency, we can simplify the phase error signal based on Equation (3.1) to the form shown in Equation (3.1). While this term is nonlinear, it is feasible to derive a linearized model of the phase detector (PD) for small phase deviations, considering that $\sin\left(\phi - \phi_o\right) = \left(\phi - \phi_o\right)$.

$$v_{err\_pd} = \frac{V}{2}\left\{\sin\left(\phi - \phi_o\right)\right\} \quad (3.2)$$

The linearized model of the power-PLL (pPLL), taking into account the aforementioned assumptions, is shown in Figure 3.2. This model establishes a relationship between the phase of the input signal and the phase of the output signal. Consequently, it becomes feasible to employ conventional control theory in the design

of the pPLL, aiming for optimal settling time and stable operation, as documented in references [30] and [41].

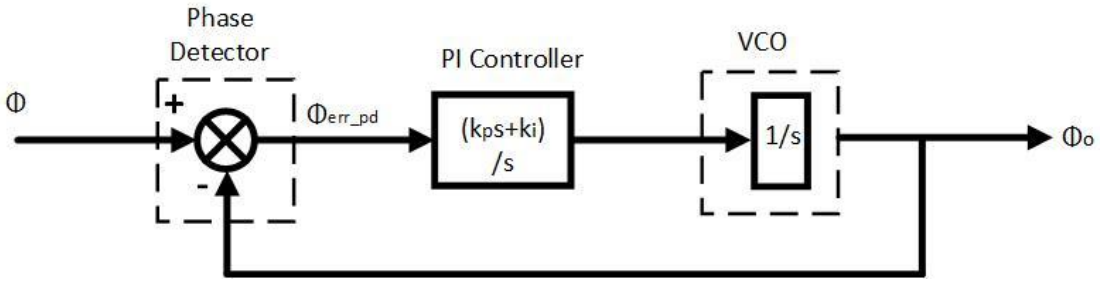

Figure 3.2: Linear Representation of a PLL model

Although the power-PLL (pPLL) is a simple method, it has certain drawbacks. One such drawback is its sensitivity to changes in the grid voltage, particularly during voltage sag conditions, which can adversely affect the transient response. Additionally, the pPLL may exhibit a poor transient response due to the characteristics of the low-pass filter (LPF) employed.

Several approaches have been suggested to address the issues mentioned above in the power-PLL (pPLL). One such method is the DFAC (Double Frequency Amplitude Compensation) technique, introduced in [33]. This method involves canceling out the double frequency component and implementing amplitude compensation in the DQ (Direct-Quadrature) frame. Another approach, proposed by Thacker et al. [31], focuses on eliminating the double frequency term by subtracting a specific term ($\sin\theta_o \cos\theta_o$) from the error signal and utilising a peak voltage tracker for ensuring unity input voltage to the PLL regardless of the grid voltage magnitudeHowever, the performance of the PLL is affected by changes in the utility voltage since instantaneous peak voltage detection is not feasible [40]. To overcome this limitation, various PLL variants have been proposed. One such variant is the enhanced-PLL (EPLL) [37, 41], which employs an adaptive notch filter to eliminate the unwanted double frequency component. Additionally, there are other types of PLLs based on the conventional PLL, including the complex coefficient filter-based PLL described in [42], as well as the variable time delay-based PLL [41].

3.1.3. Synchronous Rotating Frame (SRF)

The conventional PLL is constrained by its limited bandwidth due to the requirement of rejecting the 2nd harmonic, leading to a suboptimal transient response. As a solution, an alternative approach involving a synchronous rotating frame-based phase detector

(PD) can be employed. This method was initially introduced in [32], which presented the design of a three-phase PLL suitable for operation under distorted utility conditions. The application of this method in single-phase systems has also been discussed in [30-33].

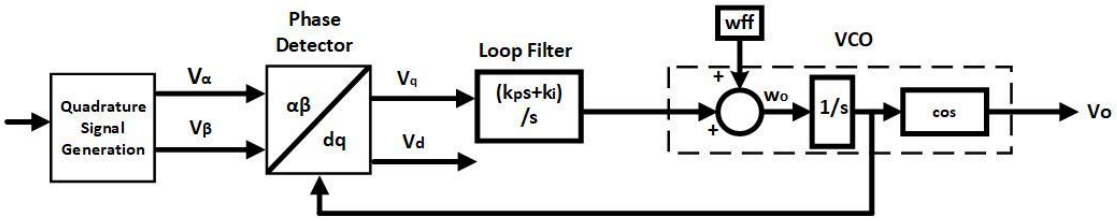

Figure 3.3: Structural Diagram of a SRF model

Figure 3.3 illustrates the fundamental block diagram of the SRF (Synchronous Reference Frame) based PLL method. The essence of the SRF PLL is centered around converting the utility voltage vector into a quadrature synchronous reference frame, achieved through the application of the Park transform. The DQ transformation requires the generation of an orthogonal signal (v_β) which is 90° phase shifted to the input signal (v_α). The stationary-to-synchronous frame along with v_α and v_β are defined in (31).

The output signals of the DQ transformation block can be simplified. Therefore, it can be seen that at steady state ($\omega = \omega_o$), the error signal of the SRF PD block (v_q) is free of the double frequency component that was seen in the pPLL. Hence it is possible to have a larger bandwidth for the PLL resulting in a faster transient response [33]. Since the quadrature signal is used as the closed loop control variable, PLL lock occurs when ($\theta - \theta_o$) becomes equal to 90° (v_q is zero).

$$\begin{aligned} v_d &= V\sin\left(\left[\omega-\omega_o\right]t+\left[\phi-\phi_o\right]\right) \\ v_q &= -V\cos\left(\left[\omega-\omega_o\right]t+\left[\phi-\phi_o\right]\right) \end{aligned} \tag{3.3}$$

In the case of the three-phase SRF PLL, the generation of stationary frame signals (v_α, v_β) relies on the utilization of the Clark transform. However, for the single-phase SRF PLL, various methods are employed to generate the orthogonal signal. These methods include the inverse Park transform [35, 36], Hilbert transform, transport delay [41], second-order generalized integrator (SOGI) based method [38], as well as recent advancements based on the discrete Fourier transform [43].

The different methods used for quadrature signal generation (QSG) in synchronous rotating frame (SRF) PLLs involve trade-offs in terms of performance and complexity. The inverse park transform-based PLL, for example, requires a complex tuning procedure for the PI controller due to the interdependence of the two nonlinear loops [41]. On the other hand, the Hilbert transform-based PLL faces a trade-off in filter order, where a low-order filter results in poor harmonic rejection and a higher-order filter introduces time delay [41]. Additionally, the transport delay-based SRF PLL, while relatively easy to implement, exhibits phase angle errors when the frequency deviates from the nominal value due to the fixed delay length of the FIFO buffer [39].

The SOGI PLL has become widely recognized for its simplicity and fast response to transients compared to other types of PLLs, although it has a lower capability for rejecting harmonics compared to the pPLL method. The next section will discuss the fundamental structure and operation of the SOGI PLL, followed by the presentation of an improved version of the control scheme using SOGI PLL.

3.1.4. Second Order Generalized Integrator (SOGI) based PLL

The SOGI (Second-Order Generalized Integrator) based PLL, introduced by Mihai Ciobotaru et al. [38], comprises a unique QSG (Quadrature Signal Generator) block integrated with a conventional synchronous DQ frame PLL. Figure 3.4 depicts the structure of the SOGI QSG block. The transfer functions for the in-phase (v_α) and quadrature (v_β) signals are defined in equations (3.4) and (3.5) respectively.

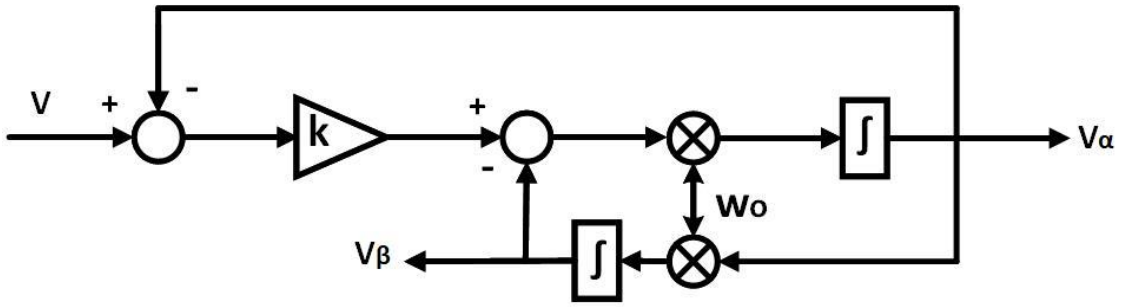

Figure 3.4: Block Diagram of SOGI-PLL

$$G_{SOGI\_\alpha}(s) = \frac{V\alpha}{V}(S) = \frac{k\omega_o s}{s^2 + k\omega_o s + \omega_o{}^2} \tag{3.4}$$

$$G_{SOGI\_\beta}(s) = \frac{V_\beta}{V}(S) = \frac{k\omega_o{}^2}{s^2 + k\omega_o s + \omega_o{}^2} \tag{3.5}$$

Hence, it is evident that the closed-loop transfer function of the in-phase output signal from the SOGI block, as described in equation (3.5), exhibits the characteristics of a

resonant band-pass filter. The parameter ω_o sets the center frequency, typically at 50Hz. The complete structure of the PLL is shown in Figure 3.5.

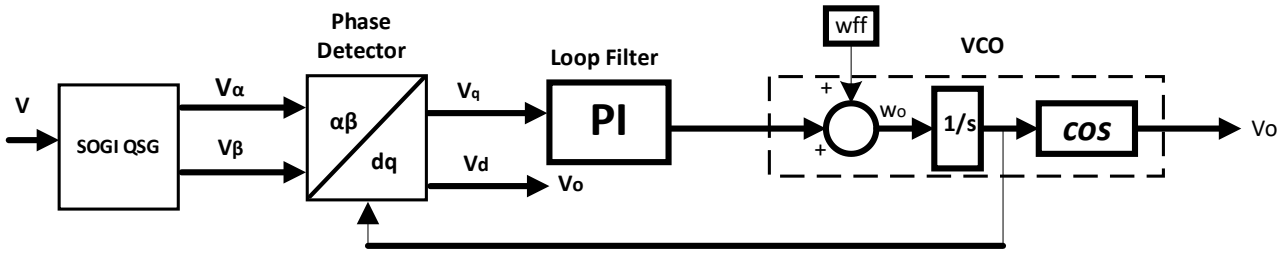

Figure 3.5 SOGI PLL representations

Additionally, an optimized design approach for tuning the SOGI PLL, considering the delay of the SOGI block, is presented in [41]. This methodology ensures a rapid transient response and robust disturbance rejection capability. In this chapter, this design methodology serves as a benchmark for comparing the improved SOGI PLL and the PIIR PLL. Based on the optimized design presented in [41], the SOGI gain (k), proportional gain (k_p), and integral gain (k_i) are set to 2.1, 137.5, and 7878, respectively, for a nominal grid frequency of 50 Hz.

The PLL enables the generation of the reference signal for current and calculates the grid frequency which makes it an elemental subsystem of the PFC-HMF controller. This section describes the operation of the used SOGI-PLL and two techniques that improve the PLL's execution.

A bandpass and a low-pass filter are used in the SOGI-PLL to process the PCC voltage. The filter is typically made out of a single SOGI section that can be used to build both a bandpass and a second-order lowpass filter. Typically, the gain K is set at 0.707 to produce a Butte-worth filter. Since the maximally linear phase response is in the Bessel filter [9, 10], it is suggested in this work that K be chosen to produce a Bessel filter, = 0.866, to neatly preserve the voltage waveform phase. If the PCC voltage is extremely contaminated, it is suggested that the harmonic attenuation be increased by using numerous SOGI sections. It is suggested that in certain scenarios, the coefficients for the “n” SOGI sections will correspond to the factored form of a higher order (2n) Bessel filter. Two orthogonal components, and, are produced by the bandpass and low-pass filters' outputs, and both of these components are input into a standard dq-PLL to determine the grid frequency and phase. The process necessitates using a coordinate transformation provided by the equation,

$$\begin{bmatrix} V_{ad} \\ V_{aq} \end{bmatrix} = \begin{bmatrix} \cos\theta i & \sin\theta i \\ -\sin\theta i & \cos\theta i \end{bmatrix} \begin{bmatrix} V_{\alpha} \\ V_{\beta} \end{bmatrix} \quad (3.6)$$

here V_{ad} gives information about the amplitude of the input signal and V_{aq} provides information about the phase error. The trigonometric operations make the algorithm computationally expensive but since the SOGI-PLL is a frequency regulator working upon two integrators cascaded to each other in a closed-loop system, working as an ideal integrator at a particular frequency this adaptive filter with the help of Mason formula given above in equation.

3.2 SOGI Based Controller Design.

Proportional-integral (PI) controllers are applied to control the PFC converters as seen in Figure 2.12 With an external control loop for the voltage control and an inner control loop for the current, the PFC controller keeps the DC link voltage nearly constant and the input power factor close to one. As a result, the control technique aids in controlling output parameters with great switching efficiency.

This technique's proposed control mechanism is straightforward and easily implementable in practice. The block diagram of the chosen control method is shown in Figure 3.6. While V_{DC} indicates the boost converter's actual output, V_{ref} is the reference voltage that is anticipated to be present there.

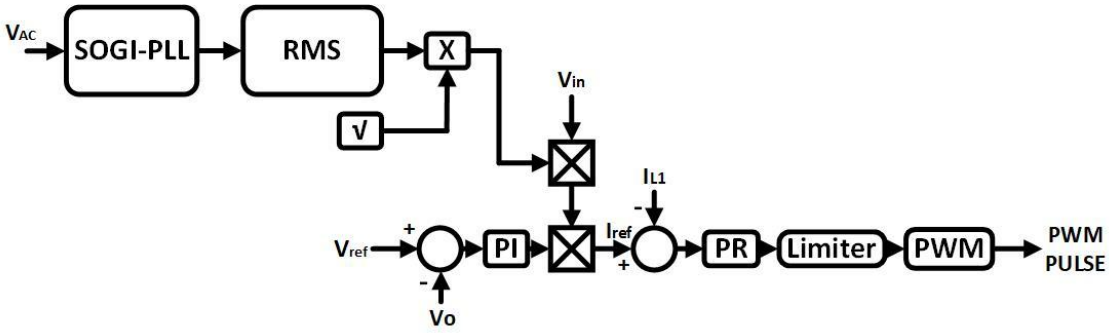

Figure 3.6: SOGI based Closed loop control scheme

It shows the proposed control scheme with SOGI filter in it creating a reference template for harmonic mitigation technique (HMT).After processing the error signal, the voltage controller (Pid controller) generates a controlled signal for the current I_S. The $I_S.\sin\omega t$ is created by multiplying this current signal by a unit template generated by a phase-locked loop (PLL). To create the reference current signal, the load current I_L is then subtracted from the sinusoidal signal I_S. The circuit provides the absolute value of the i_S* reference current signal since the boost inductor current cannot be varied. The actual signal i_C and the required reference signal i_S* are given to the current controller

to produce the proper gating signal. A hysteresis current controller has been selected as the current controller. As shown, the lower and the upper hysteresis bands are produced by adding and deducting a band of value "h" from the reference signal i_S*, respectively. Now the pulse is severed when the current crosses the upper hysteresis band, or i_S*+h, causing the current to fall and flow through the load. The inductor current is driven to align within the width of the hysteresis band. Similarly, when the value of the current goes lower than the lower hysteresis band i.e. i_S*-h, the pulse gets connected and is given to the switch, making the linear increment in the current. The power switch is switched using this approach to follow the reference current instruction, and the resulting current drawn by the load will be virtually sinusoidal, have a low total harmonic distortion (THD), and have a low harmonic content. As a result, the power factor of the system increases.

3.3 Simulation and Results.

For better understanding of concept in this chapter a simulation model of PFC boost converter was created using MATLAB/Simulink which initially was working under ideal condition as given in (2.1) supply voltage of which was later polluted intentionally with 10% of grid voltage distortion producing the harmonics in supply current. Results of this model with the conventional and proposed control scheme were taken and studied. The experiment was completed in 3 different case scenarios.

- Performance of PFC system with the sinusoidal grid voltage.
- Performance of PFC system with the distorted grid voltage.
- Performance of PFC system with distorted grid voltage with the proposed control scheme.

While the first case “Performance of PFC system with the sinusoidal grid voltage.” Was already discussed and showcased in “2.11.1”, in the second case 10% distortion in grid voltage is introduced resulting in poor power factor.

3.3.1 Performance of PFC system with distorted grid voltage with the proposed control scheme.

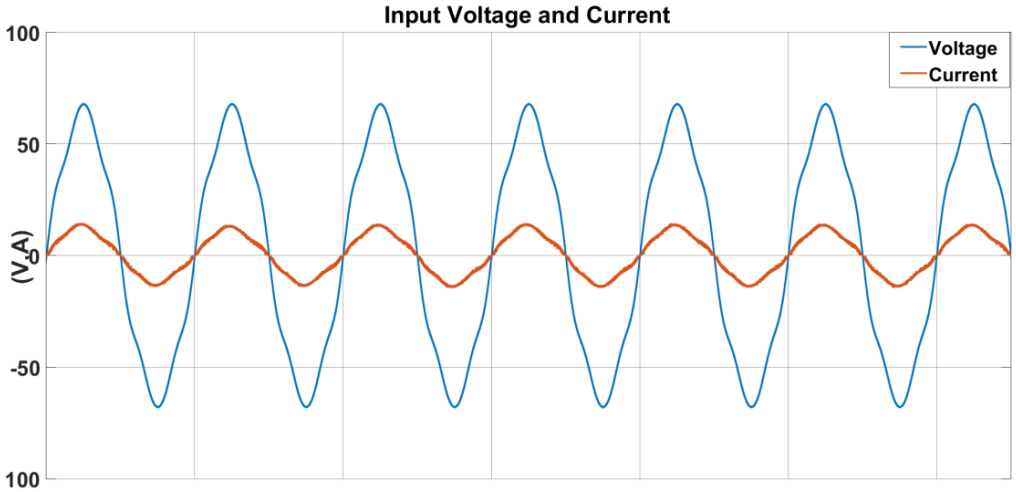

(a)

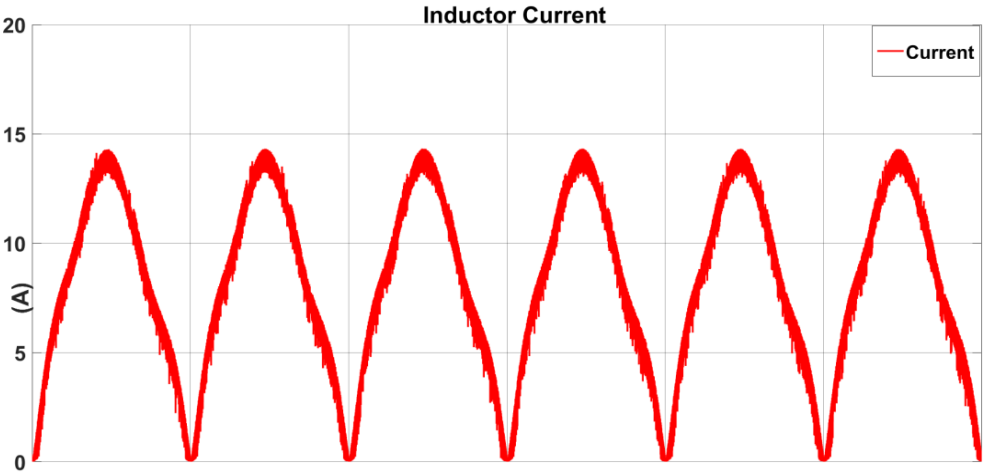

(b)

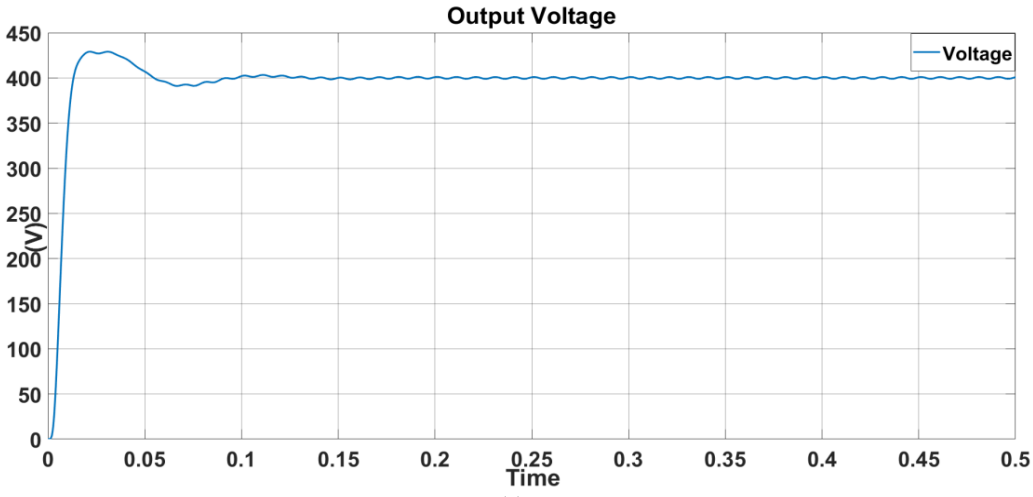

(c)

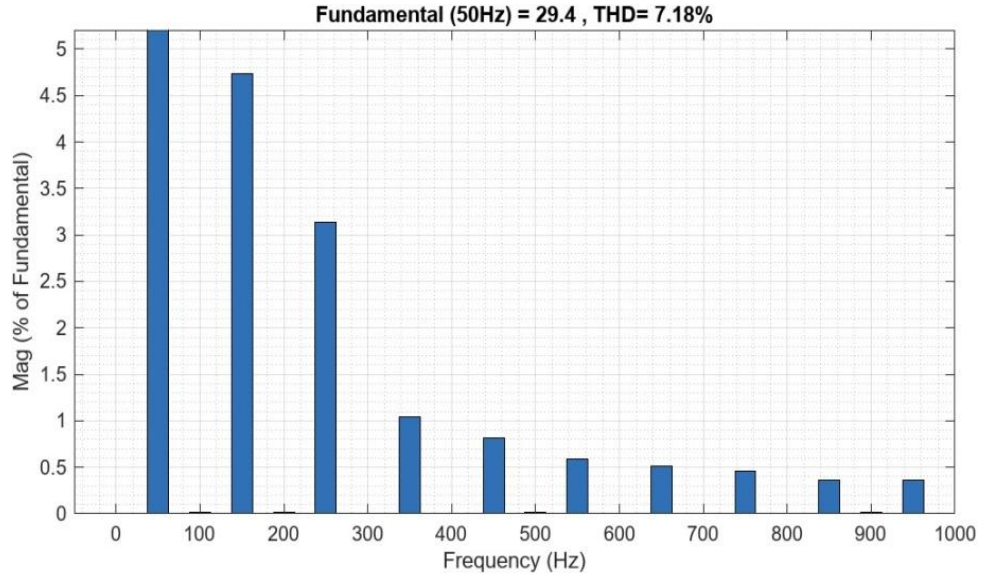

(d)

Figure 3.7: (a) Input Voltage and Current waveform, (b) Inductor Current waveform, (c) output voltage waveform, (d) FFT analysis of input current when SOGI control scheme is use on polluted

In the third case the distortion is introduced into the supply voltage. The results have been taken with the proposed control algorithm which involves a SOGI-PLL block. Here Figure 3.7 shows various results of the system with compensation on a PFC boost converter. Figure 3.7(a) shows the good improvement in the waveform of input current from the supply in phase with the input voltage with harmonics. Now after the harmonic component of the system has been compensated with the PLL the inductor current can be seen well in shape as observed in Figure 3.7(b). And Figure. 3.7(c) shows the DC voltage value at the PFC boost converter output. Fast Fourier transform (FFT) analysis of the input current gives the value of THD at 7.18% which is desirable (less than 10%).

3.4 Conclusion

This chapter gives a brief idea of why grid synchronization is an important factor and how does PLL plans a role in it and then using the MATLAB Simulink is used to present and analyze the PFC boost converter with the conventional and proposed control method. A 230V is given as the input voltage and 400VDC is regulated at the output. The analysis of the circuit, both with and without the additional harmonic pollution in the supply voltage scheme, is displayed. When the grid voltage is undistorted, the closed-loop control in the traditional PFC control scheme produces satisfactory results. When 10% of grid voltage distortion is considered, the supply current and rectifier output voltage get affected. Problems in the form of distorted supply current and poor pf are observed. A SOGI-PLL block is designed to filter the distorted voltage, regain the improved pf, and result in low THD. Thus, grid power quality is ensured with the designed control scheme modification discussed.

CHAPTER 4

BACK-END DC-DC CONVERTER

4.1 Introduction

The back-end DC-DC converter is a vital component in an electric vehicle (EV) charger system. Its main purpose is to convert the high-voltage DC power from the charging infrastructure or grid into the appropriate voltage level needed for charging the EV battery. This converter performs voltage conversion, adjusting the input voltage to match the battery's requirements. It also handles power conversion efficiently to minimize energy losses during the charging process. The converter incorporates control and protection mechanisms, including feedback loops and fault detection, to ensure safe and reliable charging. Communication interfaces may be included for bidirectional power flow and data exchange with the charger, vehicle, and power grid. The converter strives for high efficiency and compactness, utilizing advanced power semiconductor devices and optimizing space utilization. In summary, the back-end DC-DC converter is a crucial component that enables efficient, safe, and intelligent power conversion in an EV charger system.

The chargng charcteristics of a Li-ion cell are discussed in section 1.4. In electric vehicle (EV) battery banks, Li-ion cells are often connected in a series-parallel configuration to increase energy capacity by raising the voltage and current ratings. To harge the high voltage battery in constant current (CC) and constant voltage (CV) modes, a second-stage DC-DC converter is employed in the on-board charger (OBC). As explained in the previous chapter (Chapter 2), the front-end AC-DC power factor correction (PFC) converter generates a DC output voltage of 400 V with a ripple voltage of 10 V peak-to-peak. The nominal voltage of the battery ranges from 320 V(depleted condition) to 420V(Full Charge Condition).To accommodate the fluctuating input voltage from the first-stage AC-DC converter and provide a wide range of output voltages, a DC-DC converter is utilized as the second-stage converter. In addition to the high voltage battery pack used in electric vehicles (EVs) or hybrid electric vehicles (HEVs), there is also a low-voltage auxiliary battery present. The auxiliary battery is a 12 V battery that supplies power to electronic loads in the vehicle such as lights and music systems. In conventional internal combustion engine vehicles and even in EVs, alternators are typically used to charge the auxiliary battery while driving. However, this method of charging incurs losses as electrical energy is

converted into mechanical energy and then back into electrical energy, requiring additional power converters.

To minimize these losses, the on-board charger is modified to function as a Low-Voltage DC-DC Converter (LDC). This modification allows the OBC to supply power directly from the propulsion battery to the auxiliary battery during the driving stage [25]. By eliminating the need for the alternator and additional power converters, the losses associated with charging the auxiliary battery can be reduced.

4.2 DC to DC Converters Classification.

Within this section, the categorization of DC/DC converters is presented, based on:

4.2.1 Isolation

DC-DC converters can be classified based on their isolation characteristics. Isolation refers to the presence of a galvanic barrier between the input and output sides of the converter, providing electrical isolation and serving different purposes in electrical systems, offering distinct advantages and applications.

Non-isolated DC-DC converters do not provide electrical isolation between the input and output sides. They are used when the input and output share a common ground reference. Non-isolated converters are typically more compact, simpler, and less expensive compared to their isolated counterparts. They are commonly used in battery-powered systems, automotive electronics, and low-power applications. Non-isolated converters such as buck, boost, buck-boost, and SEPIC converters are widely employed to step up or step down voltages efficiently.

On the other hand, Isolated DC-DC converters provide electrical isolation between the input and output sides of the converter. They employ a transformer to transfer energy from the input to the output. This isolation ensures that there is no direct electrical connection between the input and output, which is crucial in certain applications. Isolated converters are commonly used in situations where safety, noise reduction, and voltage level shifting are required. They provide galvanic isolation, protecting sensitive electronics from high voltages, ground loops, and potential electrical hazards. Isolated converters are often found in industrial applications, power supplies, medical devices, and communication systems.

The choice between isolated and non-isolated DC-DC converters depends on the specific requirements of the application. Designers must carefully consider the trade-

offs and select the appropriate type of converter based on the specific needs of their system.

4.2.2 Switching

DC-DC converters can be categorized as either a hard-switching or a soft-switching topology. In a later (soft switching), a resonant circuit is employed to facilitate the MOSFET switching, thereby reducing switching losses and minimizing electromagnetic interference (EMI). By utilizing the resonant circuit for transistor time commutation, the converter achieves improved efficiency and lower levels of EMI compared to hard-switching topologies.

In a hard switching based DC-DC converter, the switching devices are operated at a predetermined switching frequency. However, operating at high frequencies can result in increased electromagnetic interference (EMI) and higher stress on the power electronic switches (PES). To mitigate these issues, snubbers can be incorporated to eliminate the electrical stress across the PES. Additionally, incorporating a low-pass filter helps minimize the impact of EMI. It is worth noting that hard-switching DC/DC converters generally have lower efficiency compared to soft-switching DC/DC converters.

4.3 Operating Modes for EV Charger

On Analyzing the power flow between the grid and the battery pack. On-board charger can be divided into two types:

(a) Active power transfer

(b) Reactive power transfer

While G2V (Grid-to-Vehicle) and V2G (Vehicle-to-Grid) refer to different modes of operation in the context of electric vehicle (EV) charging and grid integration, DC-DC converters are not directly involved in these modes but here we will understand the

1. G2V (Grid-to-Vehicle): G2V mode refers to the process of charging an electric vehicle from the electric grid. In this mode, only active power transfers from the grid to the vehicle's battery through an AC/DC charger. The charger converts the AC power from the grid to DC power suitable for charging the EV battery. The DC power is then managed by the vehicle's power electronics and distributed to the battery for storage.

2. V2G (Vehicle-to-Grid): V2G mode enables bidirectional power flow between an electric vehicle and the electric grid, hence capable to transfer both active and reactive power. In addition to charging the vehicle, the EV battery can also supply power back to the grid when required. This mode allows electric vehicles

to act as mobile energy storage units that can contribute power to the grid during peak demand periods or other grid support services. V2G implementation typically involves bidirectional AC/DC converters, which facilitate the power flow between the vehicle and the grid.

4.4 Non- Isolated DC – DC Converter

Non-isolated DC-DC converters are highly favored in a range of applications, including battery-powered devices, automotive electronics, portable electronic devices, and distributed power systems. Their compact and cost-effective design makes them a popular choice. One of the key advantages of these converters is their ability to assist the charger in regulating the voltage and current provided to the EV battery, ensuring both efficient and safe charging.

Various non-isolated DC-DC converters are recommended for bi-directional as mentioned in literature sources [42-43]. And among all a commonly used topology is Half-Bridge converter, given in Figure 4.1 which can either operate in Boost or in Buck mode as per the requirement by using two active switches.

The converter consists of two power switches, typically MOSFETs or IGBTs, arranged in a half-bridge configuration. The midpoint of the half-bridge is connected to the common node of the two DC voltage sources. The two switches are controlled in a complementary manner to regulate the power flow and voltage conversion.

In buck mode, when the input voltage is higher than the output voltage, one switch (typically the upper switch) is turned on while the other switch (typically the lower switch) is turned off. This allows current to flow from the input source through the on

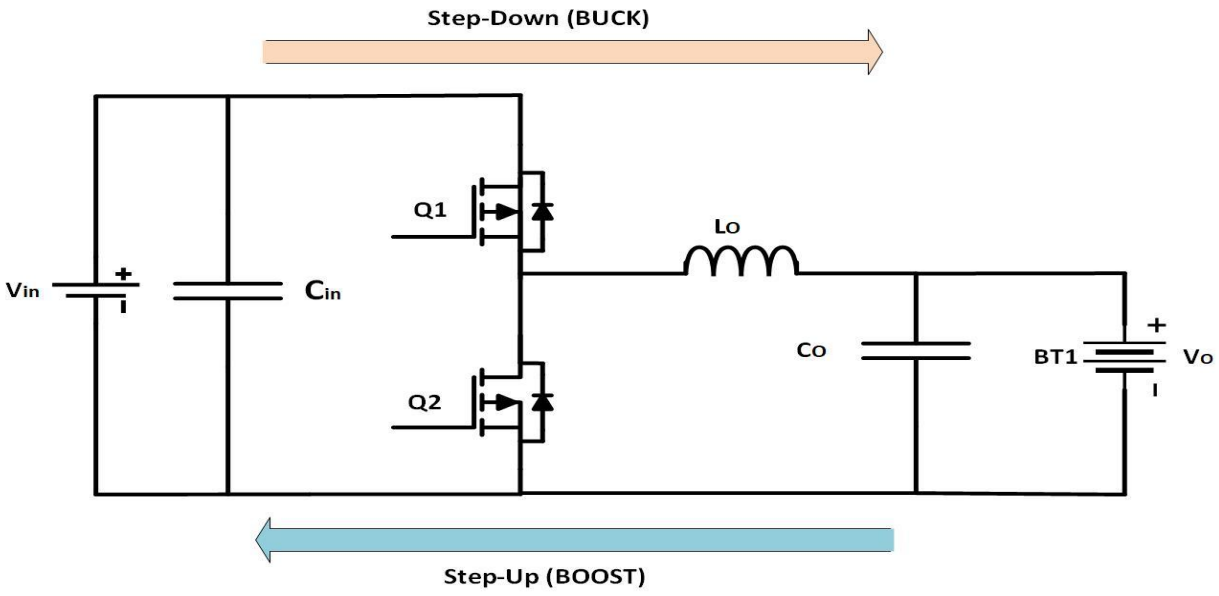

Figure 4.1: Circuit Diagram of a Half-Bridge Buck/Boost DC – DC Converter

switch, the load, and then to the output source. The diode connected in parallel with the off switch provides a freewheeling path for the current during this mode.

In boost mode, when the input voltage is lower than the output voltage, the switch states are reversed. The lower switch is turned on while the upper switch is turned off. This enables current to flow from the input source through the on switch, the load, and then to the output source. The diode connected in parallel with the off switch provides the freewheeling path during boost mode.

To ensure this bidirectional power flow, the converter needs to handle the reverse current flow. When the direction of power flow is reversed, the corresponding switch is turned off, and a diode connected in parallel with each switch allows the current to circulate in the opposite direction through the freewheeling path.

4.4.1 Bidirectional Controller

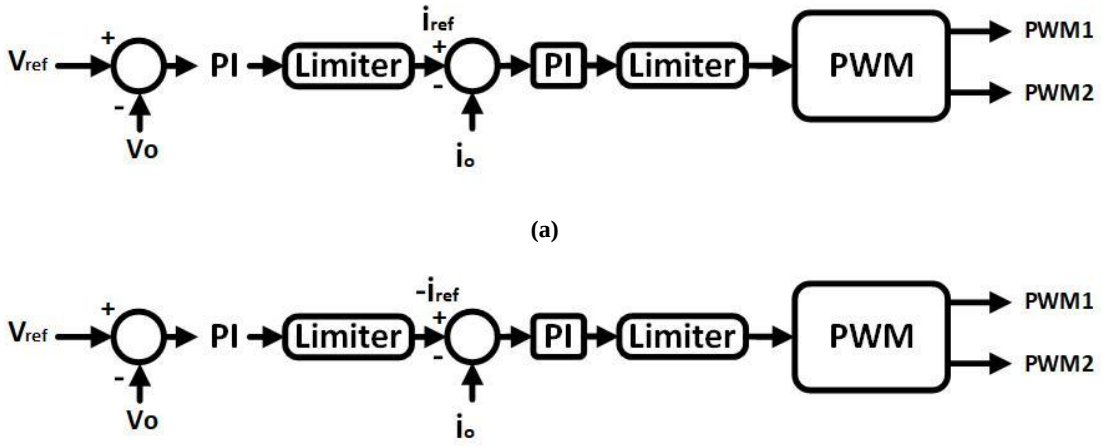

Figure 4.2: Controller Block Diagram for (a) Battery Charging, (b) Battery Discharging.

The controller needs to handle bidirectional power flow. It should ensure smooth transitions between buck and boost modes and adjust the switching of the power switches accordingly. This is achieved by monitoring the voltage and current polarities and controlling the switch states accordingly using PI controller .Figure 4.2 gives a control strategy for DC-DC converter. A PI controller is used to regulate the battery current during charge and discharge current operation. Reference value of current (iref) is kept positive for charging and negative for discharging. Limiter controller incorporates current limit protection to prevent excessive current flow and protect the converter and load.

4.4.2 Converter Design

Inductor Current (i_L) slope is given as

$$\frac{di_L}{dt} = \frac{V_L}{L} \tag{4.1}$$

where L is the value of inductance and V_L is the value of voltage across the inductor.

When the converter is working in step-up mode then the power from battery is being transferred to the grid and second switch (Q2) is in ON state, then the inductor voltage is

$$V_L = V_O \tag{4.2}$$

Substituting the value of (4.2) in (4.1)

$$\frac{di_L}{dt} = \frac{V_o}{L} \tag{4.3}$$

From equation (4.3) inductor current slope is observed to be positive and when diode across switch (Q1) is in forward biased then the inductor current slope becomes negative and inductor voltage becomes,

$$V_L = V_O - V_{in} \tag{4.4}$$

Similarly in step-down mode, slope for inductor current is negative when first switch (Q1) is in ON state and positive when diode across Q2 is in forward bias.

Inductor at the output filter (Lo) is calculated by assuming the converter to be working in Step down mode as is given as

$$L = \frac{V_O \times (V_{in} - V_O)}{I_{ripple} \times f_{sw} \times V_{in}} \tag{4.5}$$

Vo is the output voltage of converter, Vin is the supply voltage, Iripple is the ripple current of the output current, fsw is switching frequency of the converter.

Similarly, Capacitance of the output filter can be calculated by

$$C = \frac{I_{ripple}}{8 \times f_{sw} \times V_{ripple}} \tag{4.6}$$

Vripple is the value of ripple of the output voltage.

4.5 Isolated DC – DC Converter [42-44]

As mentioned previously, the selection of a DC/DC converter is influenced by various factors. These factors include the power to be transferred and whether a step-down or step-up converter is necessary. Additionally, the requirement for isolation also plays a significant role. In the case of an On-Board Charger (OBC), a step-down converter is needed since the input voltage is higher than the output voltage. Furthermore, galvanic isolation is necessary, which entails the use of a transformer.

Table 3 Power Levels of Isolated DC-DC Converters.

DC-DC Converter Topologies	On Board Charger Power Levels.
Full Bridge LLC	**3.3kW**
Full Bridge Phase Shift	**11kW**
Half Bridge LLC (3 Phase)	**>11KW**

The information provided leads to the selection of a Phase shift full bridge topology for level-1 and 2 chargers, as shown in Figure 4.1.

The equation for output voltage in PSFB can be expressed as

$$V_O = 2 * V_C * n * D \tag{4.7}$$

where, V_O is the demand voltage of battery load from the converter for charging, V_C is the input fed to the DC-DC Converter from the previous state and n is the ratio of secondary to primary side of transformer and D is the duty cycle for the converter.

The Value of D should be less than 50% for avoiding the saturation of the core [11].

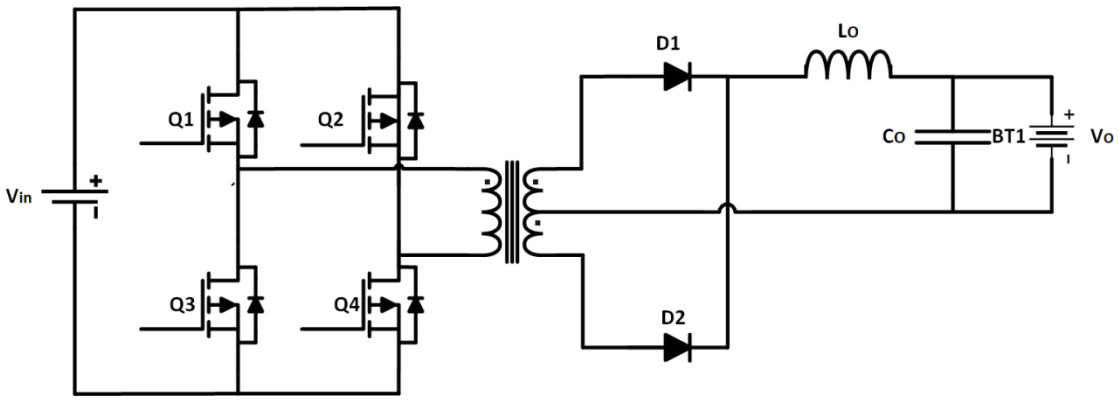

Figure 4.3: Circuit Diagram of a Phase Shift Full Bridge (PSFB) DC-DC Converter.

4.5.1 DC/AC Stage

This stage corresponds to an inverter component that transforms a direct current signal into an alternating current signal. The selection of a full bridge converter (as shown in Figure 4.1) is based on the power transmission requirements. A full bridge inverter

allows for a maximum output voltage that is twice that of a half bridge inverter. It also enables lower switch currents and output currents compared to a half bridge inverter for the same power. Furthermore, the transistors used in the full bridge inverter are smaller in size. In scenarios involving very high power, a full bridge inverter requires fewer parallel devices compared to a half bridge inverter.

The operation of the full bridge converter is straightforward. It employs a bipolar voltage switching topology, wherein the transistors are switched in pairs. Specifically, transistors T1 and T4 form one pair, while transistors T2 and T3 form the other pair. Each transistor is turned "on" during one half of the period and "off" during the other half. It is important to note that switch T1 cannot be turned "on" simultaneously with T4. The control of the full bridge converter can be achieved through two different methods.

1) Simultaneous

2) Phase Shifted

The output voltage V_O of the full bridge converter is regulated and controlled using a pulse width modulation (PWM) scheme. In this scheme, a saw tooth waveform is generated and compared with a voltage control signal from the control circuit. The result of this comparison determines the width of the pulses in the PWM signal, which in turn controls the average voltage applied to the load and regulates the output voltage V_O.

During the first half period of operation, the switch pair T1 and T4 conduct electricity as long as the saw tooth signal is lower than the control signal. Once the sawtooth signal surpasses the control signal, these transistors cease conducting until the second half period. In the second half period, the switch pair T2 and T3 take over and conduct electricity until the saw tooth signal once again exceeds the control signal. This sequence of operation repeats in subsequent periods.

Another control method is phase-shift control, which offers a convenient way to achieve zero voltage switching, thereby reducing switching losses. This control technique involves manipulating the timing of turning on opposite pairs of transistors in the bridge configuration, allowing the stored energy to be utilized for charging and discharging the capacitance of the bridge switches during a freewheeling stage. This phase shifting of the ON times of the transistor pairs helps minimize the losses associated with switching.

4.5.2 Transformer design (AC-AC)

This section focuses on the design considerations for two key components of an isolated DC/DC converter: the high-frequency transformer and the output inductor. It covers the various aspects and factors that need to be taken into account when designing these components to ensure the proper functionality and performance of the converter.

A transformer is composed of multiple coils that are magnetically linked. In the discussed converter, the transistors switch at a high frequency, typically around 20 kHz, resulting in an output signal with a high frequency. The universal electromagnetic force (EMF) equation for transformers can be expressed as follows:

$$E = KNfaB \tag{4.8}$$

Where E is the winding voltage, f is the frequency, N the number of turns, a the core cross-sectional area and B the peak magnetic flux density, K is 4.44 for sinusoid and 4 for rectangular wave.

Due to the relationship described, when the frequency is high, the core section of the transformer is reduced, and vice versa. However, operating at a high frequency introduces additional challenges. The Eddy current losses increase with the square of the frequency and decrease with the material resistivity of the transformer. To mitigate these losses, an insulating ferromagnetic material is used for the magnetic circuit of the high-frequency transformer. Since the DC/DC converter employs a full bridge configuration, the high-frequency isolation transformer must support bidirectional core excitation. The type of AC/DC converter being used also influences the transformer design, whether it is a center-tapped transformer or a conventional transformer. Both types need to operate effectively at high frequencies. In this specific DC/DC converter, a two-winding coil transformer is required.

4.5.2.1 Magnetic behavior [43]

When a magnetic core material is exposed to an external magnetic field, denoted as H, the alignment of molecules within the material occurs gradually. This magnetization process involves overcoming energy barriers, causing a delay in the magnetization relative to the applied field. As a result, a hysteresis loop is formed, as illustrated in Figure 4.4, depicting the relationship between the applied magnetic field and the resulting magnetization.

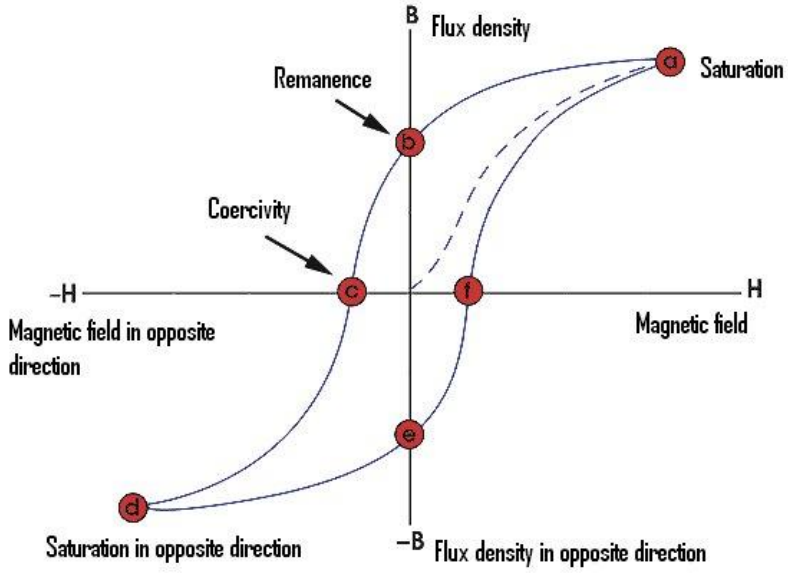

Figure 4.4 – Typical BH-curve of magnetic material

A magnetic core initially possesses zero magnetism and is represented at the origin (0) in the figure, where B = 0 and H = 0. When the magnetic core is subjected to an external magnetic field, the magnetic field within the core, denoted as B, begins to increase. However, this increase is non-linear and eventually levels off as the core becomes fully saturated. This saturation point, denoted as point a, indicates that further increases in the external magnetic field will no longer affect the core's magnetization.

As the external magnetic field is subsequently reduced, the magnetic field within the core also decreases until it reaches point b. At this stage, the core is no longer influenced by an external field, yet it retains a certain level of flux density. This remaining flux density within the core, known as residual magnetism, is commonly referred to as remanence. When the direction of the external field is reversed, the magnetic field within the core will reach point c. This specific point where the field crosses zero is known as the point of coercivity.

The same process described above will repeat when the external field is reversed. The field within the core will once again reach saturation, this time at point d.

4.5.2.2 Core material selection

Softcore materials are commonly used in high-frequency applications due to their low sensitivity to external magnetic fields and hysteresis [47]. The choice of core material depends on factors such as the level of core saturation, temperature, and specific application requirements. Temperature is particularly important as it can affect the magnetization of the core, with the temperature at which the core loses its

magnetization referred to as the Curie (TC). Few commonly used cores include ferrites, iron powder, and soft iron. Ferrite cores offer advantages such as high permeability and low operational losses compared to other materials. In this thesis, the focus is primarily on planar transformers that utilize ferrite core materials.

The performance curve represents the power handling capability of different ferrite core materials at a specific power loss density [47]. By examining the curve, it becomes evident that selecting a suitable core material is crucial for high-frequency applications. In this case, ferrite core materials like 3F3, 3F4, 3F35, and 3F36 exhibit favorable characteristics for operation at 600 kHz, making them suitable choices for such applications.

4.5.2.3 Transformer Setup [43]

In the conventional approach, the design of high-frequency transformers takes into account the maximum operating flux density, Bmax. This value is influenced by factors such as the shape of the transformer core and the type of core material employed. Following Faraday's law of electromagnetic induction, the generation of electromotive force, V, is a result of the rate at which the magnetic flux, φ, changes with respect to time, t.

$$V_1 = -N\frac{d\phi}{dt} \tag{4.9}$$

In this equation, N represents total number of turns in the coil. However, the magnetic flux φ is determined by the magnetic flux density BAC, which flows through the cross-sectional area A_c of the core.

$$\phi = B_{\max} A_c \tag{4.10}$$

From eq 1 and 2 we get

$$V_1 = -NA_c\frac{dB_{\max}}{dt} \tag{4.11}$$

The voltage V_1 on the primary side during the time interval from 0 to DTs is equivalent to the input voltage Vin of the converter. The maximum voltage applied on the primary side results in the peak flux density $B_{\max}$. This relationship provides the solution for as follows:

$$N_1 = \frac{V_d DT_s}{A_C B_{\max}} \tag{4.12}$$

The primary voltage V_d will reach its maximum when the duty cycle reaches its lowest value. Consequently, the number of turns N_1 can be calculated as follows:

$$N_1 = \frac{V_{d,\max} D_{\min} T_s}{A_C B_{\max}} \tag{4.13}$$

From equation (4.13), it is evident that the peak flux density (Bmax) decreases as the number of primary turns (N_1) increases. Consequently, core losses decrease while resistive losses increase. This represents a tradeoff between core losses and resistive losses. In scenarios where the transformer operates under heavy load conditions, a design with larger core losses and smaller resistive losses may be preferable..

To determine the appropriate wiring, it is necessary to calculate the RMS currents for the primary and secondary sides using equations (2.1) and (2.2).

$$\begin{aligned} I_{P,RMS} &= \sqrt{\frac{1}{2T_S}\int_0^{2T_S} i_1^{\,2}(t)\,dt} \\ &= \frac{n_2}{n_1} I_{O,\max}\sqrt{D} \\ I_{S,RMS} &= \sqrt{\frac{1}{2T_S}\int_0^{2T_S} i_2^{\,2}(t)\,dt} \\ &= \frac{1}{2} I_{O,\max}\sqrt{1+D} \end{aligned} \tag{4.14}$$

Litz wire is a popular choice for winding transformers in Switch Mode Power Supplies (SMPS). It is specifically designed to minimize losses caused by the skin effect and proximity effect in the conductors. To achieve this, Litz wire is composed of multiple thin wires, each coated with an insulating film.

The skin effect, which is typically a concern at high frequencies, can be disregarded in the case of this transformer that utilizes Litz wire.

4.5.2.4 Transformer losses

Magnetization losses

The presence of wires in the transformer results in the generation of magnetization inductance, which needs to be energized by a current for the transformer to function effectively. However, this current leads to the occurrence of magnetization losses within the transformer.

The calculation of the magnetization inductance can be expressed as follows:

$$L_m = A_L N_1^2 \tag{4.14}$$

where A_L is the inductance factor and can be found in datasheets for specific cores

The magnetization current can then be as

$$\Delta \mathrm{I_m} = \frac{V_d D T_S}{L_m} \tag{4.15}$$

Resistive losses

In order to evaluate the resistive losses in the transformer, it is necessary to determine the total length of the wire. Based on this information, the total resistance on both the primary and secondary sides can be determined.

$$R_1 = \frac{\rho_{cu} L_1}{A_{C1,bundle}} \tag{4.16}$$

$$R_2 = \frac{\rho_{cu} L_2}{A_{C2,bundle}} \tag{4.17}$$

Where ρ_{cu} is the resistivity of copper wire and it is measured to be around 1.68×10^{-3}.

The total resistive loss calculated is

$$P_{cu} = R_1 I^2_{P,RMS} + R_2 I^2_{S,RMS} \tag{4.18}$$

Core-losses

The core loss in the transformer, which arises from the characteristics shown in Figure 2.10, can be determined by referring to the power loss diagram provided in the data sheet of the specific core material. By knowing the volume of the core and utilizing the equations derived from the data sheet, the core loss P_{core} can be calculated equation 4.19.

$$P_{core} = C_m f^x B^y \left(c_{t0} - c_{t1} T + c_{t2} T^2\right) \tag{4.19}$$

where $C_m, x, y, c_{t0}, c_{t1}, c_{t2}$ are parameters which have been found by curve fitting of the measured power loss data. T is the temperature

The total maximum power loss for the transformer is then

$$P_{tot} = P_{core} + P_{cu} \tag{4.20}$$

4.5.3 AC/DC Stage

There are two possible approaches to implement this converter. The first approach involves utilizing a center-tapped transformer with a diode half bridge, while the second approach utilizes a transformer with a diode full bridge configuration. In this

work, the first method, utilizing a center-tapped transformer, has been selected. It is worth noting that this type of converter exhibits a lower diode voltage compared to the half bridge configuration. Additionally, this configuration allows for improved current flow through the transformer windings.

4.5.4 LC OUTPUT FILTER [41]

A typical LPF shown in figure 4.3 is made for filtering out the ripples from both the output voltage and the current.

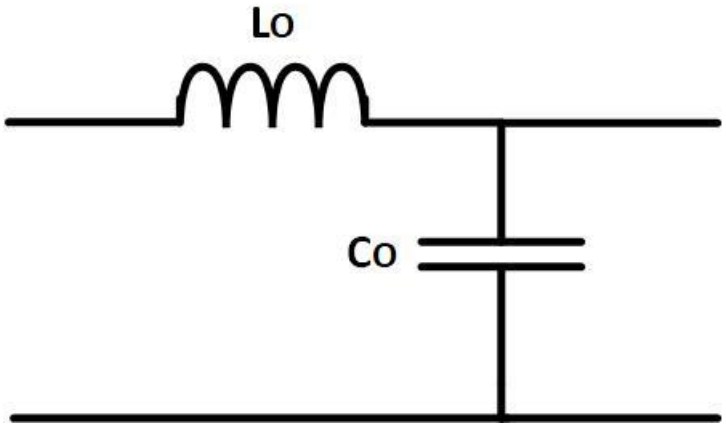

Figure 4.5 – Output low pass-filter

The inductor used in the converter must have a sufficient value to ensure that the output current ripple remains within acceptable limits. Typically, a current ripple between 5-10% of the average load current is considered acceptable**.**

For these calculations the inductor current from zero to DTs is considered. The voltage over the inductor is given by

$$V_L = L\frac{di_L}{dt} \tag{4.21}$$

And the inductance can be calculated by

$$L = \frac{V_L}{\frac{di_L}{dt}} \tag{4.22}$$

A minimum value of the inductance can be calculated when the voltage across the inductor reaches its maximum $V_{L,\max}$.

$$L_{\min} = \frac{V_{L,\max}}{\frac{ripple.I_{L,\max}}{t_{on}}} \tag{4.23}$$

By analyzing the network, the value of voltage across the inductor can be expressed as

$$V_L = V_{oi} - V_o$$

Where, $V_{oi} = \frac{N_2}{N_!} V_d$ (4.24)

Substituting it in above equation we get,

$$V_L = \frac{N_2}{N_1} V_d - V_o \quad (4.25)$$

And the maximum voltage across the inductor will be achieved under condition

$$V_{L,\max} = \frac{N_2}{N_1} V_{d,\max} - V_{o,\min} \quad (4.26)$$

The maximum average inductor current is given by

$$I_{L,\max} = \frac{P_{O,\max}}{V_{O,\min}} \quad (4.27)$$

And hence the inductor value at which the CCM condition can be achieved is expressed as

$$L_{\min} = \frac{\frac{N_2}{N_1} V_{d,\max} - V_{O,\min}}{\frac{ripple.I_{L,\max}}{t_{on}}} = \frac{V_O(1-D)}{2 * \Delta i_{LO} * f_{SW}} \quad (4.28)$$

Similarly in order to calculate the filter capacitor value, the following relation is considered.

$$i_C(t) = C \frac{dV_C}{dt}$$

Under normal working condition it is assumed that all the ripple current from the inductor goes through the capacitor as well and the ripple of the output voltage is under 5%, With these considerations the maximum allowed value of capacitance of the output capacitor is

$$C_{\max} = \frac{i_C(t)}{\frac{dV_C}{dt}} = \Delta_{iL} * \frac{D}{f_{SW} * \Delta V_O} \quad (4.29)$$

4.6 Efficiency Enhancement Strategies

4.6.1 Zero voltage switching (ZVS)

Zero Voltage Switching (ZVS) is a technique used in power electronics to minimize switching losses and improve efficiency in high-frequency switching applications. It is commonly employed in switch-mode power supplies (SMPS), DC-DC converters, and other power electronic systems.

In traditional power electronic circuits, when a switch (such as a Mosfet) is turned on or off, there is a brief period of time during which the voltage across the switch is neither zero nor the full supply voltage. This transitional period results in switching losses, as energy is dissipated in the form of heat. ZVS aims to eliminate these losses by ensuring that the switch is turned on or off when the voltage across it is very close to zero.

The ZVS technique typically utilizes resonant circuits, which consist of an inductor and a capacitor connected in parallel or series with the switch as can be seen in Fir.. By carefully designing the circuit parameters and controlling the timing of the switch, ZVS can be achieved.

During ZVS operation, when the switch is turned on, the resonant circuit stores energy in the inductor and capacitor. This energy is then released when the switch is turned off, allowing the current to continue flowing through the inductor and maintaining the voltage across the switch at or near zero. By avoiding the voltage transition, the switching losses are significantly reduced.

There are several benefits associated with ZVS:

1. Reduced switching losses: ZVS reduces the power dissipation during switching, leading to improved efficiency.

2. Lower electromagnetic interference (EMI): Since the switching transitions occur at or near zero voltage, the high dv/dt (change in voltage over time) and di/dt (change in current over time) stresses are reduced, resulting in lower EMI emissions.

3. Increased power density: ZVS enables higher switching frequencies, which allows the use of smaller and lighter passive components, such as inductors and capacitors, leading to higher power density in the system.

4. Improved reliability: The reduction in switching losses and stress on components can improve the reliability and lifespan of the power electronic system.

However, implementing ZVS requires careful circuit design and control strategies. The resonant circuit parameters need to be properly selected, and the timing of the switch must be precisely controlled to achieve ZVS operation. Furthermore, ZVS is more commonly used in medium-to-high power applications due to the additional complexity and cost associated with its implementation.

Overall, ZVS is an important technique in power electronics that helps improve efficiency, reduce losses, and enhance the performance of high-frequency switching systems.

4.6.2 Synchronous rectification

In a typical rectification circuit, a diode is used to convert alternating current (AC) into direct current (DC) by allowing current flow in only one direction. However, diodes have a voltage drop across them, which leads to power loss and reduced efficiency. Synchronous rectification addresses this issue by using controlled switches that have lower conduction losses.

In synchronous rectification the diodes of output rectifiers are replaced with actively controlled switches, for system to offer several advantages such as

1. Improved efficiency: Synchronous rectification reduces the voltage drop across the rectifier, leading to lower conduction losses and improved overall efficiency of the power conversion system.
2. Lower power dissipation: The reduced voltage drop results in less power dissipation, reducing the heat generated by the rectification circuit and allowing for higher power density designs.
3. Enhanced control: With actively controlled switches, the rectification process can be precisely controlled, allowing for better regulation and response to load changes.
4. Reduced electromagnetic interference (EMI): Synchronous rectification can help reduce EMI emissions by minimizing the diode reverse recovery losses, which are a significant source of high-frequency switching noise.

It's important to note that synchronous rectification requires careful control and coordination of the switch timings to avoid shoot-through currents (simultaneous conduction of the diode and switch). Proper gate driver design and control algorithms are necessary to achieve optimal synchronous rectification operation.

4.7 Simulation and Results

A non-isolated DC – DC converter capable of bidirectional power flow and an isolated DC-DC converter, both to function as backend convert for EV charger are simulated using MATLAB/Simulink at standard power ratings with battery acting as load[].

4.7.1 Non-isolated Converter

A Half-Bridge Buck-Boost converter is designed for the given specifications.

Input Voltage (Vin) is kept constant at 400VDC and the output is desired to be of 120VDC, the ripple in output current is set at 10% and in voltage at 1%, switching frequency (Fsw) is 10kHZ and input.

Using equation (4.5) and (4.6) the value of output filter inductance and capacitance are

$$L = \frac{160.(400-160)}{0.625*10k*160} = 15mH \tag{4.30}$$

$$C = \frac{0.625}{8*10k*1.6} = 5\mu F \tag{4.31}$$

This model is working in both G2V (Grid to Vehicle) and V2G (Vehicle to Grid) mode. The converter is designed to operate at 120V delivering or demanding 12A of load from the battery.

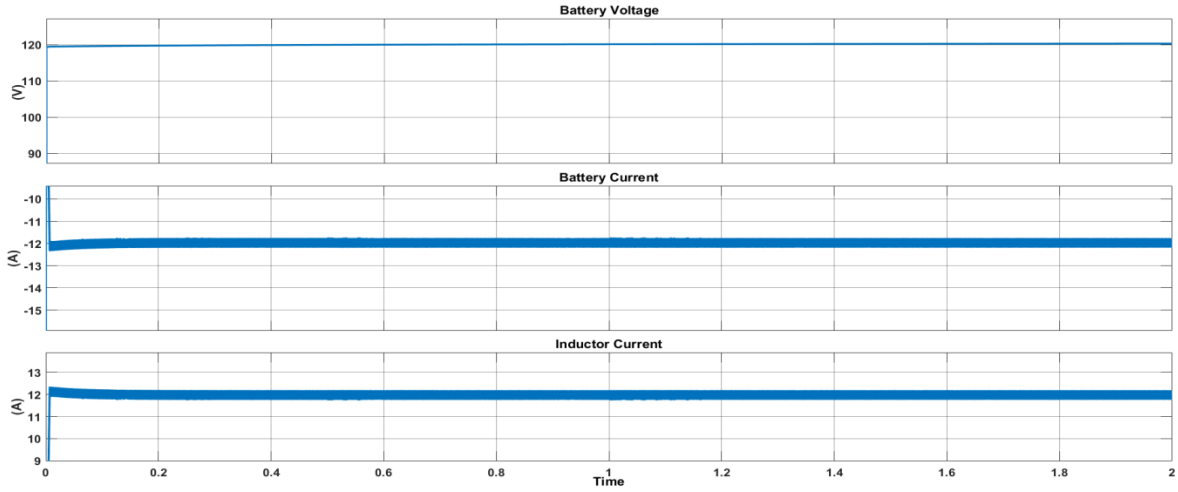

Figure 4.6: Output Voltage of DC – DC Converter given to battery, Battery Current in charging mode, Inductor current at the convert load.

Figure 4.4 shows that when battery is acting as a load to the system and is demanding the load current of 12A at 120V from device and the converter is fulfilling the same demand by producing the current of same magnitude as inductor current. This mode of operation is G2V mode.

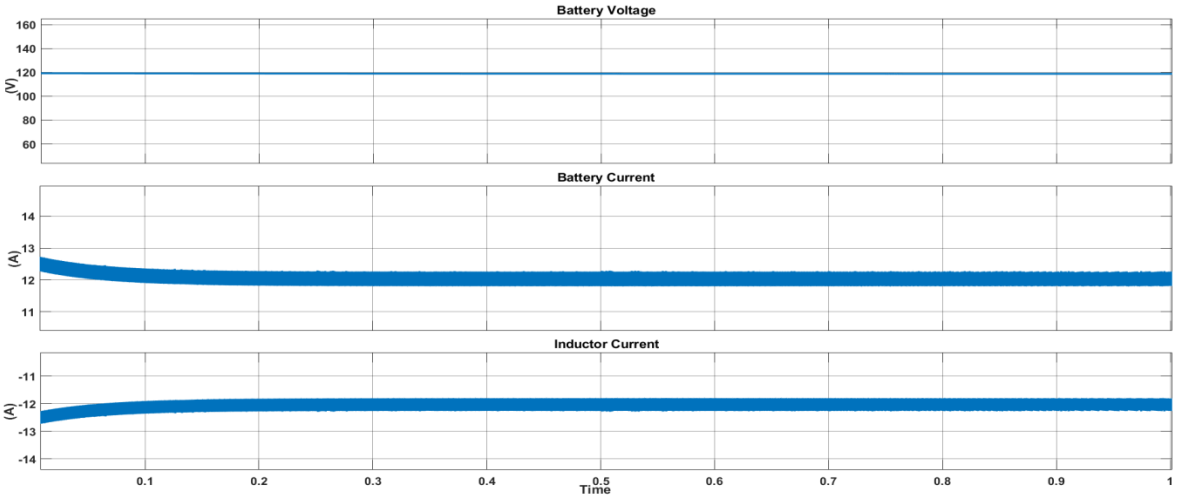

Figure 4.7: Output Voltage of DC – DC Converter given to battery, Battery Current in discharging mode, Inductor current at the convert load.

In second mode of operation called V2G mode, the battery starts acting as source instead of load and starts supplying the current back to grid, the same case observed in figure 4.5 where the battery is supplying the current of 12A to the grid at 120V and negative value of inductor current verifies the backward flow of the current.

4.7.2 Isolated Converter

A phase shifted full bridge DC – DC Converter designed for stepping down input of 400VDC to 55VDC at switching frequency of 50KHz.

Turns ratio of the high frequency transformer is

$$\frac{N_2}{N_1} = \frac{V_O}{V_{in}} = 0.1375 \tag{4.32}$$

LC filter at the output is given by equation (4.29) and (4.29)

$$L_{\min} = \frac{V_O(1-D)}{2 * \Delta i_{LO} * f_{SW}} = 94\mu H \tag{4.33}$$

$$C_{\max} = \Delta_{iL} * \frac{D}{f_{SW} * \Delta V_O} = 62\mu F \tag{4.34}$$

It is a unidirectional converter and hence only supports one direction of flow of the power, which is when battery is in charging mode. Figure 4.8 gives the battery voltage, battery and inductor current in charging mode.

Figure 4.9 shows the phase shift in the waveform of the voltage fed to primary end of the high frequency transformer followed by the waveform at the secondary end of the transformer.

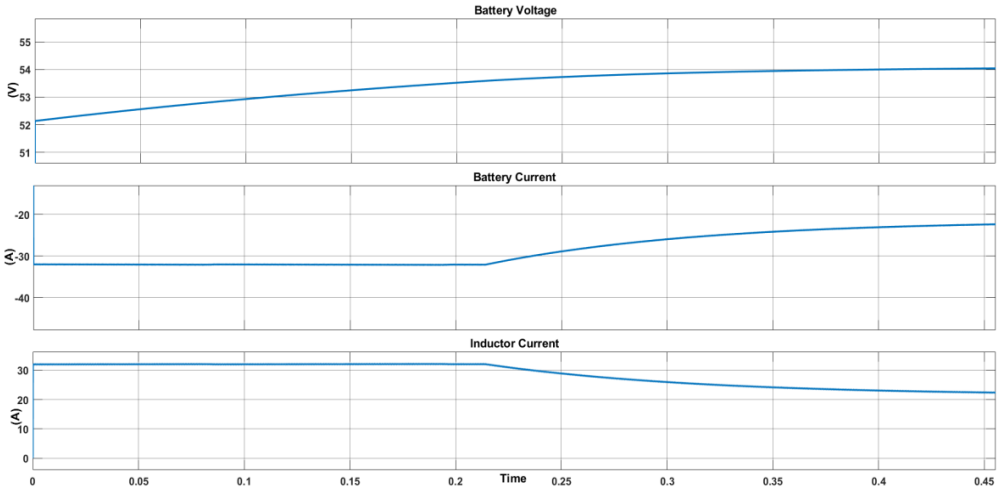

Figure 4.8: Output Voltage, Battery current in charging mode, inductor current at the output.

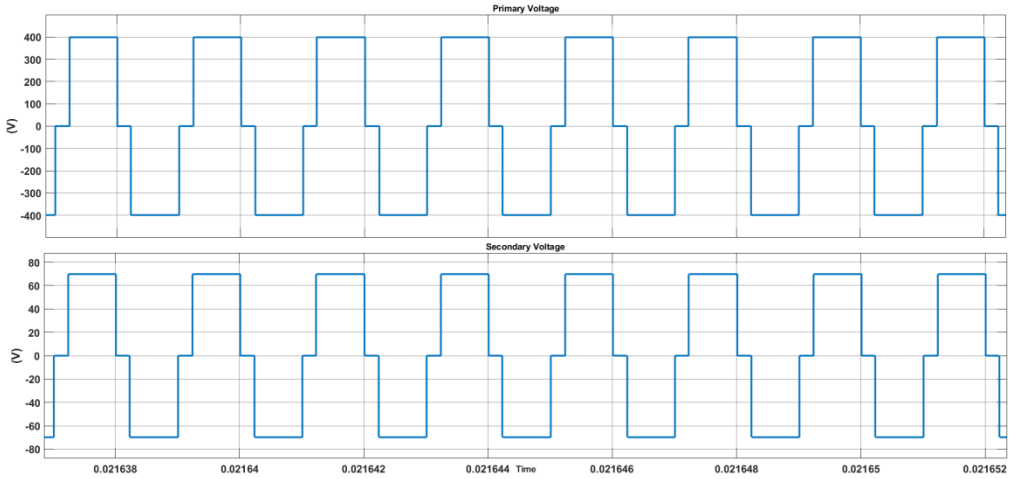

Figure 4.9: Voltage waveform of the Primary and Secondary terminal of transformer

4.8 Conclusion

The DC-DC converter, which is the second stage of the On-Board Charger (OBC), plays a crucial role in regulating the voltage and current of the battery. In this chapter, the commonly used charging method for Li-Ion batteries, known as CC/CV mode charging, is achieved through the implementation of a DC-DC converter. This mode involves charging the battery in two phases. Initially, the battery is charged from 40 V to 200 V using a constant current of 12A (CC mode). Subsequently, the charging continues in a constant voltage (CV) mode, where the battery voltage is maintained at a fixed level. It's important to note that the designed DC-DC converter allows for bidirectional power flow, enabling efficient energy transfer between the charger and the battery.

By raising the switching frequency, it is possible to reduce the size of the magnetic components in the converter. The main source of power loss occurs during rectification on the low voltage side. To enhance efficiency, it is crucial to minimize this power loss. One solution to address this is by utilizing a center-tap configuration, which only requires two components, compared to the four components needed in a full-wave bridge configuration. However, it's important to note that the center-tap configuration may require double the amount of wire on the low voltage side of the transformer, and in certain cases, a larger core compared to the full-wave bridge configuration. Consequently, this could potentially increase the weight of the system.

CHAPTER 5

DESIGN OF A 1KW AND 2KW CHARGER

5.1 Introduction

Designing an onboard charger involves several considerations, including the power requirements, charging standards, safety features, and physical implementation. The general outline of the design process of any onboard charger can be layer out as:[44,45]

1. Determine Power Requirements:
    - Determine the maximum power rating required for the charger based on the battery pack's capacity and desired charging time.
    - Consider the input voltage range available from the vehicle's electrical system.
2. Select Charging Standards:
    - Identify the charging standards compatible with your target application (e.g., AC Level 1, AC Level 2, DC Fast Charging, etc.).
    - Ensure compatibility with the vehicle's electrical system and battery pack.
3. Choose Power Conversion Topology:
    - Select an appropriate power conversion topology based on factors like power level, efficiency, and size constraints.
4. Safety Features:
    - Incorporate safety features, such as over current protection, overvoltage protection, short circuit protection, and temperature monitoring, to ensure safe and reliable charging.
    - Implement galvanic isolation between the input and output sides for safety and to comply with regulations.
5. Control and Monitoring:
    - Develop control algorithms to regulate the charging process, monitor battery parameters (voltage, temperature, state of charge), and adjust charging parameters accordingly.
    - Implement a communication interface (e.g., CAN bus) to exchange data with the vehicle's onboard systems.
6. Heat Dissipation and Thermal Management:
    - Design an effective heat dissipation system to manage the heat generated during charging.
    - Use appropriate heat sinks, cooling fans, or other thermal management techniques to maintain optimal operating temperatures.
7. Physical Design:
    - Develop a compact and robust physical design for the onboard charger, considering space constraints and installation requirements.
    - Choose suitable materials and components for durability and reliability.
8. Electromagnetic Interference (EMI) Mitigation:

- Apply proper filtering and shielding techniques to reduce electromagnetic interference generated by the charger.
- Comply with relevant EMC (Electromagnetic Compatibility) standards.

9. Testing and Certification:
    - Thoroughly test the onboard charger under various operating conditions to ensure compliance with safety and performance standards.
    - Obtain necessary certifications and approvals required for automotive applications.

Here in this Chapter, all these parameters are kept in mind and different rating Electric Vehicle Chargers are designed. Power requirement refers to the amount of electrical power needed to charge an electric vehicle (EV) battery within a desired time frame. It is a fundamental consideration in the design of an EV charger. The power requirement depends on factors such as the battery capacity, charging time, and the available input voltage from the electrical grid or power source.

1. Battery Capacity: The battery capacity of an EV is typically measured in kilowatt-hours (kWh) and represents the amount of energy the battery can store. The power requirement for charging the EV depends on the battery's capacity. For example, if the EV battery has a capacity of 40 kWh, and you want to charge it within 4 hours, the average charging power required would be 10 kW (40 kWh / 4 hours = 10 kW).

2. Charging Time: The desired charging time is an important factor in determining the power requirement. It varies depending on the user's needs and the charging infrastructure available. Faster charging times require higher power levels, while slower charging times can utilize lower power levels. Charging times can range from a few minutes for fast charging to several hours for overnight charging.

3. Input Voltage: The available input voltage from the electrical grid or power source also affects the power requirement. The EV charger must match the voltage input to the vehicle's onboard charging system. The charger's power output must align with the available voltage to ensure efficient and safe charging.

   It's worth noting that power requirement considerations extend beyond the charger itself. Infrastructure limitations and the capacity of the electrical grid must also be taken into account. Higher power requirements may necessitate upgrades to the electrical infrastructure to handle the increased load.

   In summary, determining the power requirement involves considering the battery capacity, desired charging time, and available input voltage. By

accurately assessing these factors, the EV charger's power output can be optimized to meet the changing needs of the EV owner while ensuring safe and efficient charging.

5.2 Charging Standards in India. [1,6]

In India, electric vehicle (EV) charging standards are primarily influenced by the standards adopted globally, such as those established by international organizations like the International Electrotechnical Commission (IEC) and the Society of Automotive Engineers (SAE). Here are the commonly followed charging standards in India:

1. Bharat AC 001 (AC Level 1):
    - Also known as Bharat Slow, this standard utilizes a single-phase alternating current (AC) power supply for charging.
    - It operates at 230 volts with a maximum current of 10 amperes (2.3 kW).
    - Bharat AC 001 is typically used for slower overnight charging and is suitable for EVs with smaller battery capacities.
2. Bharat AC 002 (AC Level 2):
    - Also known as Bharat Fast, this standard employs a three-phase AC power supply for charging.
    - It operates at 400 volts with a maximum current of 15 amperes (15 kW).
    - Bharat AC 002 is used for faster charging and is suitable for EVs with larger battery capacities.
3. Bharat DC 001 (DC Fast Charging):
    - This standard is used for direct current (DC) fast charging, enabling quicker charging times.
    - It typically operates at a higher voltage, ranging from 200 volts to 750 volts, with a maximum current of up to 200 amperes (150 kW or higher).

Bharat DC 001 is suitable for EVs with larger battery capacities, allowing them to charge rapidly at public charging stations.

SAE Standard			
Voltage Levels	**Typical usage**	**Interface**	**Power level (kW) Charging Time Exp.**
Level 1 (On-board 1P): Convenient			
230 (VAC)	Office or Home base charging	Any convenient outlet Possibility home or office	1.4 : 4-11 hrs
			2: 11-36 hrs
Level 2 (On-board 1P &3P): Main			
230(VAC)	Public and private based charging	Electric vehicle supply equipment Private or Public Outlets	4 : 1-4 hrs
			8 : 2-6hrs
			19.2 : 2-3hrs
Level 3 (Off Board 3P): Fast			
208 - 600 VDC	Like a filling station commercial point	Electric vehicle supply equipment Commercial similar to current filling station	50 : 0.4-1hrs
			100 : 0.2-0.5hrs

Based upon these observations, Two EV Chargers of different power ratings i.e 1KW and 2KW are designed. For 1kW rating charger a Boost PFC converter is used as a front end device followed by an Half bridge Buck boost DC-DC converter and for second design an interleaved Boost PFC Converter along a phase shift full bridge DC-DC Converter are

5.2 1KW EV Charger [6]

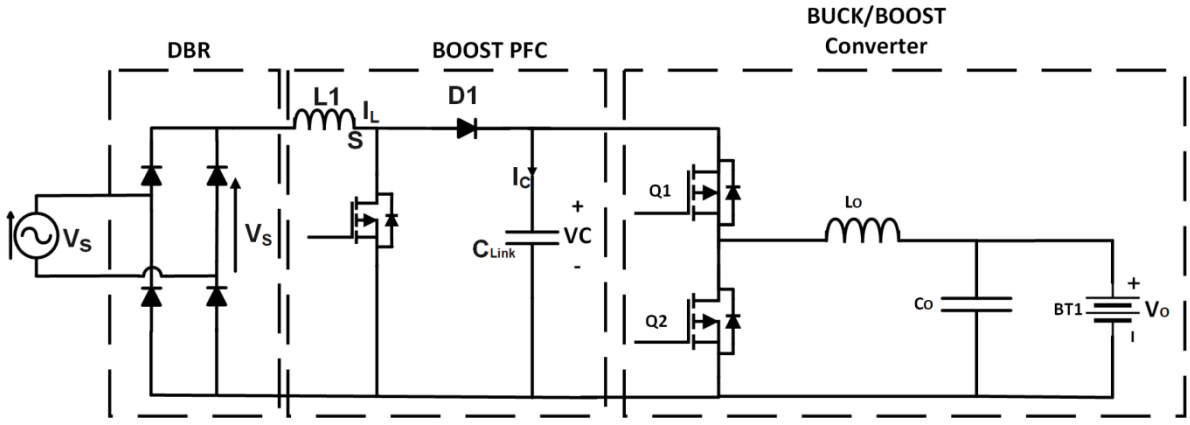

Figure 5.1: Circuit Diagram of a 1kW EV Charger with Boost PFC and Buck-Boost DC-DC

Figure 5.1 shows the complete block diagram of the proposed 1KW Charger design consisting a boost pfc as the front end device and a bidirectional buck-boost DC-DC converter acts as follow-up back end converter.

5.2.1 Boost PFC Converter Design.[41]

The boost converter works here in CCM (Continuous conduction mode) hence the energy in the inductor flows continuously during the operation of the converter as the switching device turns in before the inductor current drops to zero, keeping the inductor current continuous

A 230V AC supply is given to a rectifier circuit converting AC electrical power into DC. The Bridge rectifier is a type of arrangement with four diodes kept the result in a closed loop bridge configuration which provides the same polarity output for both the polarity of the input, the output voltage can be expressed as

$$V_{DC} = \frac{2V_{\max}}{\pi} \tag{5.1}$$

here $V_{\max}$ is the peak value of the supply voltage.

A DC-DC Boost Converter is connected at the output of the rectifier, it supplies an output voltage larger than the input voltage at the source. The relation between the voltage supplied at the source with the voltage at the output end is given as

$$V_{in} = \frac{1}{1-D} V_C \tag{5.2}$$

D is the duty cycle with V_{in} as the supply voltage to the converter coming from the rectifier and V_C as the output voltage from the PFC Converter.

Design and Calculation for boost converter filter circuit is done by first calculating the load value (considered to be resistive) by

$$R_{L(\max,\min)} = \frac{V_O}{I_{O(\min,\max)}} = \frac{400}{2.5} \tag{5.3}$$

R_L is calculated to be 160Ω.

For the calculated R_L load the value of output filter circuit are,

$$L_1 = \frac{R_{L\max} D_{\min} (1-D_{\min})^2}{2 f_{sw}} \tag{5.4}$$

For the switching frequency of 100 KHz the value of L_1 600H

And capacitance C_{Link} ,

$$C_{Link} = \frac{D_{\max} V_C}{f_{sw} R_{L\min} V_{cpp}} \tag{5.5}$$

C_{Link} is calculated to be of 180µF.

5.2.2 Buck Boost DC-DC Converter Design.

Input for this converter will be the output from the previous stage (V_C), running at the same switching frequency the is simply made of two switching devices and a output filter.

The value of inductance and Capacitance at output are given as

$$L_O = \frac{V_O \times (V_C - V_O)}{I_{ripple} \times f_{sw} \times V_C} \tag{5.6}$$

$$L_O > 2.8mH$$

Value of output inductance for this design is kept 3mH.

Similarly Capacitance is calculated by,

$$C_O = \frac{I_{ripple}}{8 \times f_{sw} \times V_{ripple}} \tag{5.7}$$

$$C_O > 9.3\mu F$$

Table 4: 1KW Charger Parameter

Parameters	Symbols	Rating
Maximum value of Single-Phase Rectified line Voltage	Vs	325V
Switching Frequency	fsw	100 kHz
Load Resistance	R_L	50Ω
Inductor	L_1	0.692 mH
Smoothing Capacitor	C_{link}	17 µF
Output filter Inductor	L_O	3mH
Output filter Capacitance	C_O	10µF

5.3 2KW EV Charge

The design of the converter is carried out for a 2 kW operation rating, working in CCM mode at the switching frequency in kHz's with assumptions such as that the switching devices are ideal is considered for ease of understanding.

5.3.1 Interleaved PFC BOOST Design [44-46]

A 230V AC (RMS) supply with a supply frequency of 50Hz is given to the filter circuit which uses a capacitor as a filter. Once after rectification, capacitors remove the ripple

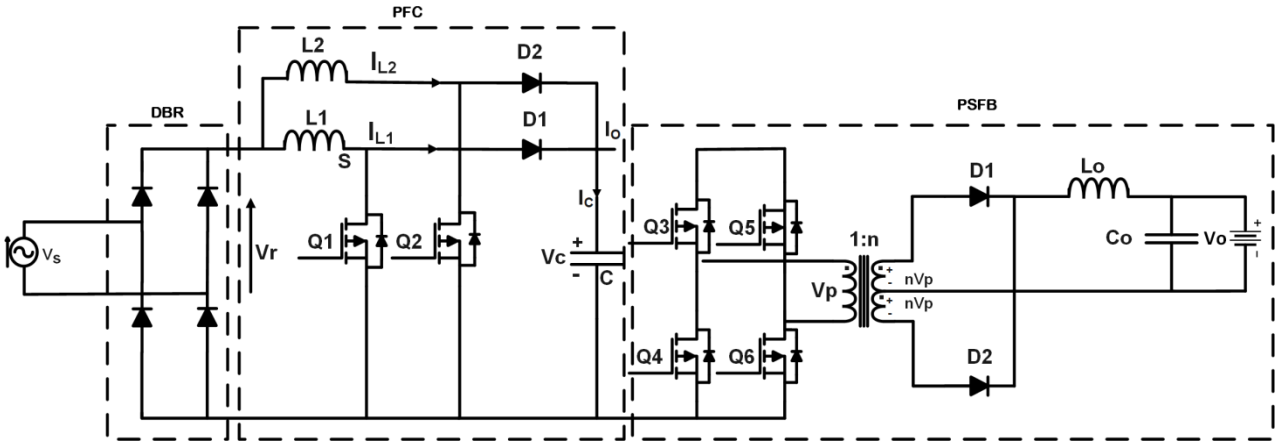

Figure 5.2: Circuit Diagram of a 2kW EV Charger with interleaved PFC and PSFB DC-DC

and smoothen the pulsating DC output so a near to constant DC voltage is supplied. For high power application, more than one boost cell can be operated in parallel to increase the power capability of the PFC circuit and reduce the capacitor current ripple, known as interleaved system.

For our system to work at the rated output power of 2kW, with the regulated DC link voltage (V_c) maintain at 400V under normal conditions. The duty cycle for the same can be expressed as

$$D = \frac{V_C - V_i}{V_C} \tag{5.8}$$

where V_i is the peak value of the voltage supply and can be represented as $\sqrt{2}$ times of AC line Voltage (V_S). At times of the lowest AC line voltage supply, i.e 200V the maximum current from the input line will pass and so will the highest value of Duty Cycle will be reached which will make the (2) as

$$D_{\max} = \frac{V_C - \sqrt{2}V_{S\min}}{V_C} = \frac{400 - \sqrt{2}(200)}{400} = 0.3 \tag{5.9}$$

Considering the inductor ripple current to be 20% of the inductor current for both of the inductor values.

$$\Delta i_{L1} = \Delta i_{L2} = \frac{P_o}{V_C}.20\%$$
$$= \frac{2000}{400} * 0.20 \quad (5.10)$$
$$= 1A$$

Major part of design process is the selection of inductor value, as that assures the proper PFC functionality. The selection of this value depends on inductor ripple current

$$L = \frac{V_i * D}{f_S . \Delta i_L} \quad (5.11)$$

From above, the value of inductor L_1 *and* L_2 are calculated as

$$L_1 = L_2 = \frac{400 * 0.3}{50000 * 1} \quad (5.12)$$
$$= 2.4mH$$

The ripple in DC link voltage (ΔV_C) is taken at 1% of its nominal value

$$\Delta V_C = \frac{1 * 400}{100} = 4V \quad (5.13)$$

From (6) the output capacitor can be estimated at the given voltage ripple.

$$C \geq \frac{P_O}{4\pi f_{Supply} * V_C * \Delta V_C} \quad (5.14)$$
$$\geq 1986\mu F$$

5.3.2 The PSFB DC-DC Conveter [47,48]

The output voltage in PSFB is,

$$V_O = 2 * V_C * n * D \quad (5.15)$$

Transformer turn ration n is

$$n = \frac{Ns}{Np} = \frac{50}{400} = 0.125 \quad (5.15)$$

where, V_O is the demand voltage of battery load from the converter for charging, V_C is the ,input fed to the DC-DC Converter from the previous state and n is the ratio of secondary to primary side of transformer and D is the duty cycle for the converter.

The output Voltage of the charger is expected to be at 48V then D is calculated

$$48 = 2 * 400 * 0.125 * D$$
$$D = 0.48 \quad (5.16)$$

The Value of Filter Inductor is calculated for 20% inductor ripple current

$$\Delta i_{Lo} = \frac{P_O}{V_O}.20\%$$
$$= \frac{2000}{48} * 0.2 \quad (5,17)$$
$$= 8.3A$$

The switching frequency (f_{SW}) of the DC-DC Converter is 500 KHz, upon substituting the parameters in chapter 4 equations we get,

$$L_O = \frac{48(1-0.48)}{2*8.3*100000} \quad (5.18)$$
$$= 15.03\mu H$$

Similarly, the output capacitor depends upon the voltage ripple and can be measured by,

$$C_O = \Delta_{iL} * \frac{D}{f_{SW} * \Delta V_O} \quad (5.19)$$

Where the ΔV_O is the output ripple voltage, kept at 1%, giving the output capacitance to be around 100uF.

The simulation model is prepared with component specification as per the table below.

Table 5: 2KW Charger Parameters.

Parameter	Variable	Value
Supply Voltage	V_s	180V
Input inductor	L_1,L_2	3mH
DC-link Voltage	V_C	400V
DC-link Capacitance	C	2000 μ F
Transformer Ratio	n	0.125
Filter Inductance	L_o	15 μ H
Filter Capacitance	C_o	100 μ *F*
Output Power	P_o	2kW
Switching Frequency	F_{sw}	100Khz

5.4 Simulation and Results A simulation prototype of the suggested EV charger is simulated using the MATLAB/SIMULINK software.

5.4.1 1KW Charger Results

This charger is designed to work for bidirectional power flow when connected to a grid and battery. Current waveform is multiplied fives for observation purpose.

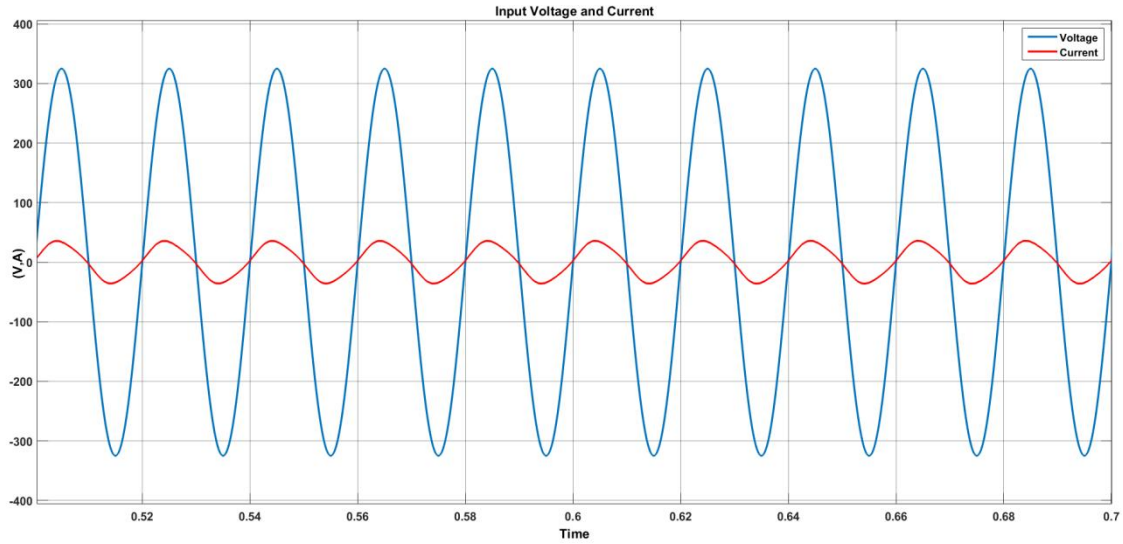

(a)

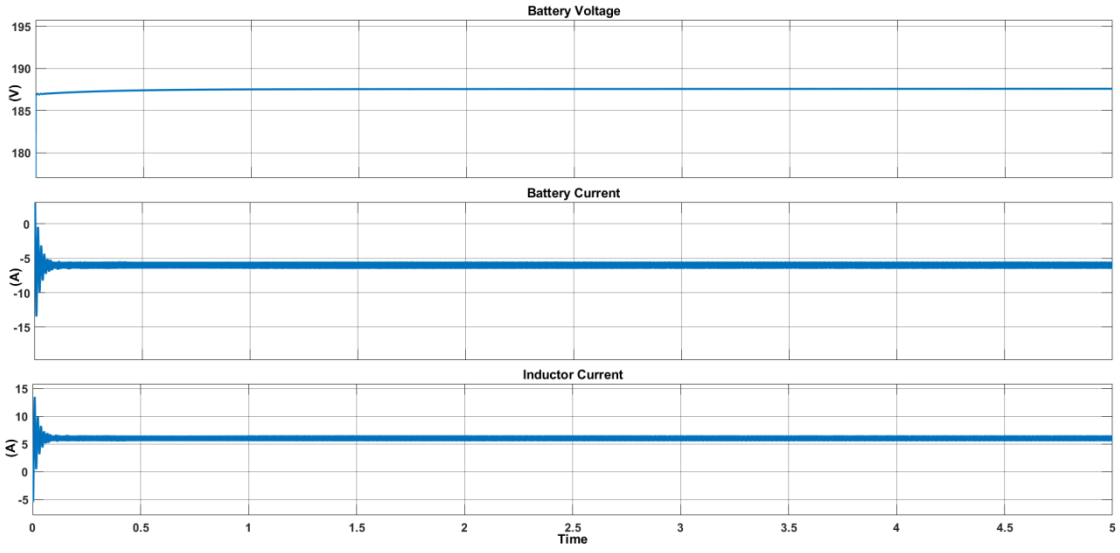

(b)

Figure 5.3 Output of the system (a) input current and voltage waveform in phase, (b) battery voltage, current and inductor current in charging mode.

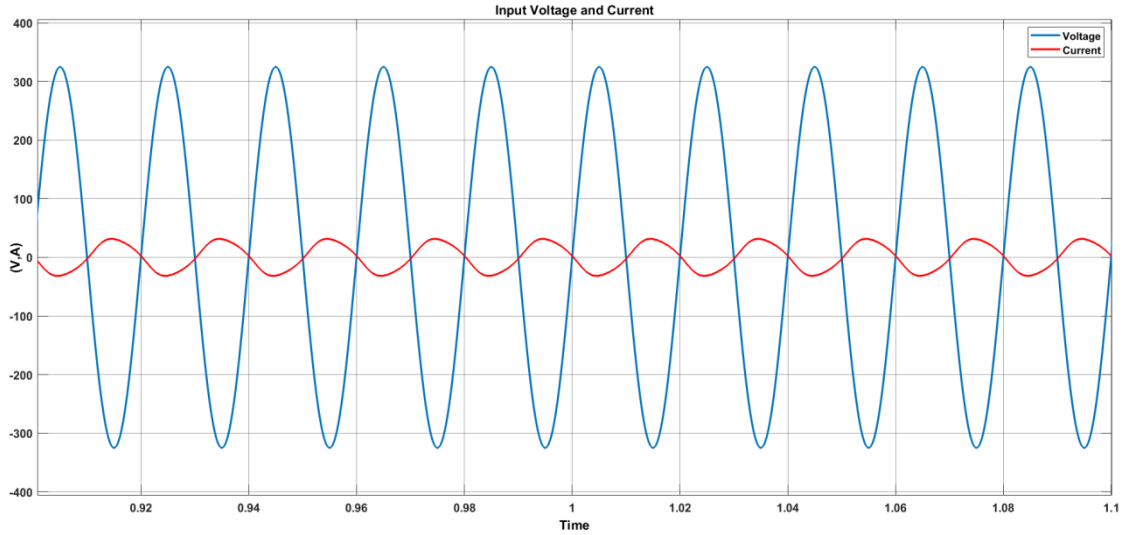

(a)

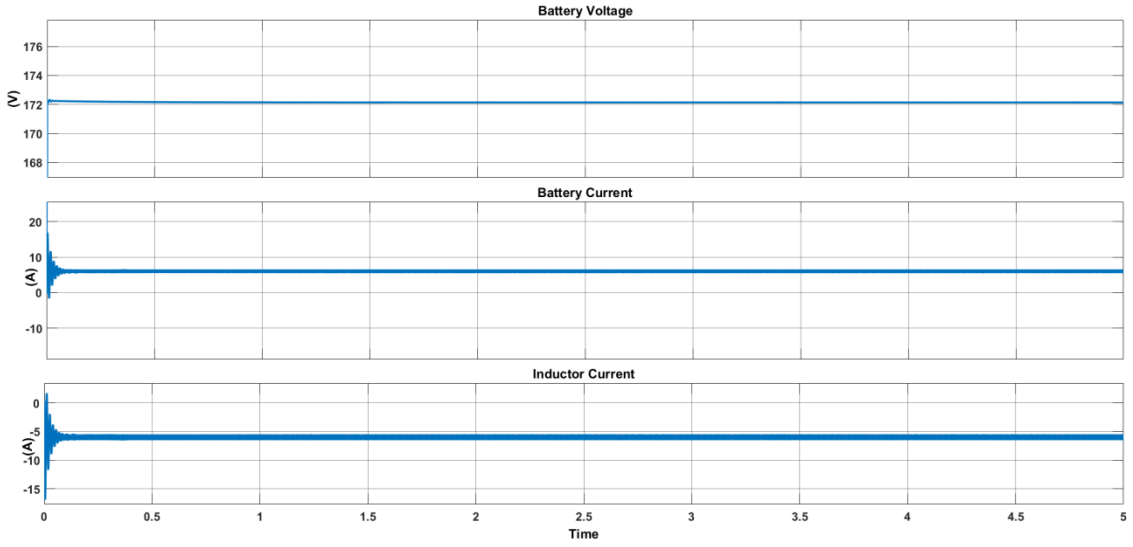

(b)

Figure 5.4 Output of the system (a) input current and voltage waveform in phase, (b) battery voltage, current and inductor current in discharging mode.

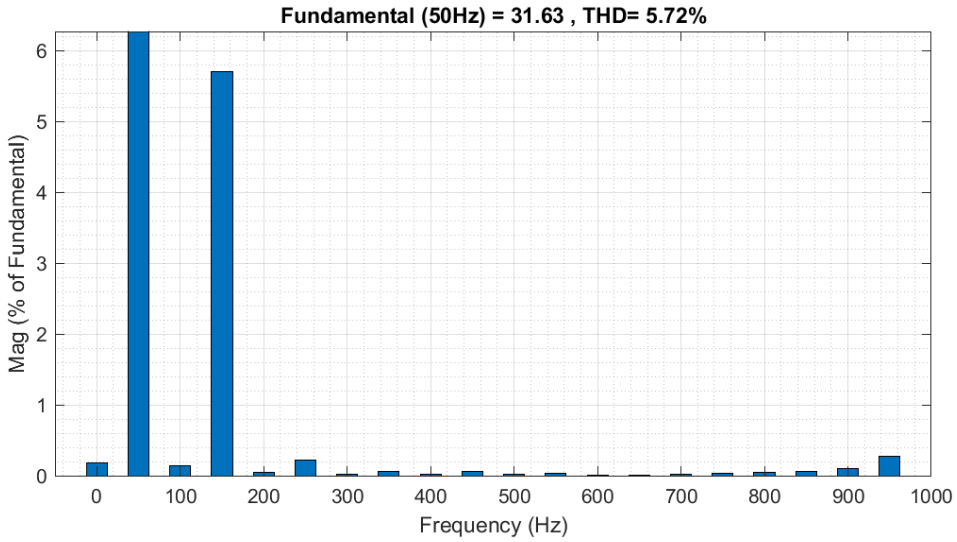

Figure 5.5: FFT analysis of an 1KW Charger

5.4.2 2KW Charger

The charger is designed for unidirectional flow of the power, from grid to battery load.

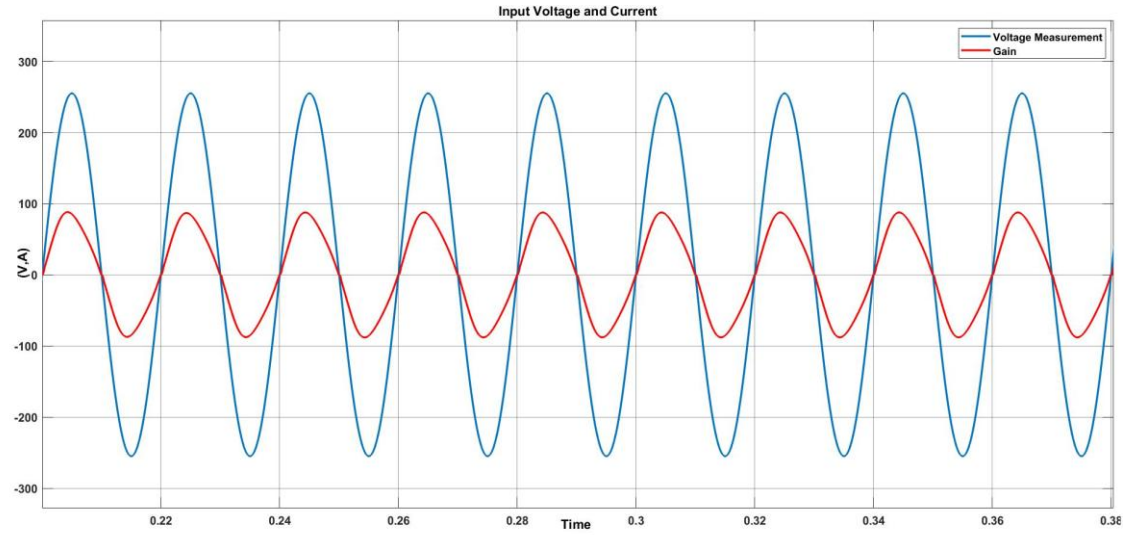

(a)

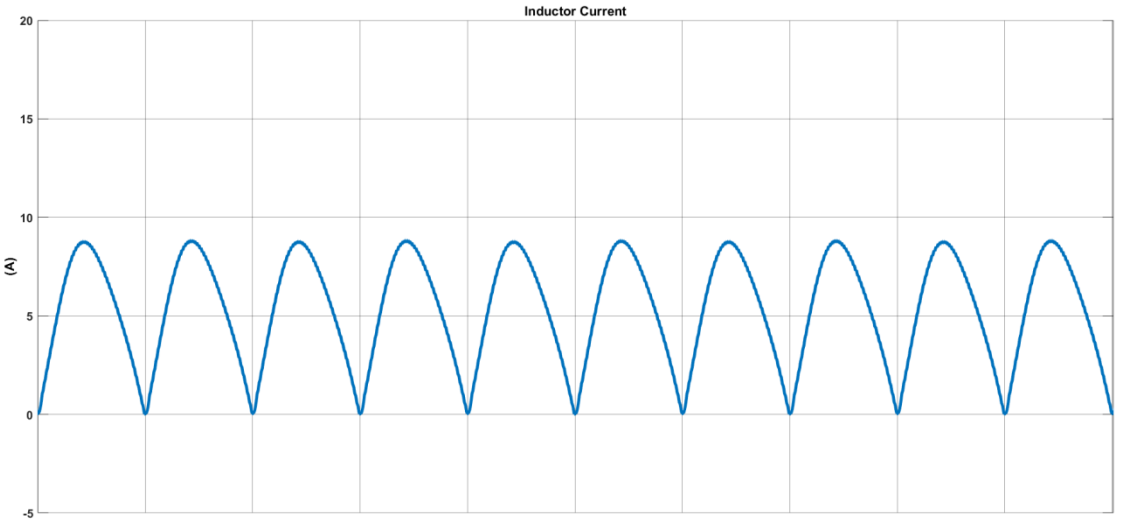

(b)

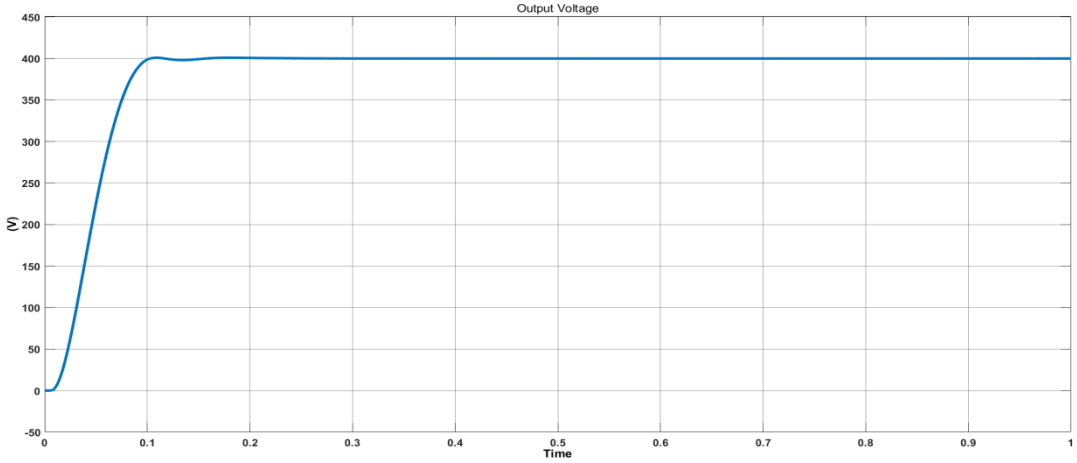

(c)

Figure 5.6: Interleaved PFC boost (a) input voltage and current in phase, (b) inductor current, (c) output V

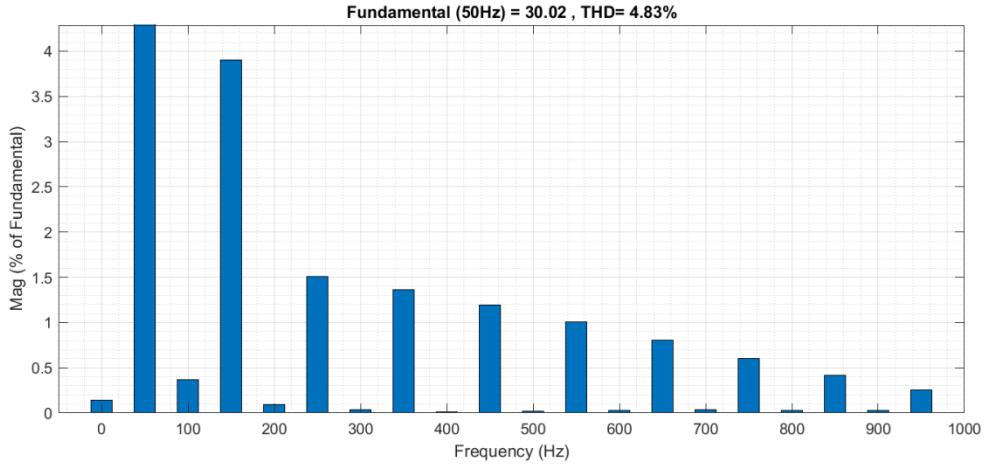

Figure 5.7: FFT analysis of 2KW Charger

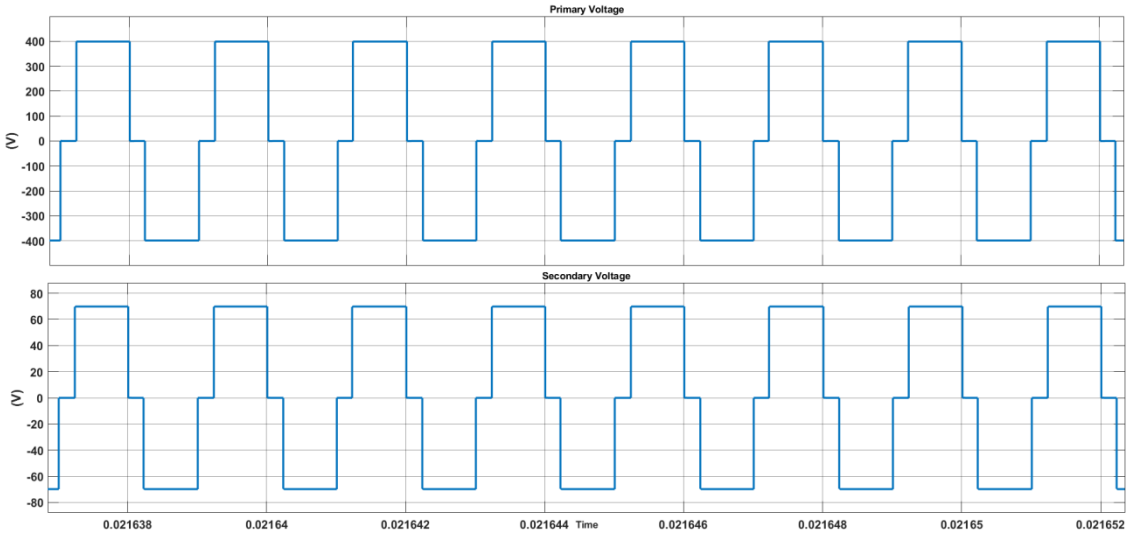

Figure 5.8: Voltage waveform at primary and secondary leg of high frequency transformer.

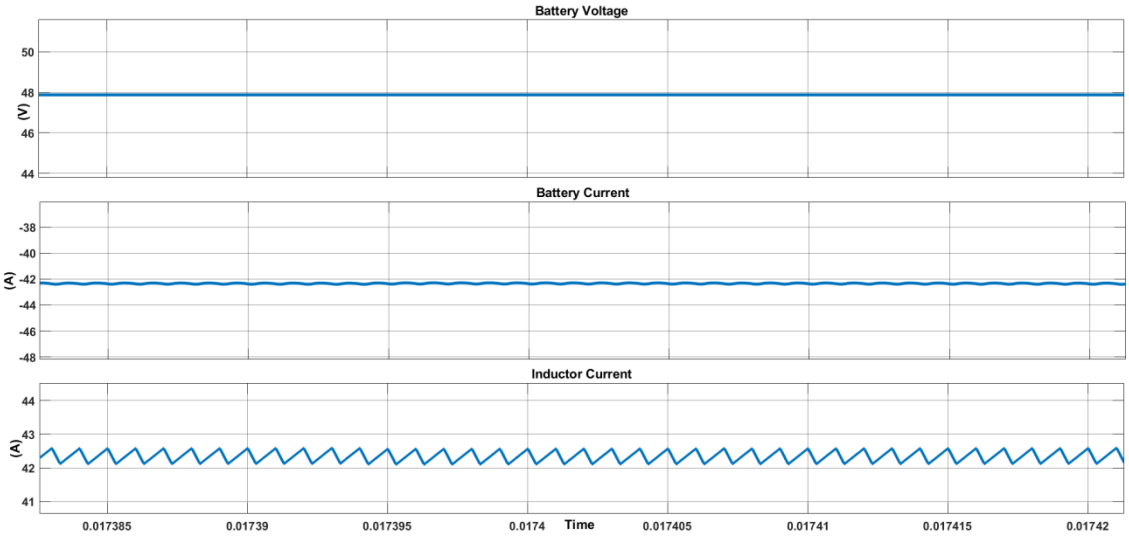

Figure 5.9: (a) Batter Voltage, (b) Battery Current, (c) Inductor Current of a 2kw Charger.

CHAPTER 6

CONCLUSION AND FUTURE SCOPE

The thesis discusses the design and challenges of an on-board electric vehicle charger for level 1 charging using a 230 V input supply. It introduces the different stages of the charger and identifies the difficulties involved. To address these challenges, various developments have been implemented. The proposed solution is a two-stage charger topology comprising an active Power Factor Correction (PFC) converter at the front end and a Bi-directional DC-DC converter. The active PFC converter, functioning as a Boost converter, achieves 5% Total Harmonic Distortion (THD) at full load and is capable of handling wide variations in loads. The thesis provides a detailed discussion of the power stage and controller design, along with simulated results.

In the second stage, a DC-DC converter is created and simulated to regulate the charging current and voltage. The converter demonstrates excellent accuracy in charging the propulsion battery using the CC/CV mode across a wide voltage range. Additionally, a V2G controller is developed for the DC-DC converter to enable power supply from the propulsion battery to the grid. The voltage and current patterns of the battery are showcased, confirming the effectiveness of the designed converter.

LIST OF PUBLICATIONS

[1] C. Sushant,Singh Alka, “A Boost PFC fed LLC Resonant Converter For Electric Vehicle Application” , ICETEST-PICC,IEEE,2023.

[2] C. Sushant, Singh Alka, “Design and Control of a 2kW Electric Vehicle Charger”, ICSSESS-SIT, IEEE, 2023. (Accepted)

REFRENCES

[1] S. S. Williamson, Energy management strategies for electric and plug-in hybrid electric vehicles. Springer, 2013.

[2] a. Emadi and K. Rajashekara, "Power Electronics and Motor Drives in Electric, Hybrid Electric, and Plug-In Hybrid Electric Vehicles," IEEE Trans. Ind. Electron., vol. 55, no. 6, pp. 2237–2245, 2008.

[3] M. Yilmaz and P. T. Krein, "Review of charging power levels and infrastructure for plug-in electric and hybrid vehicles," 2012 IEEE Int. Electr. Veh. Conf. IEVC 2012, vol. 28, no. 5, pp. 2151–2169, 2012.

[4] Kavuri Poornesh1 , Kuzhivila Pannickottu Nivya2 , K. Sireesha3," A Comparative study on Electric Vehicle and Internal Combustion Engine Vehicles", Proceedings of the International Conference on Smart Electronics and Communication (ICOSEC 2020)

[5] H. Wang, S. Dusmez, and A. Khaligh, "Design and analysis of a full-bridge LLC-based PEV charger optimized for wide battery voltage range," IEEE Trans. Veh. Technol., vol. 63, no. 4, pp. 1603–1613, 2014.

[6] Huishuang Fan, Hongqi Ben and Jichao Ning, "Output voltage ripple reduction control strategy for three-phase combined PFC converter under grid voltage unbalance," in 22nd International Conference on Electrical Machines and Systems (ICEMS),2019.

[7] Rafael Pena-Alzola, Marco Andres Bianchi, Martin Ordonez, "Control Design of a PFC with Harmonic Mitigation Function for Small Hybrid AC/DC Buildings", IEEE Transactions on Power Electronics (Volume: 31, Issue: 9, September 2016).

[8] P. Maheshwari, Y. Tambawala, H. S. V. S. K. Nunna, and S. Doolla, "A review of plug-in electric vehicles charging: Standards and impact on the distribution system," Power Electronics, Drives and Energy Systems (PEDES), 2014 IEEE International Conference on. pp. 1–6, 2014.

[9] Jinming Xu, Hao Qian, Yuan Hu, Shenyiyang bian, Shaojun Xie, "Overview of SOGI-Based Single-Phase Phase-Locked Loops for Grid Synchronization Under Complex Grid Conditions" IEEE Access 2021.

B. Whitaker, A. Barkley, Z. Cole, B. Passmore, D. Martin, T. R. McNutt, A. B. Lostetter, J. S. Lee, and K. Shiozaki, "A high-density, high efficiency,

isolated on-board vehicle battery charger utilizing silicon carbide power devices," IEEE Trans. Power Electron., vol. 29, no. 5, pp. 2606–2617, 2014

[10] V. Monteiro, G. Pinto, and J. Afonso, "Operation Modes for the Electric Vehicle in Smart Grids and Smart Homes: Present and Proposed Modes," IEEE Trans. Veh. Technol., vol. 9545, no. c, pp. 1–1, 2015.

[11] L. Solero, "Nonconventional on-board charger for electric vehicle propulsion batteries," IEEE Trans. Veh. Technol., vol. 50, no. 1, pp. 144–149, 2001.

[12] T. Konjedic, L. Korosec, M. Truntic, C. Restrepo, M. Rodic, and M. Milanovic, "DCMbased Zero-Voltage Switching Control of a Bidirectional DC-DC Converter With Variable Switching Frequency," IEEE Trans. Power Electron., vol. 31, no. 4, pp. 3273–3288, 2015

[13] B. S. S. Singh, "Single-phase power factor controller topologies for permanent magnet brushless DC motor drives," no. October 2008, 2010.

[14] B. S. S. Singh, "Single-phase power factor controller topologies for permanent magnet brushless DC motor drives," no. October 2008, 2010.

[15] J. Chen, D. Maksimović, and R. W. Erickson, "Analysis and design of a low-stress buckboost converter in universal-input PFC applications," IEEE Trans. Power Electron., vol. 21, no. 2, pp. 320–329, 2006.

[16] J. Arrillaga, B. C. Smith, N. R. Watson, and A. R. Wood, Power system harmonic analysis. 2013.

[17] D. Committee, I. Power, and E. Society, "IEEE Recommended Practice and Requirements for Harmonic Control in Electric Power Systems IEEE Power and Energy Society," vol. 2014, 2014.

[18] R. W. Erickson and D. Maksimovic, Fundamentals of power electronics. Springer Science & Business Media, 2007.

[19] Pratap Ranjan Mohanty, Anup Kumar Panda and Dhiman Das, "An Active PFC Boost Converter Topology for Power Factor Correction," Annual IEEE India Conference (INDICON), 2015

[20] Rahul Pandey and Bhim Singh, "A Power Factor Corrected Electric Vehicle Battery Charger Using Boost Converter 2018 8th IEEE India International Conference on Power Electronics (IICPE).

[21] João Paulo M. Figueiredo and Fernando L. Tofoli, "A Review of Single-Phase PFC Topologies Based on The Boost Converter," 2010 9th IEEE/IAS International Conference on Industry Applications - INDUSCON 2010.

[22] Murat Yilmaz and Philip T. Krein, “Review of Battery Charger Topologies, Charging Power Levels, and Infrastructure for Plug-In Electric and Hybrid Vehicles,” IEEE TRANSACTIONS ON POWER ELECTRONICS, VOL. 28, NO. 5, MAY 2013.

[23] wenjin Dai, and Ming Li, “Design of Single Phase Boost-PFC Converter With Fast voltage Regulator,” IEEE International Conference on Industrial Technology,2008.

[24] P. N. Ekemezie, “Design of a power factor correction ac-dc converter,” in AFRICON 2007, 2007, pp. 1–8.

[25] W. Method, W. Ma, M. Wang, S. Liu, S. Li, and P. Yu, “Stabilizing the Average-CurrentMode-Controlled Boost PFC Converter via,” vol. 58, no. 9, pp. 595–599, 2011

[26] S. Choudhury, “Average current mode controlled power factor correction converter using TMS320LF2407A,” Appl. Note SPRA902A. Texas Instruments, no. July, pp. 1–15, 2003

[27] H. Plesko, J. Biela, J. Luomi, and J. W. Kolar, “Novel concepts for integrating the electric drive and auxiliary DC-DC converter for hybrid vehicles,” IEEE Trans. Power Electron., vol. 23, no. 6, pp. 3025–3034, 2008

[28] S. Kim and F. S. Kang, “Multifunctional onboard battery charger for plug-in electric vehicles,” IEEE Trans. Ind. Electron., vol. 62, no. 6, pp. 3460–3472, 2015

[29] M. A. Khan, I. Husain, and Y. Sozer, “A Bi - directional DC - DC Converter with Overlapping Input and Output Voltage Ranges and Vehicle to Grid Energy Transfer Capability,” vol. 2, no. 3, pp. 507–516, 2014.

[30] R. Teodorescu, M. Liserre, and P. Rodriguez, "Grid Converters for Photovoltaic and Wind Power Systems," ed: John Wiley & Sons, Ltd., 2011

[31] H. Guan-Chyun and J. C. Hung, "Phase-locked loop techniques. A survey," Industrial Electronics, IEEE Transactions on, vol. 43, pp. 609-615, 1996

[32] M. Karimi-Ghartemani and M. R. Iravani, "A new phase-locked loop (PLL) system," in Circuits and Systems, 2001. MWSCAS 2001. Proceedings of the 44th IEEE 2001 Midwest Symposium on, 2001, pp. 421-424 vol.1

[33] S. Golestan, M. Monfared, F. D. Freijedo, and J. M. Guerrero, "Design and Tuning

of a Modified Power-Based PLL for Single-Phase Grid-Connected Power Conditioning Systems," Power Electronics, IEEE Transactions on, vol. 27, pp. 3639-3650, 2012

[34] A. zdemir, I. Yazici, and C. Vural, "Fast and robust software-based digital phase-locked loop for power electronics applications," Generation, Transmission & Distribution, IET, vol. 7, pp. 1435-1441, 2013

[35] A. Ohori, N. Hattori, and T. Funaki, "Phase-Locked Loop Using ComplexCoefficient Filters for Grid-Connected Inverter," Electrical Engineering in Japan, vol. 189, pp. 52-60, 2014

[36] M. M. Begovic, P. M. Djuric, S. Dunlap, and A. G. Phadke, "Frequency tracking in power networks in the presence of harmonics," Power Delivery, IEEE Transactions on, vol. 8, pp. 480-486, 1993.

[37] D. Nedeljkovic, J. Nastran, D. Voncina, and V. Ambrozic, "Synchronization of active power filter current reference to the network," Industrial Electronics, IEEE Transactions on, vol. 46, pp. 333-339, 1999

[38] R. Weidenbrug, F. P. Dawson, and R. Bonert, "New synchronization method for thyristor power converters to weak AC-systems," Industrial Electronics, IEEE Transactions on, vol. 40, pp. 505-511, 1993.

[39] R. W. Wall, "Simple methods for detecting zero crossing," in Industrial Electronics Society, 2003. IECON '03. The 29th Annual Conference of the IEEE, 2003, pp. 2477-2481 Vol.3

[40] P. Rodriguez, A. Luna, M. Ciobotaru, R. Teodorescu, and F. Blaabjerg, "Advanced Grid Synchronization System for Power Converters under Unbalanced and Distorted Operating Conditions," in IEEE Industrial Electronics, IECON 2006 - 32nd Annual Conference on, 2006, pp. 5173-5178.

[41] Gardner and F. M, "Phaselock Techniques," ed: John Wiley & Sons Inc, 1966.

[42] Utsav Sharma, and Bhim Singh, “An Onboard Charger for Light Electric Vehicles,” 2020 IEEE International Conference on Power Electronics, Drives and Energy Systems (PEDES).

[42] Ionel “Dan” Jitaru, Nicolae Daniel Bolohan, “A High Efficiency 2KW DC-DC Converter for Automotive Application,” 2012 Twenty-Seventh Annual IEEE Applied Power Electronics Conference and Exposition (APEC).

[42] Chan-Song Lee, Jin-Beom Jeong, Baek-Haeng Lee, and Jin Hur, “Study on 1.5

kW Battery Chargers for Neighborhood Electric Vehicles", 2011 IEEE Vehicle Power and Propulsion Conference.

[43] Dingsihao Lyu, Thiago Batista Soeiro, and Pavol Bauer, "Impacts of Different Charging Strategies on the Electric Vehicle Battery Charger Circuit Using Phase-Shift Full-Bridge Converter", 2021 IEEE 19th International Power Electronics and Motion Control Conference (PEMC).

[44] Mohd Shahnawaz Khan, Shelas Sathyan, Harinaik Sugali,v and S S Chandra Bommagani," Design of On-Board Battery Charger using Interleaved Bridgeless Type PFC and Phase Shifted Full Bridge Converter",2020 IEEE International Students' Conference on Electrical, Electronics and Computer Science.

[45] Fariborz Musavi, Wilson Eberle, and William G. Dunford, "A High-Performance Single-Phase Bridgeless Interleaved PFC Converter for Plug-in Hybrid Electric Vehicle Battery Chargers",IEEE TRANSACTIONS ON INDUSTRY APPLICATIONS, VOL. 47, NO. 4, JULY/AUGUST 2011.

[48] Arya P S, and Chithra R., "Phase Shifted Full Bridge DC-DC Converter", International Research Journal of Engineering and Technology (IRJET).